Technische Universität Berlin

Diplomarbeit
zur Erlangung des Grades
Diplom-Ingenieur

vorgelegt von: Andreas Vetter

Thema:

Design of a liquid metal target loop for a high power spallation source

Prüfer: Prof. Dr. Gerd Brunk, TU Berlin
Betreuer: Dr. Friedrich Groeschel, Paul Scherrer Institut

Abstract:

The Eurisol Design Studies (Eurisol DS) aim to design a new ISOL facility. The targets will consist of a 4 MW liquid metal driver target surrounded by a fission target as well as of 100 kW solid targets. The driver target will use mercury as target material and heat removal fluid.

This thesis shows the lay-out of the liquid metal loop, which is designed to evacuate 3.0 MW of thermal power. It describes the function and sizing of the piping and components.
The thesis deals with the choice of the pump, the expansion tank/gas separator and the heat exchanger using water as cooling fluid as well as instrumentation.

Zusammenfassung:

Das Projekt Eurisol Design Studies (Eurisol DS) hat zum Ziel, eine neue ISOL Anlage zu konzipieren. Das Target besteht dabei aus einem Flüssigmetall „driver target“, und einem diesen umgebenden „fission target“. Zudem sind konventionelle 100kW Targets vorgesehen. Das „driver target“ wird aus flüssigem Quecksilber bestehen, welches zugleich zur Abfuhr der Wärme genutzt wird.

Die Diplomarbeit beschäftigt sich mit der Auslegung des Quecksilberkreislaufes, wobei 3.0MW an thermischer Leistung abgeführt werden müssen. Die Funktion und Auslegung der Rohre und Komponenten wird beschrieben.
Weiterhin wird die Wahl der benötigten Pumpe getroffen, die Dimensionierung des Wärmetauschers (mit Wasser als Kühlmittel) und des Expansionstank bzw. des Gasseparator durchgeführt, sowie die Instrumentierung besprochen.

Table of Content

Table of Content I
Nomenclature III
Subscripts IV
Abbreviations V
List of figures VI
List of tables VIII
1 Introduction 1
1.1 Existing structures at PSI 2
1.1.1 Particle source 2
1.1.2 Accelerators 3
1.1.3 Target (SINQ) 6
1.1.4 Experimental devices 8
1.1.5 Schematic overview 10
1.2 Usage of spallation sources 11
1.3 History and plans of EURISOL DS 11
2 Outline of the loop 15
2.1 Basic requirements 15
2.2 Materials 17
2.3 Filter 18
2.4 Irradiation 18
2.5 Safety 25
2.6 Target heat removal 25
2.7 Pressure drops in the loop 26
2.8 Check for cavitation 29
2.9 Baseline parameters for loop 30
3 Dimensioning of the main devices 32
3.1 Pump 32
3.2 Heat exchanger 39
3.3 Expansion tank and gas separator 44
3.4 Drain Tank 47
4 Measurement devices 49
4.1 Temperature 49
4.2 Pressure 51
4.3 Level meter 51
4.4 Flow meter 52
4.5 Mercury concentration in the air 52

5 Design of the loop 53
5.1 Dimensioning of the tubes 53
5.2 Flange 55
5.3 Compensation of thermal expansion 56
5.4 Valves 57
5.5 Design 57
5.6 Operation of the loop 60
5.6.1 Installation of loop 60
5.6.2 Filling of loop 60
5.6.3 Normal operation 60
5.6.4 Draining of loop 60
5.6.5 Emergency shut down 61
5.7 Weight 61
6 Conclusion and future work 62
7 Appendix IX
7.1 Material data IX
7.2 Irradiation data XII
7.3 Tube dimension norm XIV
7.4 Heat exchanger algorithm XV
7.5 DIN 2633 XVIII
7.6 Study of tube S-arrangement XIX
7.7 Implemented matlab code XX
7.8 References XXVII
7.9 Eidesstattliche Erklärung XXIX

Nomenclature

Symbol	Name of quantity	Abridged notation in SI units
c_p	Specific heat capacity at constant pressure	J/kg℃
d	Diameter	m
h	Heat convection coefficient	W/ m^2K
k	Heat conduction coefficient	W/mK
L	Length	m
$\dot{m}$	Mass flow	kg/s
n	Cavitation number	-
Nu	Nusselt number	-
P	Pressure	bar
Pe	Peclet number	-
$\dot{Q}$	Heat flux	MW
r	Radius	m
R	Resistance (convectional)	m℃/W
Re	Reynolds number	-
S_v	Thickness (without safety)	m
T	Temperature	℃
Th	Tickness	m
U	Perimeter	m
V	Volume	m^3

w	Stream velocity	m/s
η	Dynamic viscosity	Pa s
ς	Pressure loss coefficient (coefficient of fluid resistance)	-
λ	Friction coefficient	-
ρ	Density	kg/m^3

Subscripts

0	Zero (reference value)
f	Fouling (e.g. fouling resistance)
h	Hydraulic (e.g. hydraulic diameter)
i	Inner (e.g. inner diameter)
in	Value at influx (e.g. influx velocity)
lm	Log mean (log mean temperature)
o	Outer (e.g. outer diameter)
out	Value at outflux (e.g. outflux velocity)
s	Shell (shell of tube and shell heat exchanger)
t	Tube (e.g. Tube thickness)
tb	Tube boundle (e.g. diameter of a bundle of tubes)
tot	Total (e.g. total friction loss coefficient)
tp	Tube pitch (e.g. length of tube pitch)

Abbreviations

CERN	Conseil Européen pour la Recherche Nucléaire
ESS	European Spallation Source
ISOL	Isotope-separation-on-line
LBE	Lead-bismuth eutectic
PSI	Paul Scherrer Institut
RIB	Radioactive ion beam
SINQ	Swiss Spallation Neutron Source
SLS	Swiss Light Source
SNS	Spallation Neutron Source
SYN	Research department of “Synchrotron, Radiation and Nanotechnology” at PSI

List of figures

Figure 1: Nuclei interactions [Cern summer school] 1
Figure 2: Isotopes produced by neutrons hitting lead 1
Figure 3: Proton source and Cockcroft-Walton accelerator at PSI 3
Figure 4: C-W cascade Generator [Wille] 3
Figure 5: Classical cyclotron 4
Figure 6: PSI ring cyclotron (Isocyclotron) 6
Figure 7: Principle of SINQ 7
Figure 8: SINQ target station 8
Figure 9: lead target 8
Figure 10: Image of a camera (neutron radiography left, X-ray radiograohy right) 9
Figure 11: Neutron radiography (engine) 9
Figure 12: Neuron radiography (Car heat exchanger) 9
Figure 13: PSI proton accelerators and experimental facilities 10
Figure 14: ISOL compared to In-Flight 12
Figure 15: Sketch of the target system 13
Figure 16: Schema of loop 16
Figure 17: Scheme of dose rate calculations 19
Figure 18: Total flux of gamma ray during build up (4mA proton beam) 20
Figure 19: Neutron flux depending on length of shielding 22
Figure 20: Photon rate and energy (left), dose rate (right) 22
Figure 21: Dose rate after 1m air gap 23
Figure 22: Model of drain tank 23
Figure 23: Decay heat 24
Figure 24: Dependency lambda of Re [Wagner, p.77] 27
Figure 25: Pressure in elbow 29
Figure 26: Dependencies of loop parameters 31
Figure 27: Drawing of a seal-less driven impeller pump 33
Figure 28: Removal of heat in a seal-les driven impeller pump 33
Figure 29: Saftey problem of seal-less driven impeller pumps 34
Figure 30: Cut through a cylindrical PMP 35
Figure 31: Cut through a disc type PMP 35
Figure 32: Model 36
Figure 33: Stress in x-direction 36
Figure 34: Sketch of an flat EMP (left) and an annular EMP (rigth) 37
Figure 35:Von mises stress (EMP1) 37

Figure 36: Z-Stress (EMP1) 37
Figure 37: EMP2 (left: von Mises stress, right Z-sttress) 38
Figure 38: Outlet temperatures (lay-out 1, 2 and 3) 43
Figure 39: Draft 2 of expansion tank/gas separator 45
Figure 40: Draft 2 of expansion tank/gas separator 46
Figure 41: Natural convecion for drain tank cooling 48
Figure 42: Thermocouples tip styles 50
Figure 43: Elbow 54
Figure 44: Tee 54
Figure 45: Flange, static case (left: von der Mises stress, right: z-stress; in MPa) 55
Figure 46: Flange, transient case (left: von der Mises stress, rigth: z-stress; in MPa) 56
Figure 47: Von Mises stress for tubes (S-arrangent) 57
Figure 48: Draft 1 of the loop 58
Figure 49: Draft 2 of the loop 59

List of tables

Table 1: Data for Injector 2 and Ring Cyclotron 6
Table 2: Elements and isotopes, which should be filtered 18
Table 3: Filtering methods 18
Table 4: Parameters for Orihet calculations 20
Table 5: Produced gas 21
Table 6: Some produced elements 21
Table 7: Dose rates (50cm behind shielding) 24
Table 8: Pressure drops in loop 28
Table 9: Main lay-out parameters of the loop 30
Table 10: Parameters of EMP draft (IPUL) 38
Table 11: Stresses of EMP draft 2, depending on ribs 38
Table 12: Parameters of Oak Ridge heat exchanger 42
Table 13: Main parameters of compared heat exchangers 42
Table 14: Resistance of the lay-outs 43
Table 15: Tube pitches of lay outs 44
Table 16: Cover gas pressure in draft 1 after 1l mercury leakage, depending on initial pressure (all values in bar) 45
Table 17: Cover gas pressure in draft 2 after 1l mercury leakage, depending on initial pressure (all values in bar) 46
Table 18: Thermocouples of Thermocoax 50
Table 19: Weight of loop (in tons) 61
Table 20: Mercury data IX
Table 21: Boiling temperatures of mercury: IX
Table 22: Vapour pressure of mercury X
Table 23: Water data XI
Table 24: Young's modulus of 316L stainless steel (interpolation allowed) XI
Table 25: Linear thermal expansion coefficient (316L) XI
Table 26: Poisson coefficient (316L) XI
Table 27: Thermal conductivity (316L) XII
Table 28: Density and specific heat (316L) XII
Table 29: Decay heat (after 200d build up) XII
Table 30: Gamma spectrum (short term) XIII
Table 31: Gamma spectrum (long term) XIII
Table 32: Excerpt of DIN V EN V 10 220 (2) XIV
Table 33: Study of tube S-arrangement XIX

1 Introduction

This diploma thesis was carried out at the Paul Scherrer Institut (PSI), Switzerland. The research institute was founded in the 1960s with a focus on nuclear energy. Since then, PSI has extended the scope of its activities into new fields such as life sciences, astronomy, and renewable energy amongst others. Nuclear physics still plays a large role at the institute and this thesis was placed under the auspices of the department "Condensed Matter Research with Neutrons and Muons (NUM)".

The subject of the thesis deals with the design of supply devices of a new, more powerful spallation source. Spallation refers in this context to the spallation of an atomic nucleus. In general, this is achieved by accelerating a species of particles, in our case protons, which then hit a target material, whereby the nuclei are split. Depending on the material of the target, it emits different amount of neutrons, protons, alpha, beta and gamma rays. The emitted protons can cause further spallation, so called delayed spallation.

There are three kinds of hit processes. They can be distinguished by the type of nuclei division. In addition to spallation, there exist fragmentation and fission. The fragmentation process causes a smaller and a bigger nucleus while, during fission, two similar big nuclei are produced. An example with an incoming proton beam hitting an ^{238}U nucleus is drawn in figure 1. Figure 2 shows the produced isotopes when lead is hit by fast neutrons.

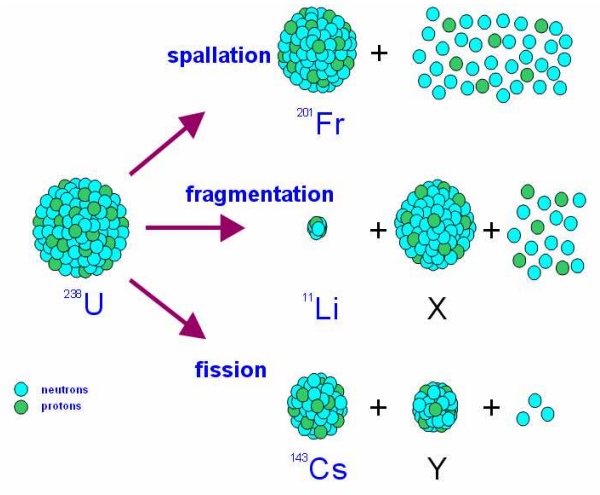

Figure 1: Nuclei interactions [Cern summer school]

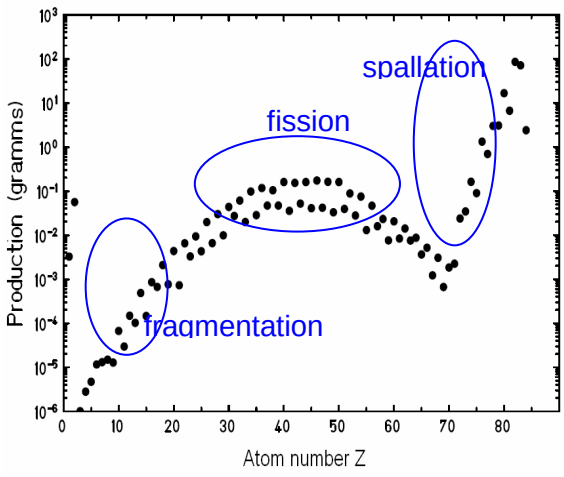

Figure 2: Isotopes produced by neutrons hitting lead

Within these examples, the hit nuclei (in this case ^{238}U or lead, respectively) form a so called target. The new planed spallation source shall use accelerated protons as "source" particles. As target material, mercury is foreseen amongst other materials. The name of the overall project is EURISOL DS.

1.1 Existing structures at PSI

The aim of this chapter is to give an idea of existing atomphyisics/nuclearphyisics research centres. They are located in Europe, North America and Japan. One of the most popular is CERN, in Geneva. Of course, all of these institutes differ from each other, both in their research scope as well as in applied devices. However, there are some devices which can be found in every institute. These include a source of the particles, that should be accelerated; accelerators; a target and some experimental devices. In the following some existing devices at PSI should be introduced. This should help the reader to get a first impression of this kind of research.

1.1.1 Particle source

Particles must be charged, as they are accelerated in electric fields. At PSI, facilities for electron and proton acceleration exist. The facility for electrons (SLS) will not be examined within this thesis.

To extract positive ions, one needs plasma, which is (partly) ionized gas. The plasma is generated by additive electrons with high kinetic energy. There are different methods for producing these fast electrons. These free electrons impact on the bound electrons of a source material and are released. The following relation illustrates the process, whereas A stands for an arbitrary atom (source).

$$e^- + A \rightarrow 2e^- + A^+$$

Hydrogen plasma is used for extracting protons at PSI. The hydrogen is filled in a tank which is connected to an extraction voltage source (60kV). In addition, there is a Cockcroft-Walton pre-accelerator (810kV). The ionisation inside the tank is done by free electrons of a filament. The emitted beam is focused by a solenoid. Figure 2 shows the Cockcroft-Walton accelerator on the left side and the proton source on the right side. The hydrogen tank has a volume of roughly 1 litre, lies inside the visible cave and has a hydrogen supply. The consumption of hydrogen is very low. The black pylons are electrical isolators. Also, the connection between Cockcraft-Walton accelerator and cave is made of very poor conductive material; hence, high voltage from the accelerator top is transferred to the surface of the cave at very low current. Within the spiral structure, lies the acceleration gap. The left part is loaded with 810kV, the right part is earthed. The shape of the metallic spiral helps to create a smooth electrical field in the direction of acceleration within the gap. The gap is filled with sulphur hexafluoride (SF_6), which is a very good isolator and reduces the risk of sparkovers.

Cockraft-Walton accelerator:

As the Cockroft-Walton accelerator is directly linked with the proton source, it shall be discussed shortly within this chapter. Cockcroft-Walton accelerators are electrostatic accelerators. The danger of sparkovers prohibited high voltages before Cockcraft and Walton invented a new accelerator with a cascade generator in the 1930's. Within several steps, the input voltage is increased. This first type provided 400kV.

C-W generators connect Grainacher circuits in series. A generator supplies sinus voltage. Figure 4 shows three

circuits in series. Each circuit consists of two diodes and two capacitors. Each capacitor conserves either negative or positive voltage and thus, the voltage is doubled with each circuit [Wille].

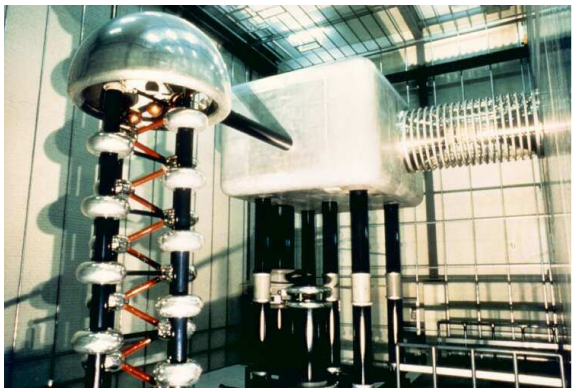

Figure 3: Proton source and Cockcroft-Walton accelerator at PSI

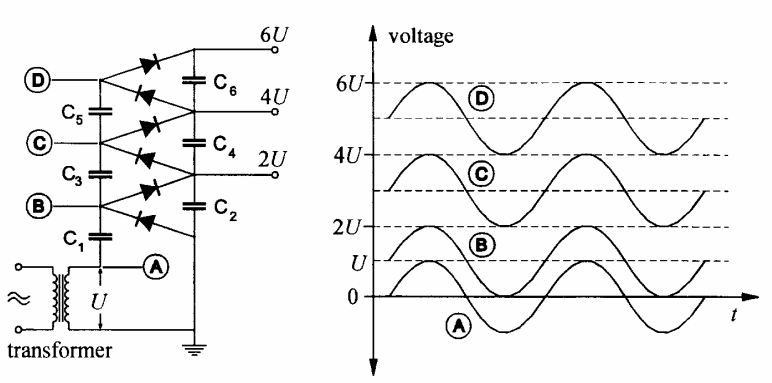

Figure 4: C-W cascade generator [Wille]

Proton beamline and buncher:

The protons are diverted by magnets to hold them on the beamline. The width of the beam coming from C-W accelerator is about 2cm. The beam can be focused or defocused by quadrupols.

The beam at the beginning of the beam line is continuous. For further acceleration with PSI facilities, continuous wave beam is required. This is done by a buncher, which utilizes the "phase focusing effect". The buncher separates the protons into bunches. The time between the bunches and the length of the bunches depend on the accelerators. Bunch width at PSI is 0.3ns and time between two bunches is 19.75ns. The protons are now prepared for acceleration.

1.1.2 Accelerators

Beside the Cockraft-Walton accelerators, there exists a great variety of diverse accelerators. There are two subdivisions of accelerators: one using DC for acceleration, like Cockraft-Walton, and AC accelerators. Except the Cockraft-Walton accelerators, PSI proton accelerators use AC. A good introduction to accelerators is given by [Wille] and [Hinterberger].

Protons from the Cockcroft-Walton accelerator are led to a second accelerator, the so called Injector 2. It is called "injector" because it accelerates the protons to a defined energy, and with that energy, they are injected into a third accelerator (called Ring Cyclotron), which accelerates the protons to the desired final energy. PSI has also an Injector 1, that operates independent of Injector 2 and the Cockroft-Walton accelerator. Injector 1 shall not be discussed. The partitioning of the acceleration into diverse accelerators is due to the fact that accelerators have only a certain acceleration energy range. Both Injector 2 and Ring Cyclotron are Isocyclotrons. The parameters of these two PSI cyclotrons are shown in table 1 at the end of this paragraph.

There are three types of Cyclotrons: classical cyclotron, synchrocyclotron and isocyclotron. All of them accelerate the ions in a ring shape to save space compared to a linear accelerator (LINAC) which accelerates the ions on a straight line. The latter two are further developments of the classical cyclotron. Accordingly, classical Cyclotron is explained first.

Classical cyclotron:

The ions are accelerated within an electric field produced by cavities, which are connected to a high frequency (sinus) generator. As the ions are accelerated by a high frequency field, the beam is pulsed. They are focused in the longitudinal way by an effect called "phase focusing". Therefore, so called bunches of ions are produced. This type of beam is called continuous wave. Synchrocyclotrons (amongst others) produce a so called "pulsed beam", as the time between the bunches is much bigger.

The ion beam is led on its circular path by magnetic fields. These are produced in a very common way by coils and magnetic yokes. The acceleration of the ion beam starts in the middle and the ion path travels outward in a helical (in a plane). Either an ion source is in the middle of the cyclotron or the ion beam is led from outside into the middle. In this case, the injected beam has to be pulsed, and furthermore, to be adjusted in such a way that it does not hit one of the accelerated bunches. Figure 5 shows the sketch of a classical cyclotron. The cavities are called "Dee" because of their form.

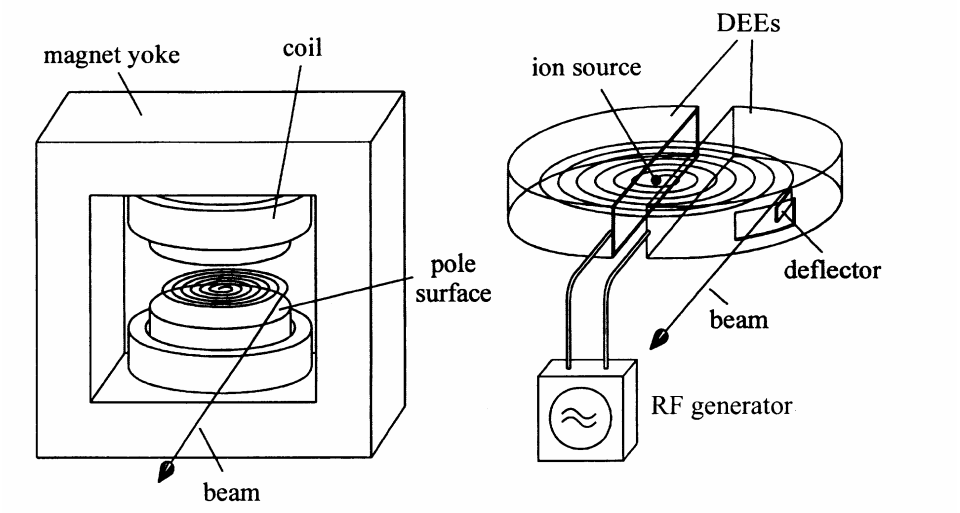

Figure 5: Classical cyclotron [Wille]

The ions in the middle are accelerated by the electrical field. There are mechanic filters which secure that only those ions with the maximal energy increase come to the circular acceleration path. These arrive in the magnetic field and are led in a circuit back to the gap between the Dees. Meanwhile, the polarity of the electrical field is reversed and the ion bunch is once more accelerated in the gap. After being deflected once more by the magnetic field the bunch reaches the point of the first accelerations this time a little bit further outside the middle. So there are two accelerations per revolution. The revolution frequency has to be equal to the frequency of the electrical field (or has to be k times higher, where k is a natural number) to ensure maximal acceleration in between the gaps. The revolution frequency (also called "cyclotron frequency"), ω_{cyc}, can be determined by the equation of

motion and the law of Lorentz (formula 1 for non relativistic calculations). Formula (2) describes the electrical side. The generator frequency, ω_{gen}, is fixed at all times and invokes proportionally the frequency of the electric field, ω_e, between the gaps.

$$\omega_{cyclotron} = \frac{1}{2\pi} \cdot \frac{qB}{m} \qquad (1)$$

$$U = U_0 \cdot \sin \omega_{gen} \quad \propto \omega_e \qquad (2)$$

The maximal acceleration of protons in a classical cyclotron was 22MeV. The cyclotron was located in Oak Ridge (USA) and had a diameter of 2.18m. The number of revolutions inside the cyclotron was 50.

The main problem of the classical cyclotron occurs when relativistic velocities of the ions shall be reached. Relativistic mass increases with speed and, therefore, the cyclotron frequency, ω_{cyc}, gets lower; as one can see in formula (1). The cyclotron frequency, ω_{cyc}, and the frequency of the electric field are not synchronous anymore. There exist two solutions of that problem, the synchrocyclotron and the isocyclotron. Cyclotrons are not used anymore.

Synchrocyclotron:

The synchrocyclotron supply lower frequencies of the electrical field, ω_e, in the outer regions of the cyclotron. In that way, both frequencies are synchronised again. This is achived by changing the resonance frequency of the cavity. Therefore, the shape of the cavity is deformed a little bit. These cyclotrons were built mainly in the 1950's with energies for protons between 50-800MeV. As the cyclotron frequency, ω_{cyc}, is not constant only one bunch can be accelerated at each time ("pulsed beam"). Otherwise, an injected bunch would collide with an accelerated one. The maximal pulse rate of a synchrocyclotron was 300Hz (Los Alamos). Unfortunately, the result is a very low current of the beamline. Isocyclotrons do not have this disadvantage. Nowadays, all synchrocyclotrons are out of use.

Isocyclotron:

This cyclotron holds the cyclotron frequency, ω_{cyc}, stable by increasing the magnetic field with higher mass (see formula 1). The increase of the magnetic field leads to the defocusing of bunches in axial direction. The defocusing problem was solved through the use of focusing magnets (quadrupols) which were combined in an alternating arrangement of focusing and defocusing quadrupols. This is called "edge focusing". The beam of isocyclotrons is of high quality and provides high current. Isocyclotrons reach energies for protons up to 600MeV. Figure 6 shows an existing accelerator at PSI, an isocyclotron. The grey boxes are cavities, the green are magnets.

Figure 6: PSI ring cyclotron (Isocyclotron)

	Injector 2	Ring Cyclotron
Injection Energy [MeV]	0.870	72
Extraction Energy [MeV]	72	590
Number of revolutions	100	Ca. 200
Beam Current [mA, DC]	1.85	1.6
Accelerator Frequency [MHz]	50.633	50.633
Time Between Pulses [ns]	19.75	19.75
Bunch Width [ns]	Ca. 0.3	Ca. 0.3

Table 1: Parameters of Injector 2 and Ring Cyclotron

1.1.3 Target (SINQ)

There are several targets at PSI. The first (thin) targets of the beam line (Target M, Target E) are pion production targets. Proton energy is thereby lowered from 590MeV to 570MeV. Part of the beam is also led to further experimental facilities. The proton beam arrives at the final target with a current of 1.3mA (at 570MeV this results to 0.75MW). The target material is lead. The target is embedded in the SINQ (SINQ – "Swiss Spallation Neutron Source") target station. First, the target station will be shortly presented, then the target.

Target station

The proton beam enters the target station from below, this maximizes the space available for experimental devices which are located horizontally around the target. The whole target station is enclosured by a massive shielding block (concrete and steel). The proton beam spallates lead nuclei. Result is, amongst others, emitted neutrons and heat production. Therefore, the target is connected to a cooling loop.

The target is surrounded by two types of moderators. Moderators lower the kinetic energy (to a "feasible" one) of the neutrons due to elastic hits between nuclei. At SINQ D_2O is a standard moderator resulting in "thermal

neutrons" of 25-50MeV (2187m/s-3093m/s). D_2 decreases the kinetic energy of the neutrons to 1-5MeV (437m/s-978m/s). These neutrons are called "cold neutrons". Depending on the experiment, neutrons with higher or lower energy are advantageous. Two experimental facilities will be presented in chapter 1.1.4.

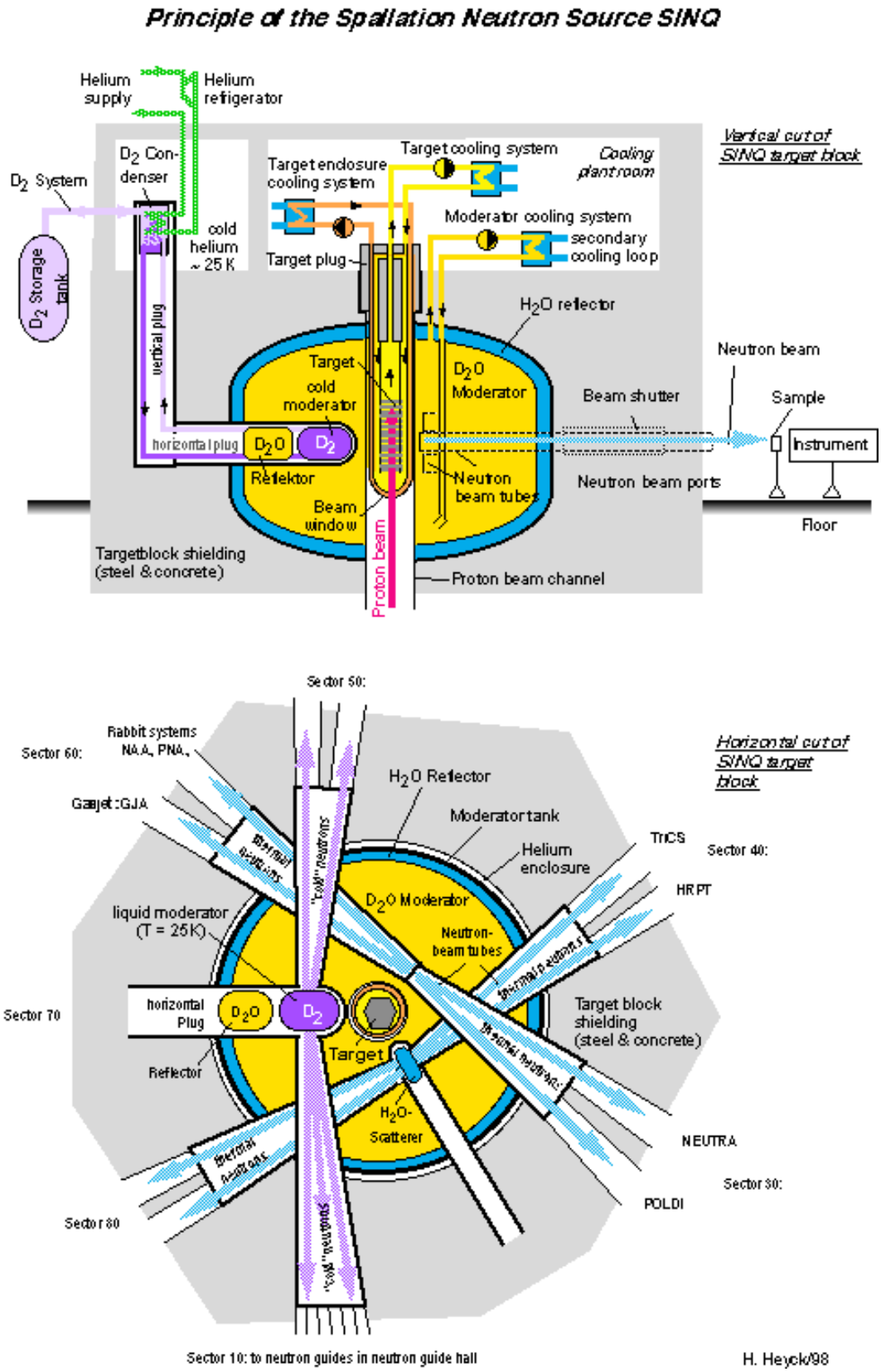

Figure 7: Principle of SINQ

Target

The target consists of several hundreds of lead rods. They are welded on a hexagonal stainless steel mantel. The target is about 50cm long and the diameter is about 10cm. It is cooled by heavy water (target cooling system). Water and beam travel longitudinal through the target. From September to December 2006 the shown solid target (figure 9) was replaced by a liquid metal target (Megapie project).

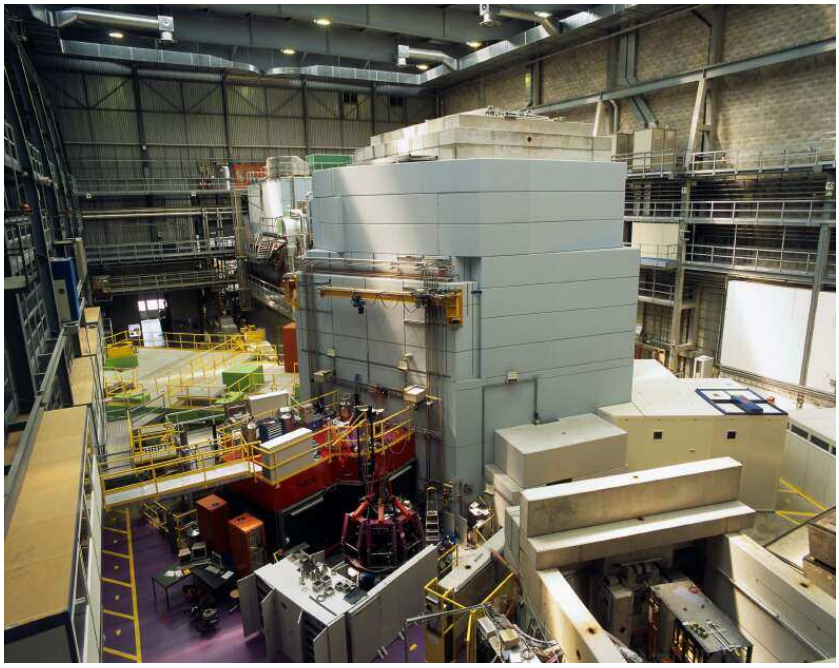

Figure 8: SINQ target station

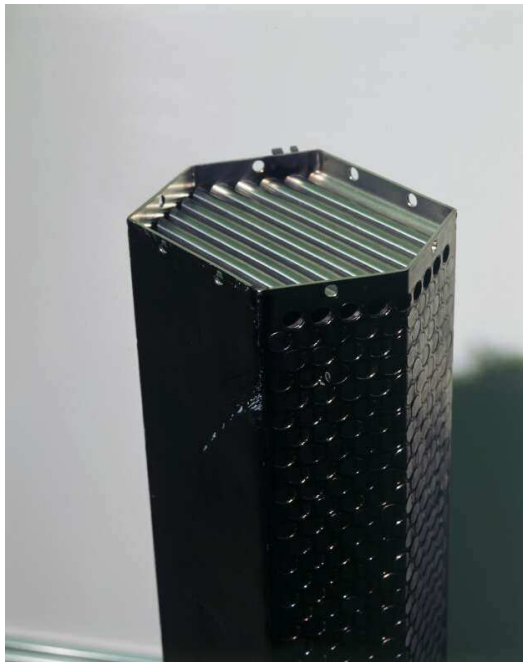

Figure 9: lead target

1.1.4 Experimental devices

There is a huge variety of experimental devices at the end of the beam line. These devices depend, of course, on the facilities producing the beam line. With higher research demands and further developed experimental applications new facilities are necessary. Two very practical applications at SINQ are presented below. Both use the thermal neutron flux from SINQ.

Neutron transmission radiography (Neutra)

The neutrons are bundled by a collimator inside Neutra. This beam then penetrates an object. The neurons interact with the object materials (absorption, scattering, refraction). A detector behind the object registers the incoming neurons. The detector provides a 2-dimensional image. Real time imaging and 3-d images are also possible at Neutra facility.

Whereas x-rays interact mainly with heavy materials (e.g. lead shielding at medicinal x-ray), neutrons interact well with lighter materials. Therefore, it is a very interesting method for looking inside technical devices such as engines. Figure 10 illustrates the difference between x-ray and neutron radiography. The investigated object is a

camera. Neutrons interact mainly with the plastic, x-rays with the metal. In figure 11 one can see inside an engine with neutron radiography. Experiments from car companies were carried out at PSI.

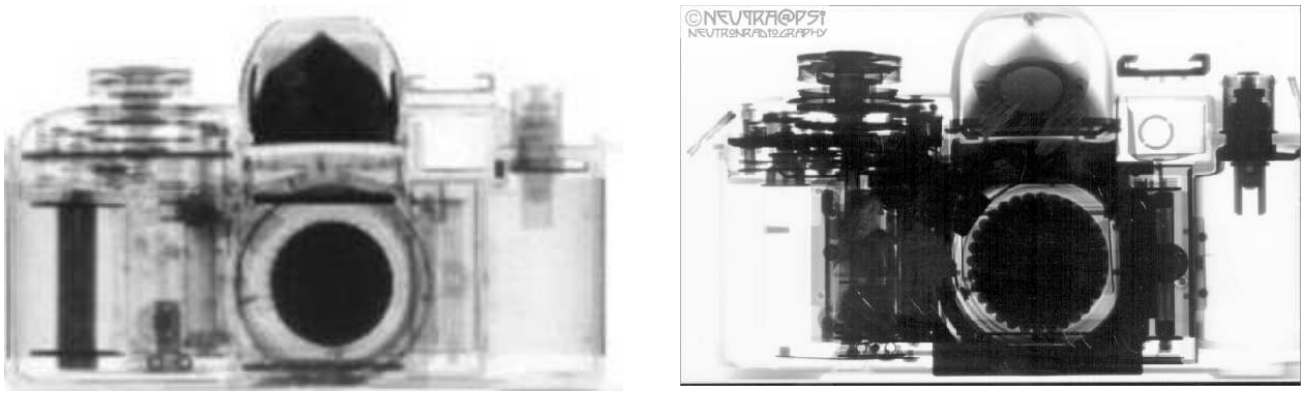

Figure 10: Image of a camera (neutron radiography left, X-ray radiograohy right)

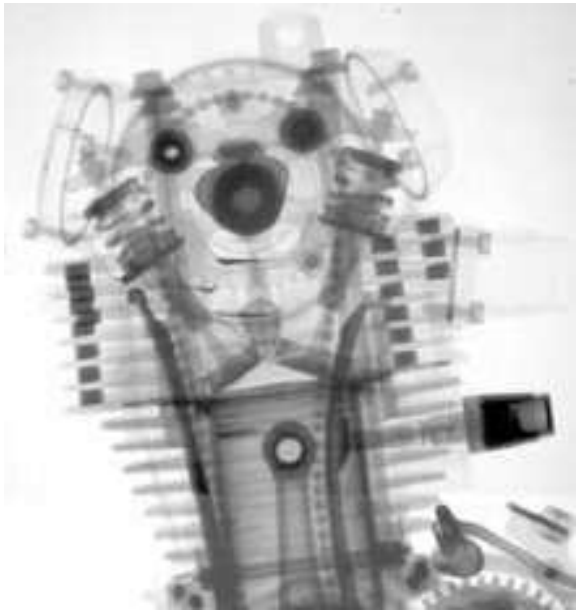

Figure 11: Neutron radiography (engine)

Figure 12: Neuron radiography (Car heat exchanger)

Production of isotopes (PNA)

At SINQ special isotopes can be produced. This is carried out at PNA ("Präperative Neutronenaktivierung"). The assay is put into a fused glas ampul which is then given into an aluminum container (6cm length, diameter 2cm). The container is transported by a helium pneumatic delivery system to the beam position. There the assay is irradiated from two minutes up to one week, depending on the material.

Isotopes produced in this fashion are delivered to research institutes, universities, hospitals and the industry. These isotopes are used mainly as tracers. For example, Br-83 is used to follow radioactive flow in rock. Producing isotopes is also one of the tasks of the Eurisol facility. With higher beam power it is possible to produce very rare isotopes.

1.1.5 Schematic overview

The overview of PSI proton accelerators and the adjacent experimental hall facilities are illustrated in figure 13. PSI also has an electron accelerator with an experimental hall, the so called Swiss Light Source (SLS). This shall not be discussed within this thesis. Thanks to the dimensioning axis, one can get a feeling of the overall size of the facilities.

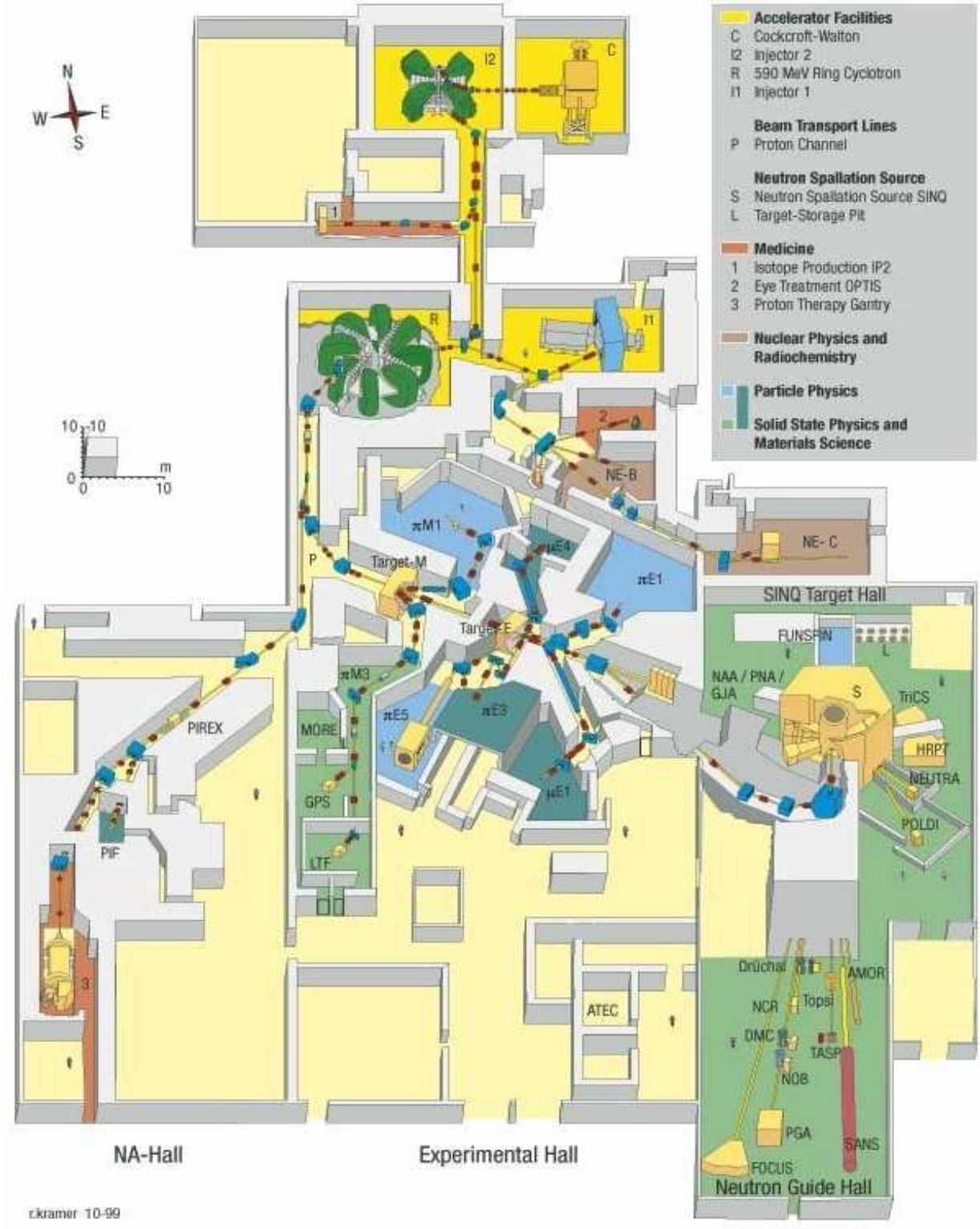

Figure 13: PSI proton accelerators and experimental facilities

The proton beam is not only used for SINQ but also directly for experiments and medical application, e.g. eye treating. Persons with eye cancer are treated in a special laboratory. The proton beam has excellent properties for tackling cancer, it can be focused very exactly on the cancer area and destroy it without damaging other regions.

1.2 Usage of spallation sources

Beside the two given examples in 1.1.4, spallation sources have many uses. They can help to carry out experiments in the following research fields:

- Nuclear structures in extremely small ranges
- Nuclear astrophysics and nucleosynthesis
- Fundamental interactions and symmetry laws.

As isotopes can be created with unusual properties (e.g. spin or total angular momentum), new information on special nuclear structures can be found, as well as information on atomic interactions relevant to astrophysics. For a better understanding of the universe, a greater knowledge of such interactions is important because "almost all elements have been produced through nuclear reactions taking place in stars or during explosive stellar events". [Eusisol_a, p.14] Further research work can be done on fundamental interactions theory, which could use measurements of β-decay; Solid-State-Physics; or Medical Applications as well [Eurisol b, p.11ff]. In addition, neutrons have some interesting properties (e.g. wave length about 1 to 10 Angstrom) which can be very useful in material science.

1.3 History and plans of EURISOL DS

The main aim of Eurisol DS is to produce and investigate radioactive ion beams (RIB), consisting of interesting isotopes. First of all, there are two very important methods of producing RIBs. Fundamentally, in the ISOL method, small particles (like protons) hit a thick target with material of a high mass number. On the other hand, in the In-Flight method, a heavy ion beam hits a thin target. Both methods have their advantages. The ISOL method produces RIBs with relatively long half-lives (larger than 1ms) and of a very good quality over a wide range of energy. "The In-Flight method allows one to produce RIBs with very short half-lives, down to a few hundreds of nanoseconds" , but of a poor quality [Eurisol_a, p.18]. Figure 1 presents schematically the two methods. It should be mentioned that one can obtain RIBs also with other methods, such as chemical separators.

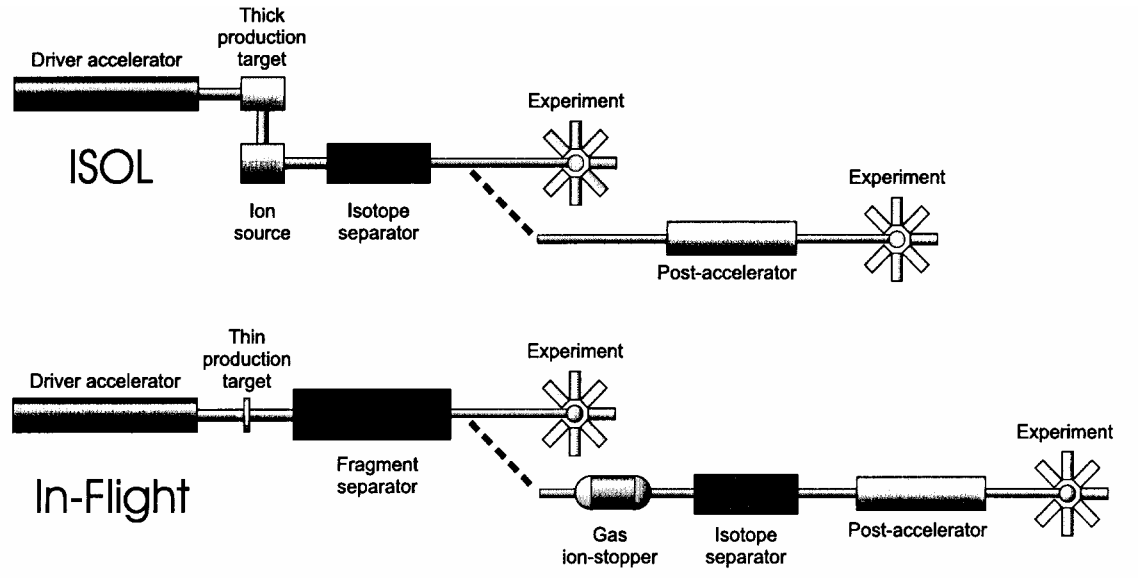

Figure 14: ISOL compared to In-Flight

The so called „Nuclear Physics European Collaboration Committee“ (NuPECC) started discussions on the demand for a new RIB source in a report entitled "Nuclear Physics in Europe: Highlights and Opportunities" (1997). A study group was founded which concluded in supporting new facilities of both types. The result was a proposal for a major upgrade of an existing, In-Flight version in Darmstadt, Germany (at the Gesellschaft für schwere Ionen Forschung GSI) and the start of the Eurisol program. The initial phase of the Eurisol program started on January 1, 2000 and finished in 2003 with a primary study for a new ISOL source in Europe. After Eurisol, Eurisol DS ("Eurisol Design Studies") was officially started on February 1, 2005. Eurisol DS aims to finish the existing initial work on the design of a new ISOL source, which could be built within the next decade.

The first decision was to identify the process to produce RIBs. To increase the range of possible RIBs, Eurisol will have two "production lines". "The proposed ISOL facility would use both (a) 100-kW proton beams on a thick solid target to produce RIBs directly, and (b) a 'converter' target to release high fluxes of spallation neutrons which would then produce RIBs by fission in a secondary target." A 1-GeV linear proton accelerator was chosen as the driver accelerator, although it was also considered for accelerating heavy ions. [Eurisol_a, p.5].

The aim of that spallation source (converter target) is to emit neutrons which hit another target, the so called fission target (with an ion source inside). In this second target, the neutrons cause a further reaction of the nuclei so that it emits uncommon isotopes as RIBs which are sought after for analysis.

The converter target consists of liquid metal. The flowing liquid metal can remove the deposited heat during spallation. In comparison to solid metals no cooling system at the target is required. Liquid metal targets can provide high neutron flux as no cooling fluid occupies spallation space (see figure 15). Additionally, direct contamination of the coolant, mostly water, is avoided. This thesis deals with the supply devices for the required liquid metal loop.

The choice of the target material influences the emission rate of neutrons immensely. The higher the mass number of the material, the more neutrons can be emitted when impacted by a proton. Other motives, like operational costs or dose rates, influence the choice of the target material as well. The Eurisol project team came to the decision to take mercury as the baseline for the target material. The main advantage of mercury for the loop lay out is that it is liquid at room temperature and therefore no heaters are necessary. Figure 15 shows a preliminary sketch of this two target system.

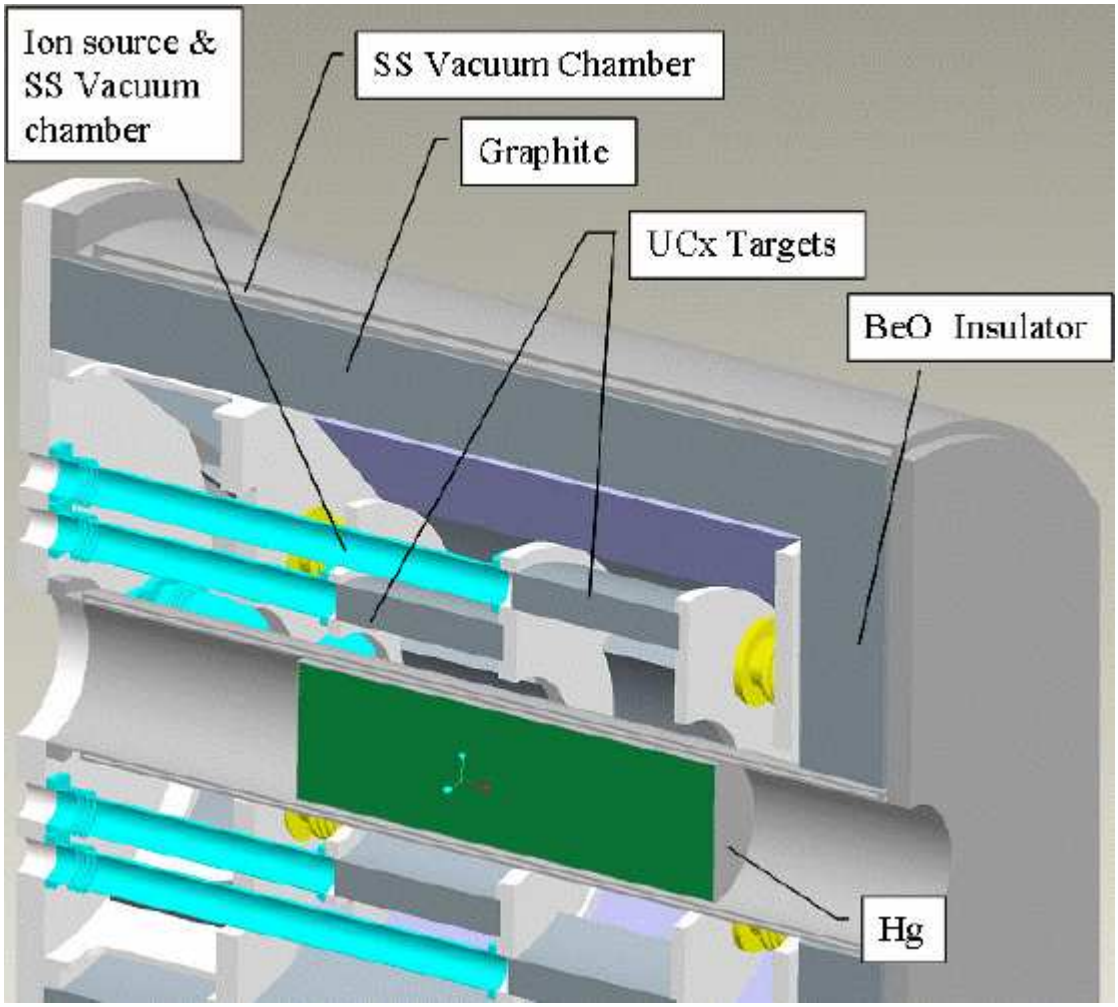

Figure 15: Sketch of the target system

To sum up, a short overview should be given. The protons are accelerated in a linear accelerator (1GeV, 4MW). They then enter the target station through a special window, after which they impact the target, which is surrounded by the fission target. As the target becomes radio active over time, shielding for the target station is necessary. The target is connected by pipes providing liquid mercury to a so called "hot cell". The hot cell provides space for the mercury loop. Hot cells are rooms built for handling irradiated devices. Such areas must be designed bearing in mind that mercury is also chemically toxic. Typical tasks including changing the target or small repairs of the loop should be carried out while remaining behind the hot cell containment wall, and using manipulators. Therefore, it is planed to assemble the target and the loop on a large trolley to be able to roll it from the beam position to the maintenance position.

This kind of research field is highly expensive. As with most nuclear research projects, there exists a network of institutes and universities that work closely together to contain costs. The Eurisol DS project is co-financed by the European Union and is divided in twelve so-called "tasks". Approximately six partners are working on each of these tasks. The tasks range from management (task 1) to more specialised aspects such as the beta beam (task 12). The area of more immediate concern to PSI, and hence the focus of this thesis, is Task 2, named "Multi-MW-Target Station", which also deals with the converter and fission target.

A basic concept for a 5MW spallation source with liquid metal was laid out in the course of a previous project, the "European Spallation Source (ESS)". The decision of the European Science Ministers in 2003 was made to cancel the project. Despite some differences between that particular project and Eurisol DS, ESS can provide useful information as a basis for this thesis.

2 Outline of the loop

Within this chapter the requirements of the planed loop are defined and an overview is given. Then, the basic calculations, which are necessary for the dimensioning of the loop, are carried out. At the end, all important parameters are summarized in table 9. The table also includes parameters, which are calculated in the following chapters. This table includes all significant values of the loop lay out. Additionally, a sketch of the dependencies of the main parameters can be found. Written matlab files can be found on the attached CD, as well as simulations with ANSYS, lay-out done with IDEAS and important documents.

2.1 Basic requirements

Lifetime

The planed EURISOL facility is very expansive. Building costs were estimated at 613 M€, give or take 20%, the operational costs at 60-65 M€ [Eurisol_a, chapter 8 and 9]. Due to these investment costs, a long life time should be secured. It is assumed that Eurisol will be competitive with future ISOL sources for 20 years. Therefore, the life time of the main devices (except target) is assumed to be 20 years, too. Measurement devices can have a shorter life time and have to be installed in such a way that one can replace them. Estimating life times of the devices under the given operational circumstances is difficult, as little comparable data exists. SNS, a spallation neutron source in Oak Ridge, USA, which was completed in May 2006, could provide information.

As the mercury, and therefore also the devices, are contaminated the exchange of defect parts of the loop is difficult. Because of that, the concept of the loop should secure the long life of all devices. Complex structures should be avoided. Furthermore, as much devices as possible should be connected together by welding to minimize the risk of leakage.

Overview

The main devices of the loop are: pump, heat exchanger and gas separator/expansion tank. The target is, of course, also part of the loop, but will not be studied within this thesis. The design of a conventional flow channel of the target is being carried out at PSI and will probably be finished in February 2007. This target is the reference target. Moreover, IPUL in Riga is currently designing an innovative cross flow target, which could be used instead of the reference target, if it is proved to be advantageous. The loop lay-out in this thesis was created for the reference target.

Within the target, the mercury is heated during radiation. The heat is removed by the mercury itself (no additional cooling), and therefore a pump and a heat exchanger are necessary.

The expansion tank provides space for the thermal expansion of the mercury. This tank is placed on the highest point in the loop. Due to the risk of cavitation inside the target (velocities up to 10m/s), additional static pressure has to be provided. This is achieved by pressurizing the cover gas inside the expansion tank. The separator separates gases, which are produced during the irradiation. A standard gas separator can work simultaneously as an expansion tank.

Furthermore, some kind of filters for separating isotopes could be built in. Possible locations for the filters could be (amongst others) behind the target, inside the expansion tank/gas separator and inside the branch near the pump. A drain tank is placed under the loop. The loop can be drained by opening valves in the supply tube, as it is built declining/inclining (no additional pressure for draining). The mercury becomes irradiated when the proton beam is on. The dose rate in the target area is very high, and therefore a shielding surrounding the target is required (Shielding I). Shielding II protects the hot cell from the decay dose, when the mercury has been drained into the drain tank.

To remove the heat from the loop as soon as possible, the heat exchanger is located after the target. This causes heat tension problems in only a few parts of the tube circuit. Moreover, the chosen pump works more efficiently with colder liquid metal. Water is strongly recommended as cooling fluid. It can be delivered from standard main water cooling loop. Figure 16 shows schematically the organization of the loop (it is not a design and more importantly it does not show the height of the loop).

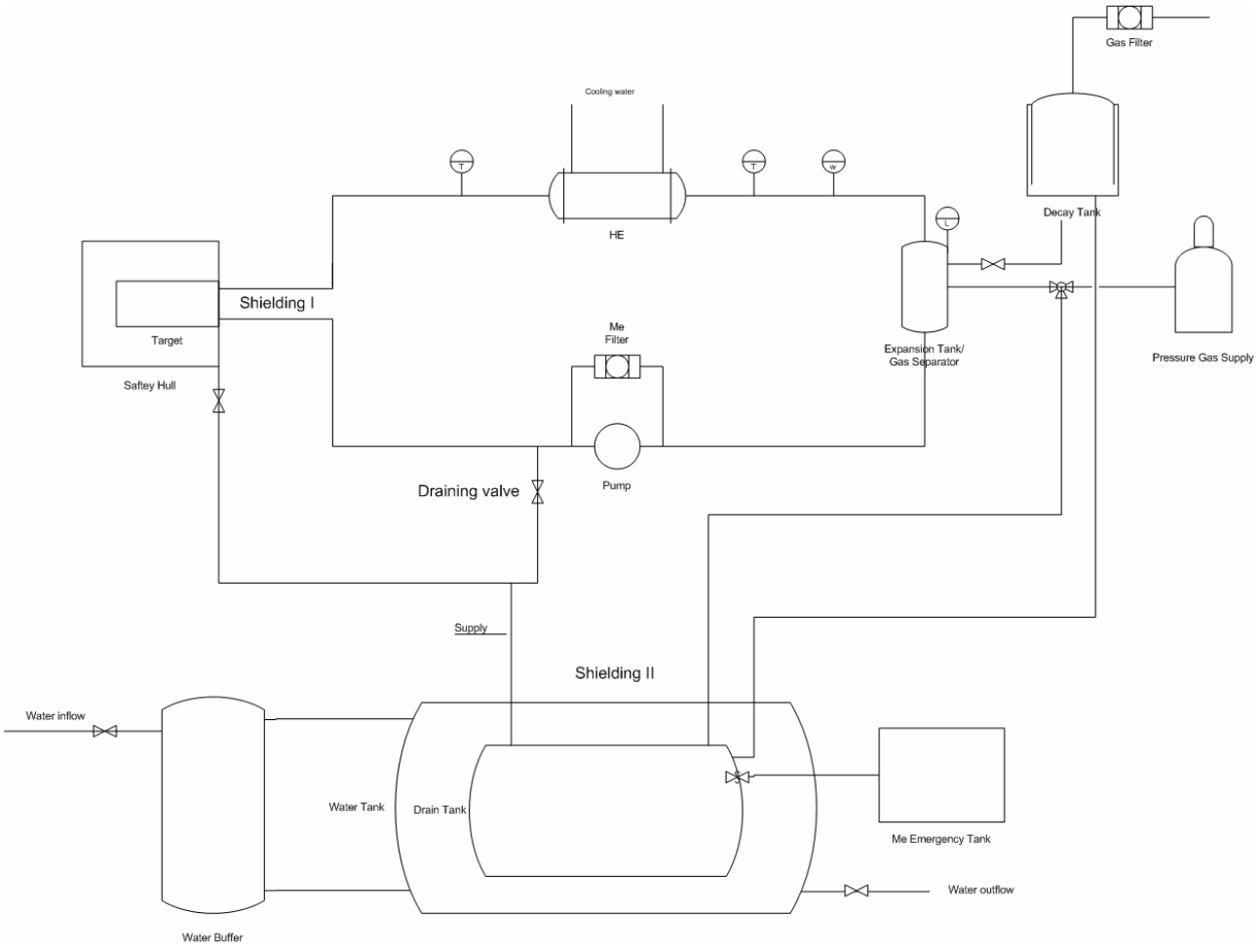

Figure 16: Schema of loop

2.2 Materials

Material data is attached in appendix (see 7.3). The materials of the loop are damaged mainly by neutrons and gamma ray.

Mercury

Mercury is the only common liquid metal at room temperature. It is a rather poor heat conductor (in comparison with other metals) and a fair conductor of electricity. It easily forms alloys with many metals, such as gold, silver and tin, which are called amalgams. The atomic mass is 200.59u.

Mercury is highly toxic. It can enter the body through the lungs, through the skin and via the digestive system. Crucial point (also for the hot cell) is mercury absorbed in the lungs. It is difficult to acquire dangerous amounts of mercury by the other routes (especially under the circumstances when entering the hot cell). Mercury in the blood has a half-life time of three days, but tissue mercury of about 90 days. The toxic limit for mercury vapour in air is 0.1mg/m^3 (for 15min exposure 0.4mg/m^3) [Merck]. Vapour pressure data of mercury is also attached in the appendix. With the help of this data and the ideal gas equation, the maximal concentration in the hot cell in case of leakage can be calculated and ranges from 5.6 mg/m^3 (10°C) to 30mg/m^3 (30°C).

Steel

The tubes, expansion tank and the pump channel are made of 316L standard stainless steel. It is very radiation resistant. As material for the heat exchanger is also foreseen 316L. However, design and thermo hydraulic analysis for the heat exchanger has still to be carried out, and different steel could also be used, e.g. T91.

Compatibility of 316L steel with flowing mercury was tested at Oak Ridge National Laboratory [OakRidge_b, see CD]. The conditions were very similar to the Eurisol loop. Main results are:

- "the compatibility of type 316L/316LN stainless steel does not depend significantly on liquid metal velocity in the range of 1m/min to 1m/s"
- Under 250°C there are no indications of corrosion (no change of weight, appearance or microstructure of tested spicesmen)

It has to be mentioned, that the exposure time of the steel specimen was maximal 1000h. Furthermore the pressure in the Eurisol loop is probably higher than at the Oak Ride experiments. Higher pressure could cause better wetting, which could led to higher corrosion. In general, mercury does not wet steel well [Kopiertes Zeug?]. Nevertheless, good compatibility (low corrosion) of steel with mercury is assumed within Eurisol loop, except inside the target.

Cover gas

The study from Zaitudinov recommends Argon as the cover gas (within the expansion tank). Air could increase the corrosion capability of mercury. [Zalavutinov, see CD]

2.3 Filter

It is considered to build filter(s) into the loop. The filter(s) could have two tasks: separating isotopes for further applications (mainly medical) and separating dangerous isotopes. For the second type one has to consider

- Toxicity (in case of an accident, e.g. air crash)
- Safe process of the loop (isotopes damaging the loop over a long term)
- Disposal of irradiated mercury
- Little radiation remaining in the tubes after draining (important for maintenance work)

Studies for Eurisol defined several isotopes as highly toxic several elements to be interested for medical applications [Eurisol_b]. The results are summarized in table 2. The influence of the produced isotopes on steel is low and the safety of the loop is not influenced. The last two points have still to be investigated in detail. First results from SNS indicate that a thin layer of radioactive material remains on the tube surface after draining the loop.

Medical application	Ir, W, Sn, Sr, Ge, Cu, Ti, Si, Al, Mg
Toxic	148-Gd, 172-Hf, 194-Au, 195-Au

Table 2: Elements and isotopes, which should be filtered

Preliminary studies of Dr. Neuhausen (PSI) suggest following separation methods.

Class of nuclides	Type of separation
Gaseous species	Evaporation in gas separator/expansion tank
Dissolved species	Metal absorbers
Hardly soluble elements	Precipitation at a cold surface
Solid particles	Floating: skimming at the gas separator/expansion tank Sedimenting: separation in the drain tank Particles dispersed in the liquid: Filtering in a bypass loop

Table 3: Filtering methods

2.4 Irradiation

The following effects of irradiation in the target have been investigated. Consequences for the lay-out of the loop are quoted in {}.

- Thermal deposit in target {heat exchanger}
- Gas production in target {gas separator/expansion tank}
- Isotope production {filter, gas separator/expansion tank }

- Irradiation from target into hot cell (mainly neutrons through shielding I) {instrumentation, shielding I}
- Short time decay (up to 1 minute) in tubes contaminating hot cell during process {instrumentation}
- Long time decay (up to several days) after shut down in drain tank {drain tank cooling, shielding II, waiting time to enter hot cell}

Not considered are delayed neutrons. In Switzerland the maximal dose rate for workers is limited to 20mS/year.

Simulation of the irradiation process was done at CERN using Fluka. The calculated nuclide inventory is saved in the file "Fluka". This file was imported into Orihet to calculate build up. The build up output file is called "BuildUp". Orihet uses this data for simulating the decay (assumed shut down after 200 days). Orhiet calculations with the same build up were carried out twice, the first time with subsequent calculation of long term decay, the second time with subsequent calculation of short term decay. Accordingly, there is one output file ("ShortDecay") for short time decay, and one output file for long time decay ("LongDecay").

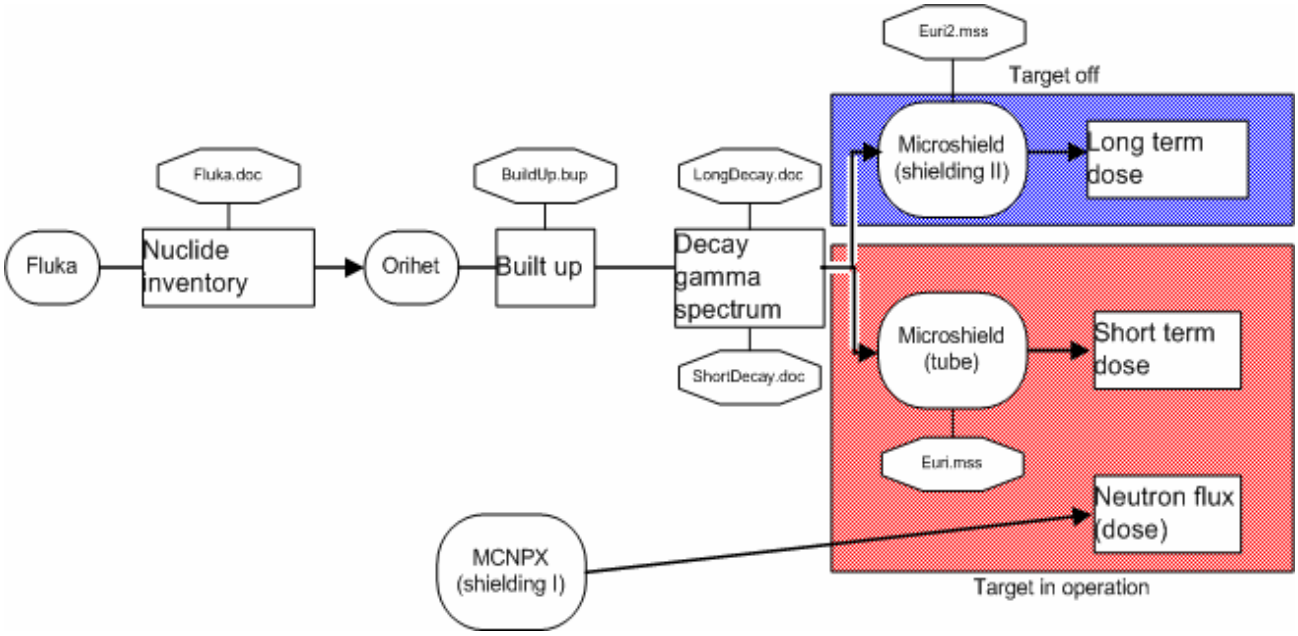

Figure 17: Scheme of dose rate calculations

The build up was simulated for 365 days with a constant proton beam of 4MW (for 1GeV protons that means 4mA current). The irradiation process is then almost saturated (see figure 18). This means the maximal possible irradiation. The decay gamma spectrum after 200 days of irradiation were used for further calculations of dose rates using MicroShield.

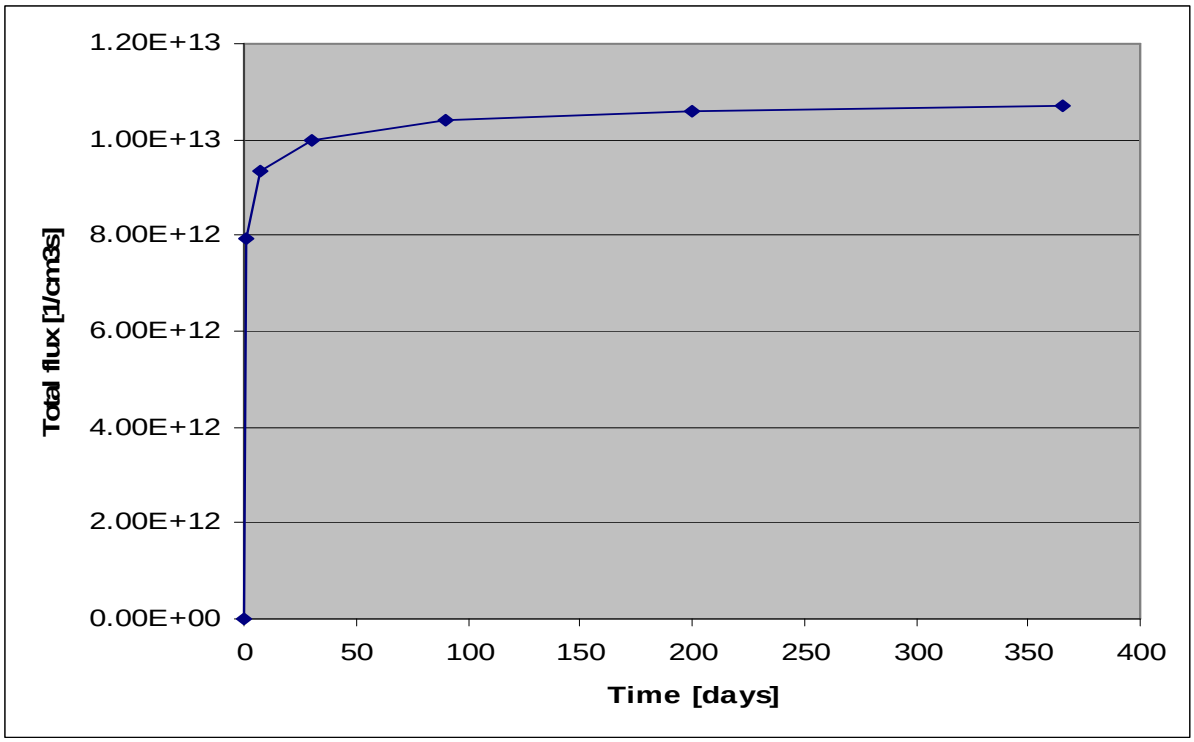

Figure 18: Total flux of gamma ray during build up (4mA proton beam)

Proton beam [mA]	4
Build up time [days]	200
Target volume [cm^3]	9680.6
Time points short decay [s]	0, 15, 60
Time points long decay [h]	0, 0.5, 1, 2, 5, 10, 24, 48, 72

Table 4: Parameters for Orihet calculations

Thermal deposit

The thermal deposit during irradiation process was calculated with "Fluka". The calculation was carried out at CERN. The result is 2.5MW (uncertainty a few percent). Thermal heat due to decay heat is within the range of a few kW (see below), and can be neglected. Considering a lay out safety of 20%, deposited heat is 3.0MW.

Gas production

Gases are also produced during the irradiation process. The largest amount of gasses produced are Hydrogen, Deuterium (1proton plus 1 neutron), Tritium (1proton plus 2 neutrons) and Helium. By that time, also noble gases accumulate in the mercury, but only in a very small amount. Therefore, they are not considered in the estimation of the total gas production, as lay out value for the gas separator. The delayed production of those four isotopes was not studied.

The file ("Fluka.lis") lists all elements and isotopes and their probability to be produced (in atoms per incoming proton per cm^3 of target). Within this simulation $6.24 \cdot 10^{15}$ protons/sec. (equals 1mA) hit the mercury target. The proton beam current in Eurisol is 4mA, hence the production rate is multiplied by 4 (assuming that the

irradiation process does not differ too much, changing the proton current). Finally, norm volumes of the four gases were calculated with the ideal gas equation.

Element	Probability [at / (pr *cm^3)] for 1mA	Produced atoms per month for 4mA	Volume per month [norm-liters] for 4mA
H	$1.86 \cdot 10^{-4}$	$1.16 \cdot 10^{23}$	4.7
Deuterium	$6.97 \cdot 10^{-5}$	$4.34 \cdot 10^{22}$	1.8
Tritium	$1.62 \cdot 10^{-5}$	$1.01 \cdot 10^{22}$	0.41
He	$3.39 \cdot 10^{-5}$	$2.11 \cdot 10^{22}$	0.85
Sum	$3.06 \cdot 10^{-4}$	$1.90 \cdot 10^{23}$	7.7

Table 5: Produced gas

Isotope production

The "Fluka.lis" file was also investigated for the production of isotopes of interest (see 2.3). Table 6 shows the production of the elements (including all isotopes, calculated with the atomic mass of the most stable isotope) during irradiation. The values can be found in the column "spallation". To verify if the masses of the elements increase or decrease in relation to the decay, masses after one month of build up are also listed ("BuildUp.bup").

Element	m [mg/month] spallation	m [mg] build up 1month		Element	m [mg/month]	Build up 1m. [mg]
Ir	1880	2630		Si	0.455	0.779
W	668	1920		Al	0.273	0.117
Sn	25.2	60.9		Mg	0.689	0.907
Sr	78.9	90.1		148-Gd	2.99	6.92
Ge	30.1	40.1		172-Hf	6.27	215
Cu	15.7	7.03		194-Au	766	57.9
Ti	2.42	4.39		195-Au	932	3600

Table 6: Some produced elements

Irradiation from target

Alpha, beta and gamma rays do not have the long range necessary for influencing the hot cell, as shielding I is several meters thick. Nevertheless, neutrons can pass this shielding. Simulation with MCNPX was carried out (Task 5) and saved in the file "NeutronsShiedling1.lis". It consists of the neutron spectrum, passing through the shielding in a straight line (less neutrons beside this line). The investigated shielding consists of 70cm of steel, followed by 4m of concrete. Total neutron flux is shown in figure 19. After 4.70m of shielding, still arrive $1.3 \cdot 10^{19}$ neutrons with an energy of minimal 100keV in the hot cell per cm^2 and year. Considering a shielding 4.5m high and 3m wide (suggested loop lay out; see 5.5), its weight is 215t; 75t of steel and 140t of concrete (steel density 7950kg/m^3 and concrete density 2600kg/m^3).

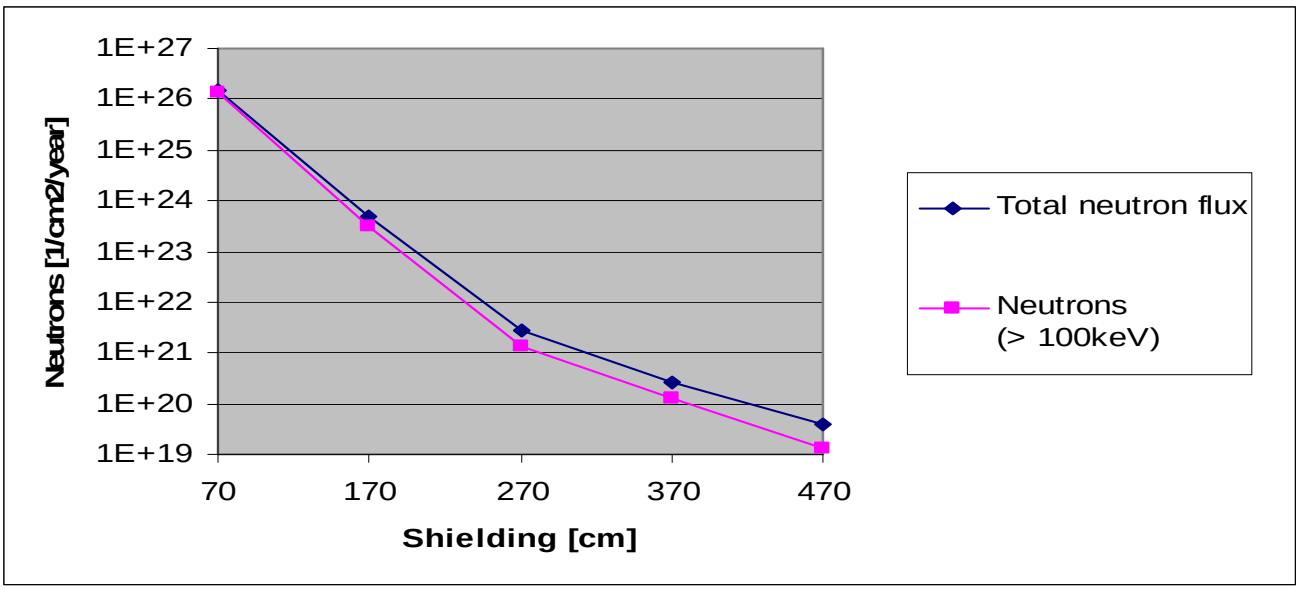

Figure 19: Neutron flux depending on length of shielding

Gamma decay dose rate in tube (short term)

Alpha and beta rays were neglected, as these have a very short range. The gamma flux distribution of mercury after 15 seconds [see Appendix] was imported to MicroShield, to calculate the invoked dose rate in the hot cell. The estimated loop circulation time of mercury is 30s. The calculated radiation inside the target distributes througout the tube. A straight tube of 150mm inner diameter with a steel wall of 5mm serves as model. It is assumed that 15t of mercury are radiated, hence, the tube has a length of 60 meter. The tube is surrounded by air. Unfortunately, MicroShield cannot handle this big geometry. MicroShield probably meshed the geometry with too big steps. The result was lower radiation near the tube (nearly zero) than at 50centimeter distance. After this distance, radiation decreased. To solve this problem, tube length was decreased to 50cm. Accordingly, the radiation output of MicroShield was divided through 120. Figure 20 shows the photon flux, the photon energy fluence rate and the deep dose equivalent rate (parallel geometry), depending on the distance to the tube. At a distance of 10cm the photon rate is $1.75 \cdot 10^8$, with a mean photon energy of $2.75 \cdot 10^8$ MeV.

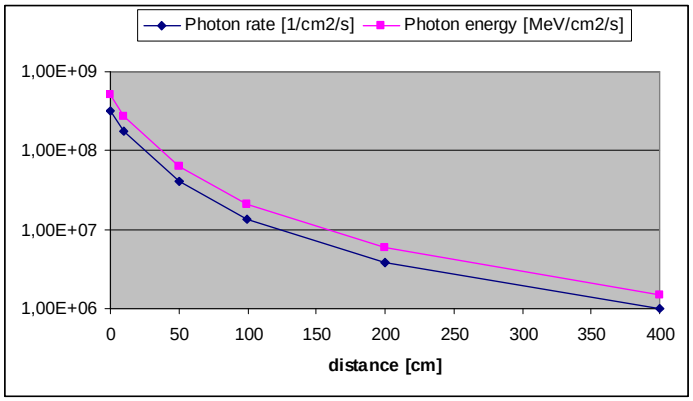

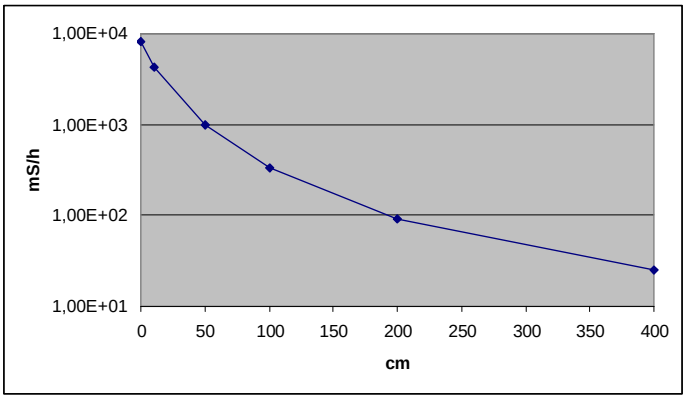

Figure 20: Photon rate and energy (left), dose rate (right)

Gamma decay dose rate in drain tank (long term)

Once more, alpha and beta rays are neglected. Aim of the shielding II is to protect the hot cell and to allow fast access to the hot cell after shut down. Maintenance work should be possible to be done within a short waiting time. Figure 21 shows the dose rate (radiated point source) without shielding at 1 meter distance from the tank, calculated by Orihet.

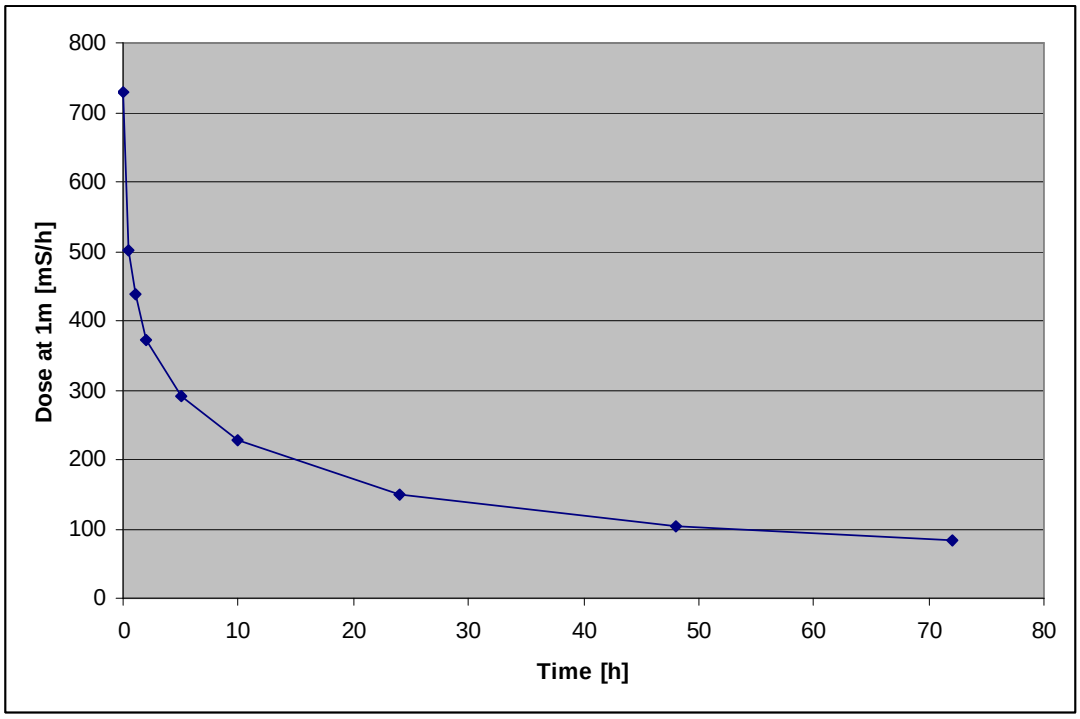

Figure 21: Dose rate after 1m air gap

Dose rate calculations with 40cm and 50cm steel shielding have been carried out for decay times of 30 minutes, two hours and five hours. The model created by MicroShield is shown in figure 22. The reference dose point in table 7 is 50 cm behind the shielding. Reference dose value is the deep dose equivalent rate (parallel geometry).

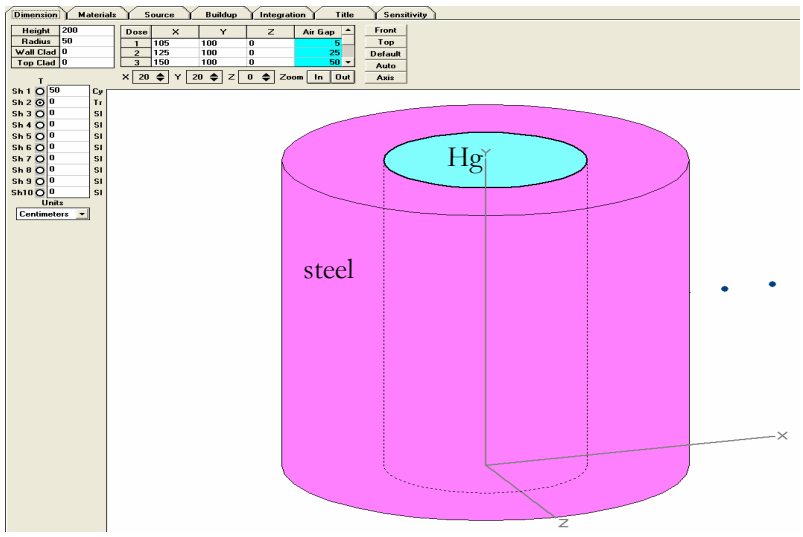

Figure 22: Model of drain tank (vertical, due to MicroShield)

Time	30 min	30 min	2 h	2 h	5 h	5 h
Shielding [cm]	40	50	40	50	40	50
Dose [µS/h]	180	8.2	120	5.2	96	4.1

Table 7: Dose rates (50cm behind shielding)

For the loop lay-out shielding of 50cm is chosen. It provides sufficient protection from radiation coming from drained mercury. Shielding on the bottom is not necessary. The additional 10cm in height (compared to the 40cm lay out) should not be a crucial point. A rough assumption could be that shielding steel saved on the bottom could be used on both sides. Accordingly, the shielding volume is the pink area, as shown in the figure. Additionally, a cooling tank is between shielding II and the drain tank, accordingly, the shielding volume is multiplied by factor 1.5. With the density of steel (8t/m³) this results to an estimated weight of the shielding of 14t (50cm) or 10.5t (40cm), respectively.

Decay heat (in drain tank, long term):

The long term decay heat is calculated by Orihet (see figure 23), the initial heat decay is 14.7kW (data is attached in appendix). As many nuclei with different half times contribute to the heat, one can not use the decay law (see red points in figure 23). The decay formula was used with a half time of 1.3 days.

$$N = N_0 \cdot e^{-\frac{\ln 2}{T_{1/2}} \cdot t}$$

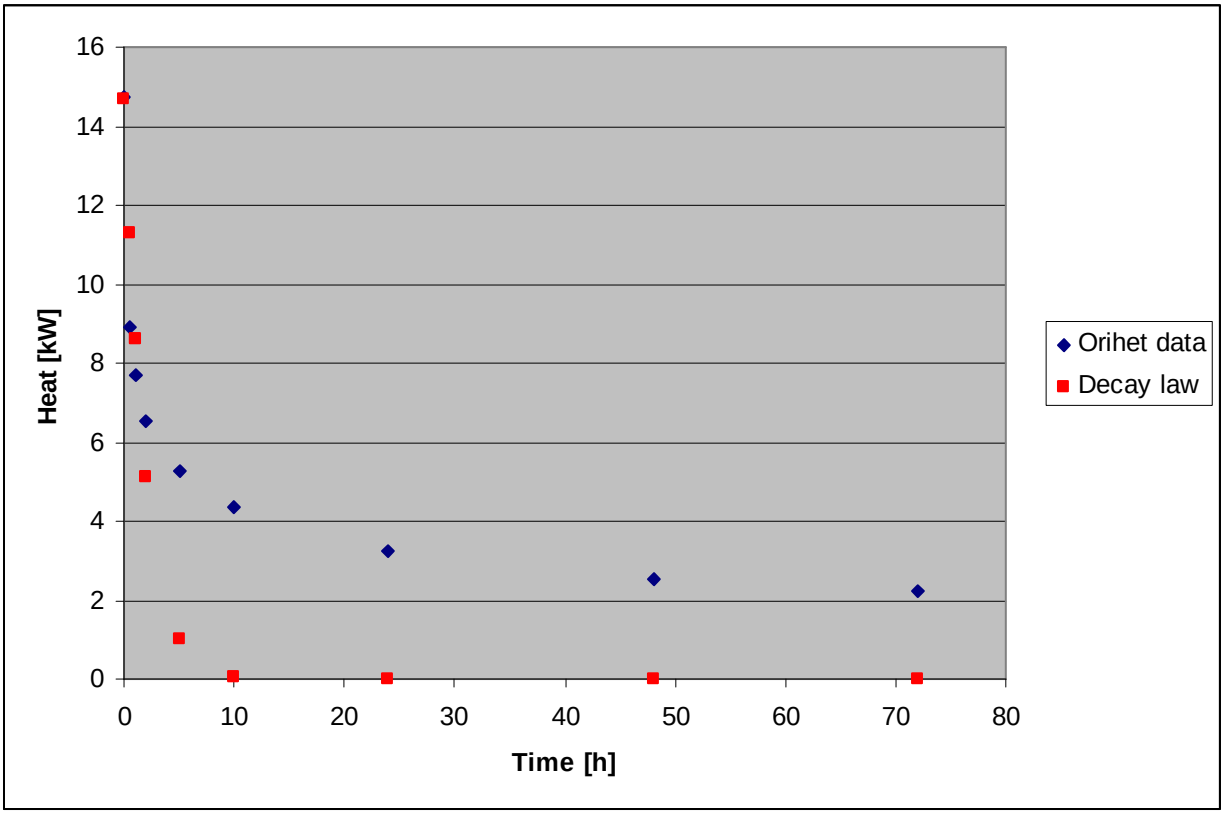

Figure 23: Decay heat

2.5 Safety

The two main dangers of the loop for personal are radiation and toxicity of mercury. Shielding I as part of the total target shielding has to minimize dose rates during service. Shielding II has to protect the hot cell and personal inside during maintenance work.

Safety against mercury was discussed within a memorandum of Dr. Riesen (PSI). The memorandum can be found on the CD ("MemorandumSaftey.doc"). Accordingly, the main points for safety (despite minimizing leakage problems) are:

- inclined colleting container beneath the target and loop
- target area and hot cell leak proof
- filter for cover gas
- hot cell visible from outside (window)
- measurement of mercury concentration in the air possible, externally and continuous.

Furthermore, safety issues during the filling of the mercury into the drain tank (installation of the loop) have to be studied, as well as fire saftey. A difficult problem will be the deconstruction of the loop. It has to be investigated where the mercury (as well as the devices) can be stored.

2.6 Target heat removal

The incoming 4MW proton beam produces 2.5 MW of heat when it hits the mercury in the target. Considering a 20% margin, 3.0MW of heat must be removed by flow of the mercury from the target to the heat exchanger. The main task of the design of the mercury loop is to prevent the mercury boiling. Boiling would increase the pressure dramatically and, therefore, inevitably damage the loop.

First of all, the nominal flow rate of the loop has to be determined. The boiling curve of mercury determines the maximal temperature inside the target. The temperature peak inside the target should have a reasonable safety margin from boiling point. According to the lay out of the reference target (December 2006), the nominal mean outflow temperature was assumed to be 180°C. This parameter depends on target design. The inflow temperature is limited by the choice of the cooling fluid inside the heat exchanger. Water is very convenient for this purpose. The heat exchanger could be connected directly to the main cooling water circuit. Water has a very high thermal capacity and does not get irradiated heavily. Temperature of cooling water was assumed to be 30°C. The main cooling water circuit will probably be cooled by a river. The nominal influx temperature of mercury in the target (equal to the outflow temperature of the heat exchanger) was specified at 60°C (compare 3.2).
Nevertheless, a different cooling fluid could decrease the mercury temperature, which would lower the

demanded flow rate of mercury. This would benefit the lay out of the pump and the target, but also imply higher thermal stresses on the heat exchanger.
Specified parameters result to a nominal flow rate, according to the heat capacity of mercury. The heat capacity in this temperature range differ only within 2%, therefore, heat capacity of 100°C was taken for calculation (instead of integration).

$$\dot{m} = \frac{\dot{Q}}{c_p dT} = \frac{3.0MW}{137.7J/kgK \cdot 120K} \cong 180\frac{kg}{s}$$

Accordingly, the nominal flow rate is 180 kg/s (48 m^3/h or 800 l/min)

2.7 Pressure drops in the loop

Pressure drops inside the loop determine the required pressure head of the pump. The pump should provide a 30% higher pressure head as the calculated pressure losses. As the loop design described in chapter 5 could be changed, a conservative estimation (except target) of the loop pressure drop was carried out. The two presented designs fulfil all lay out parameters assumed in the following paragraph.

Frictional losses *dP* increase with the square of velocity *w*. Equation 3 shows the general dependency of the pressure drop. Hence, the main part of the pressure drop is in the target, as there are very high velocities. ξ is called pressure loss coefficient.

$$dP = \xi \cdot \frac{\rho w^2}{2} \quad (3)$$

Because of the high mass flow, the tube diameter should be big enough to prevent too high pressure drops. The ESS study recommends a diameter of 15 centimetres [ESS, 4-57]. This value serves as minimal lay out value for the inner tube diameter d_i. With the nominal flow of 180kg/s and the density of mercury (assumed mean temperature 100°C) of 13385 kg/m^3, the nominal velocity within the tubes is 0.76 m/s.

$$w_{tube} = \frac{\dot{m}}{A \cdot \rho} = \frac{\dot{m}}{1/4 \cdot \pi \cdot d_i^{\,2} \cdot \rho} = 0.76\frac{m}{s}$$

The flow is a turbulent one as it shows the Reynolds number (Re>2300), with γ(100°C)=9.28 ·10^{-8} m^2/s:

$$\mathrm{Re} = \frac{wd}{\gamma} = \frac{0.76m/s \cdot 0.15m}{9.28 \cdot 10^{-8} m^2/s} = 1.2 \cdot 10^6$$

Pressure drop in the tubes:

The pressure drop in a tube is calculated with this formula:

$$\xi_{tube} = \lambda \cdot \frac{L}{d} \quad (4)$$

The friction coefficient λ can be determined by figure 24. After 20 years of operation, the tube surface is no longer smooth. As experimental data of such a mercury loop can not be found, simple estimation was done. After 20 years, the tube roughness will be between smooth and hydraulic rough. The surface roughness k was assumed 1mm. With the given Reynolds number *Re* and a diameter of 150mm, that yields to a lambda of 0.035 (see figure; d/k=150).

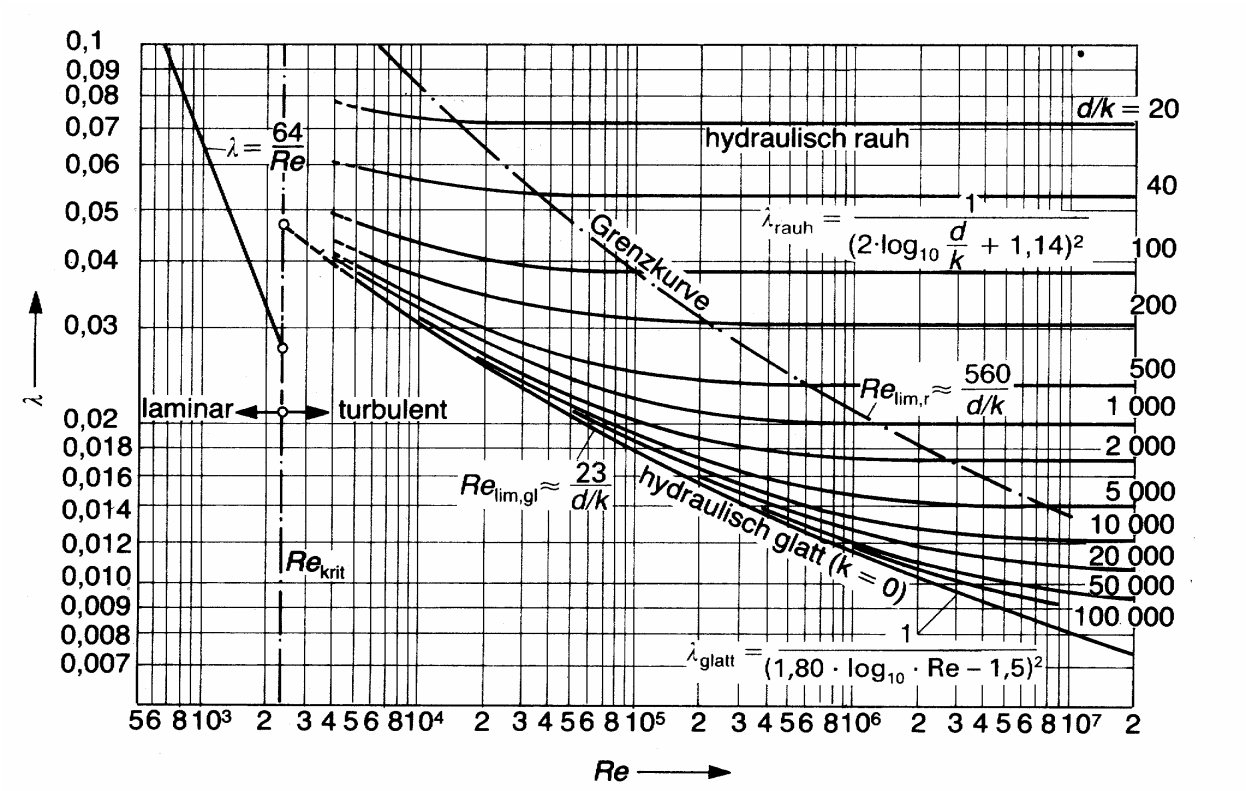

Figure 24: Dependency lambda of Re [Wagner, p.77]

The total length of the tubes is 15m. Shielding I is about 5 meters, hence, for inflow and outflow 10 meters of tubes are necessary. Tubes in the hot cell should not exceed 5 meters. The pressure drop therefore is 0.14 bar.

$$dP = 0.035 \cdot \frac{15m}{0.15m} \cdot \frac{13385kg/m^2 \cdot (0.76m/s)^2}{2} = 0.14bar$$

Pressure drop in the elbows:

The most important parameter for these kind of drops is the quotient r/d, which means the mean radius of the elbow in respect to the (inner) diameter of the tube. If this quotient is under 5, the biggest part of the loss is the drop by turn around losses [Wagner, p.98 f]. The coefficient r/d of the loop elbows should not be smaller than 1.5, which results in a (mean) radius of 22.5cm. The pressure drop for one elbow of this type is calculated according to following formulas. Six elbows would cause a total pressure drop of 0.09 bars. Elbows in the lay out of the loop (chapter 5) have a higher r/d.

$$\varsigma_{turn,90^o} = \lambda \cdot \frac{12.8}{\sqrt{r/d}} \cdot \sqrt[4]{\frac{2}{\frac{r}{d}}} \qquad for\ (1 \le \frac{r}{d} \le 2)$$

$$dP = 0.035 \frac{12.8}{\sqrt{1.5}} \cdot \sqrt[4]{\frac{2}{1.5}} \cdot \frac{13385 kg/m^3 \cdot (0.76 m/s)^2}{2} = 0.015 bar$$

Pump:

The pressure drop of the pump is assumed to be 0.9 bar (see 3.1).

Heat exchanger:

The pressure drop of the heat exchanger consists mainly of pressure drops at the inlet and outlet. The mercury there is expanded or contracted. Formula 5 and 6 describe these processes, with the smaller flow cross section A_1 of the flow and the bigger cross section A_2 [Idelchick, p.189 and 198].

$$\varsigma_{ex} = (1 - \frac{A_1}{A_2})^2 \quad (5)$$

$$\varsigma_{con} = 0.5 \cdot (1 - \frac{A_1}{A_2})^{\frac{3}{4}} \quad (6)$$

The mercury is expanded first into a reservoir, from which it is divided into the small tubes. After flowing through these tubes the mercury flows into a second basin, from which it is led into the tube again. The heat exchanger consists of 660 tubes (inner diameter 11.8mm). The main tube diameter is 150 mm, the velocity in the main tube, w_m, is 0.76 m/s, the velocity in the small tubes, w_t, is 0.3 m/s.

$$dP = (\zeta_1 w_m^2 + \zeta_2 w_t^2 + \zeta_t w_t^2 + \zeta_3 w_t^2 + \zeta_4 w_m^2) \frac{\rho}{2} = 0.15 bar$$

Considering merging effects the result is multiplied by three. Assumed pressure drop is 0.45bars.

Pressure drop in the expansion tank/ gas separator

Pressure drop in the expansion tank/ gas separator was carried out for draft 2 (see 3.3). With formulas 5 and 6, the pressure drop is 0.11bar. The pressure drop could be minimized by smoother passages from the tubes to the tank.

Pressure drop in the target:

Pressure drop in the target was assumed to be 5 bars.

Table 8 sums up the pressure drop calculations. Pressure drop in the loop is about 1.5bar, inside the target 5bar.

	Tubes (15 m)	6 Elbows (r/d = 1.5)	Gas separator	HE (3m, 0.3m/s)	Pump	Target
dP [bar]	0.14	0.015	0.11	0.45	0.9	5

Table 8: Pressure drops in loop

2.8 Check for cavitation

Within the loop there are two endangered parts (except the target). The pump due to higher velocities there and the elbows (stream could break away).

Pump

Empirical correlation 7 implies a dimensionless value n (cavitation number) higher than 2 to prevent cavitation. The values are at the inlet of the electromagnetic pump.

$$n = \frac{2p}{\rho w^2} > 2 \quad (7)$$

With the density of mercury of 13500 kg/m³ and a velocity of 2.6m/s (see 3.1), the minimal pressure has to be 0.9bar (for n=2). Static pressure of 0.9 bar is reached by 70cm of mercury. As pressure inside pump will be higher, cavitation is not a problem.

Elbows

Flow of the mercury in the elbow was simulated with CFX in order to check for cavitation. The result is presented in figure 25. The diameter of the tube is 15cm, the radius/diameter factor is 1.5. Inflow and outflow tube are 50cm long each, the velocity is 2m/s. Boundary condition is zero dynamic pressure at the exit. The resulted dynamic pressure at the entrance is about 400Pa. The CFX files are located within the folder "AnsysFiles", as well as the geometry, which was created with ANSYS.

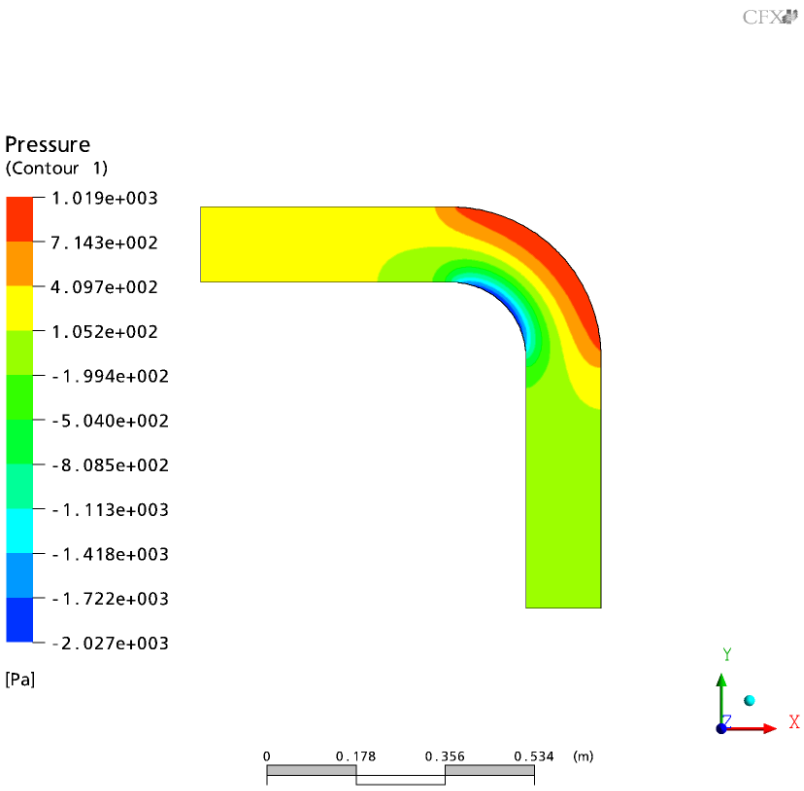

Figure 25: Pressure in elbow

The maximal pressure drop in elbow is 2027Pa. This clearly shows that no cavitation problems will occur in the elbows.

2.9 Baseline parameters for loop

The results from the calculation above are listed in the following table. To sum up, the parameter for the lay-out used in this work are also included. These parameters are determined in chapter 3.

Liquid	Mercury
Beam power	4.0 MW
Deposited heat in target	2.5 MW
Deposited heat in target with margin	3.0 MW
Nominal flow rate	180 kg/s
Cooling fluid	Water
Flow rate cooling water	24 kg/s
Tube diameter (estimated)	150 mm
Flow velocity	0.76 m/s
Nominal pressure (total pressure lay out)	40 bar
Added static pressure (max.)	20 bar
Pressure drop loop (without target)	1.5 bar
Pressure drop target	5 bar
Total pressure drop	6.5 bar
Pressure head pump (lay out)	8 bar
Nominal gas production	7.7 l/month
Nominal temperature target inlet	60 °C
Nominal temperature target outlet	180 °C
Estimated Hg inventory (incl. sump in drain tank)	20 t
Drain tank volume (lay out)	1.5 m^3
Lifetime loop	20 years
r/d minimum (for elbows)	1.5
Hg Concentration in air (nominal, maximal) [mg/m3]	<0.1, 30
Initial decay heat (max.)	14.7 kW

Table 9: Main lay-out parameters of the loop

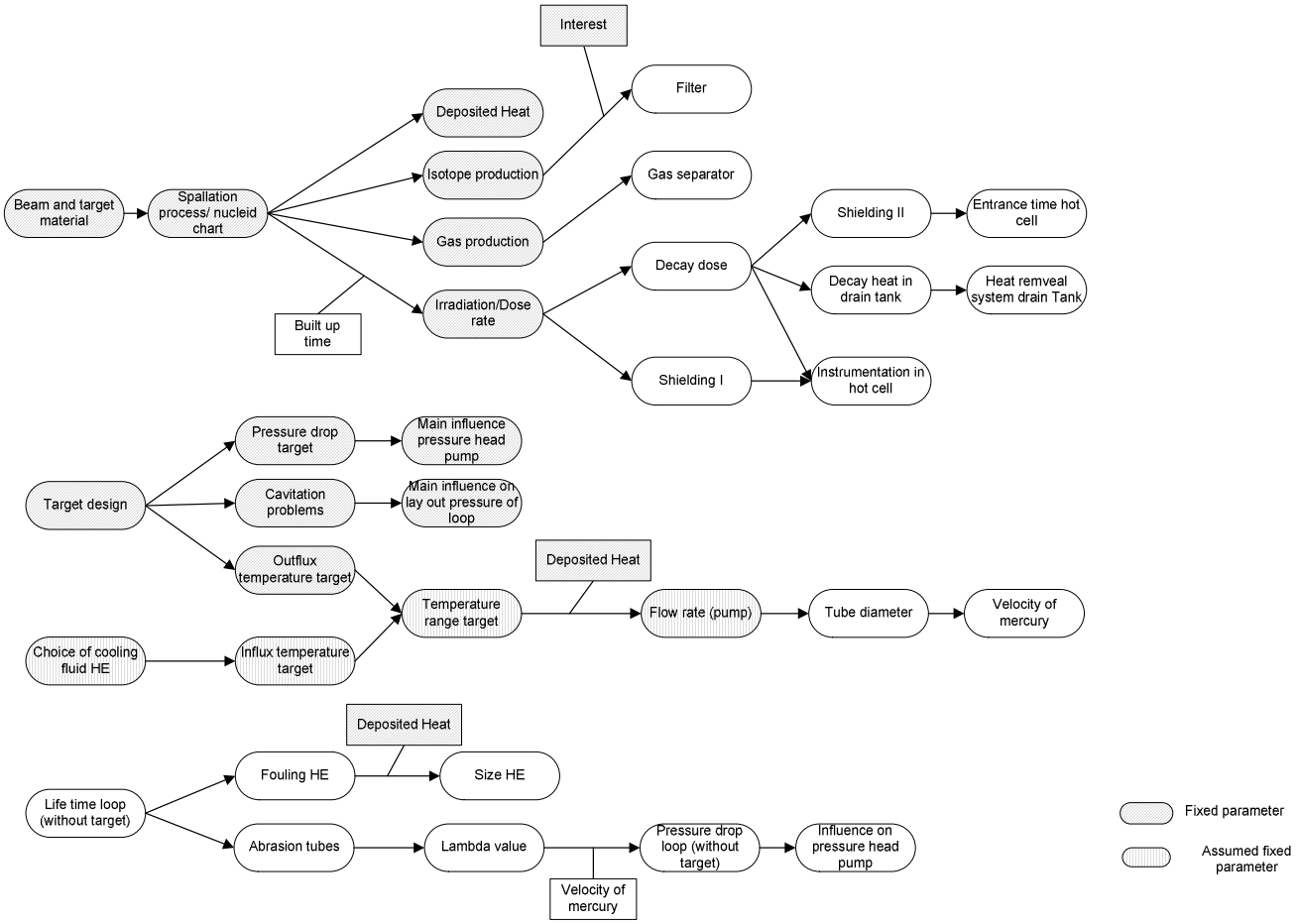

Figure 26: Dependencies of loop parameters

3 Dimensioning of the main devices

The criteria, the main devices have to handle are:

- No leakage
- Compactness
- Low pressure drop
- Long life time

As the hot cell should be small, compactness of the devices is aimed, as well as low pressure drop. Otherwise, the pump could be too weak and has to be designed bigger.

3.1 Pump

The choice of the pump is described in this chapter. Criteria for the pump were: 8 bar of pressure head, capacity of 40bar and flow rate of 180kg/s. Depending on the final design of target, the demanded pressure head could be less as well as the pressure capacity. Correlation between life time/irradiation and degeneration of the pump was not regarded. Estimation of this is difficult, as no comparable data exists.

In general, there are two main types of pumps, dynamic ones and displacement pumps. Dynamic pumps add energy continuously to pump the fluid whereas displacement pumps add the energy periodically. Displacement pumps can provide smooth flow by using several pump chambers [Karassik, 1.3, 2.27]. Smooth flow is important for the secure heat removal. In addition, the pump should be simple and reliable and no cavitation should occur.
Unfortunately, displacement pumps can not be used for the loop. Classic displacement pumps need lubrication, which is a problem. The additional lubrication material will be irradiated and could lose its capability to lubricate. Furthermore, there is the problem of sealing. Displacement pumps using membranes are very interesting, but at the moment there are no pumps with membranes which could resist the irradiation over a longer time.
The classic dynamic pump is the impeller pump. The main problem is the sealing between driveshaft and mercury tube. The risk of leakage there is too high. Three other dynamic pumps will be discussed: a seal-less driven impeller pump, a permanent magnet pump and an annular linear electromagnetic pump.

Seal-less driven impeller pump

Such pumps have a magnet coupling and, as a result, the driveshaft does not intersect the tube wall. As the loop has a very high static pressure, a seal-less magnetic driven centrifugal pump could be envisaged. The high static pressure could prevent cavitation at the impeller. A very good introduction to this kind of pumps is given by Schommer. Figure 27 shows a standard seal-less pump. The liquid is pumped with the impeller on the left hand

side, the driveshaft is on the right hand side. There is a magnetic coupling between driveshaft and internal rotor. Friction losses at the internal rotor cause a temperature rise. The containment shell is filled with the liquid which has to cool the inner parts. Therefore, a rear impeller is installed which causes a secondary flow. Figure 28 sketches out some possibilities for the arrangement of the cooling flow.

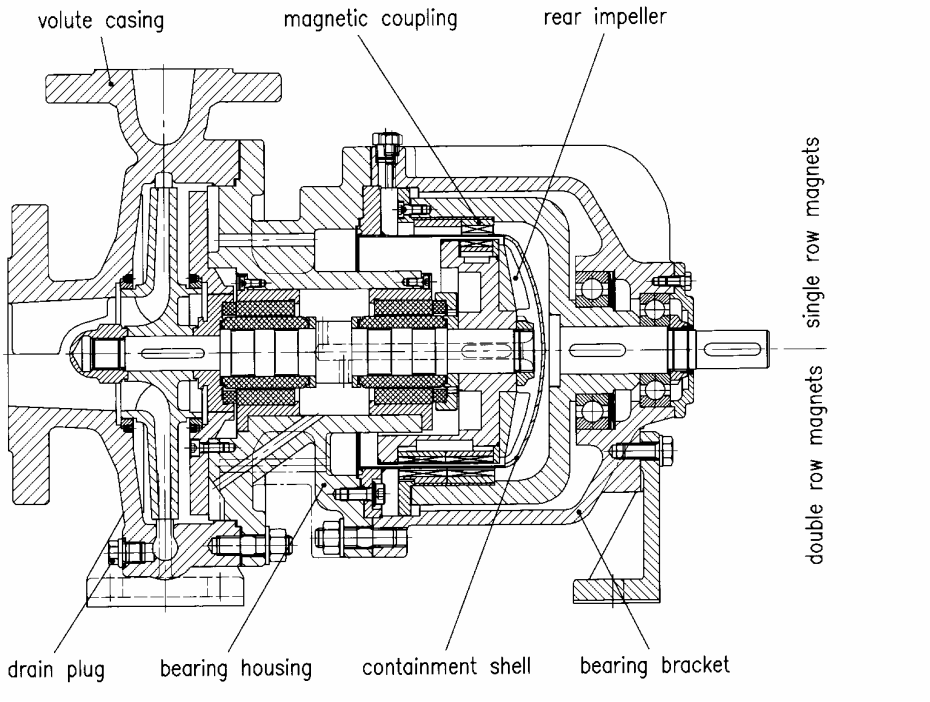

Figure 27: Drawing of a seal-less driven impeller pump

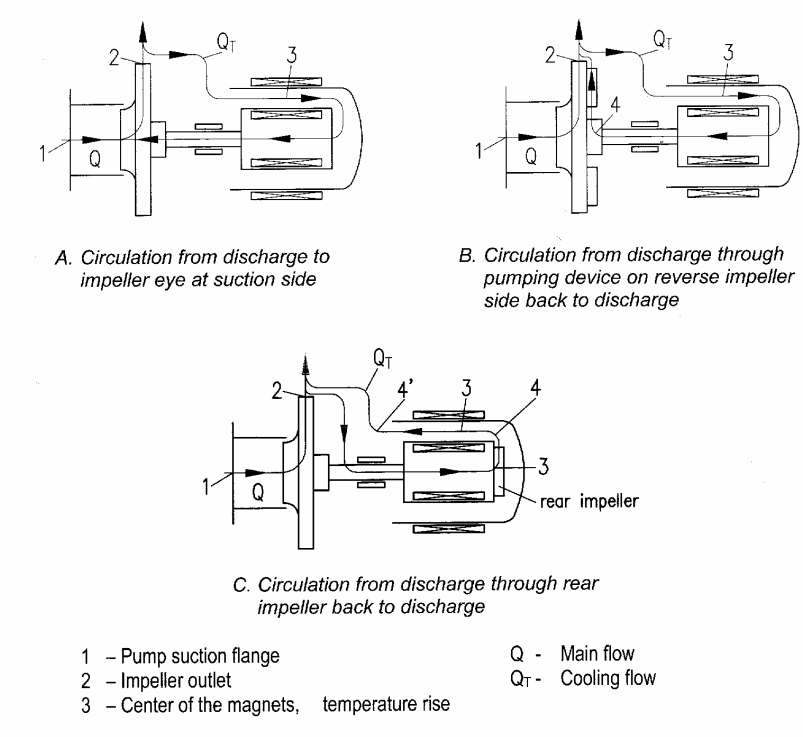

Figure 28: Removal of heat in a seal-les driven impeller pump

Unfortunately, there are problems when magnetic driven centrifugal pumps are used. The first disadvantage is that such pumps are much more complex than a permanent magnet pump or an electromagnetic pump. Indeed, the channels for the liquid metal in the latter two pumps have a very simple structure. This entails very easy thermo-mechanic calculations and ease of manufacturing. The channel parts can be welded, so that no seals are used. Seal-less driven magnetic pumps do not need seals separating the atmosphere from the liquid. But, because of rotating parts inside the liquid, there are also bearings inside the pump. As the mercury is irradiated, these bearings could be damaged after a certain time.

Another disadvantage is that the drive magnet needs bearings. Such bearings are in contact with the drive magnet, via a safety ring. If the safety ring is worn out, the drive magnet could damage the containment shell and mercury would leak outside. [Schommer, B35]. Following figure illustrates the problem with the safety ring.

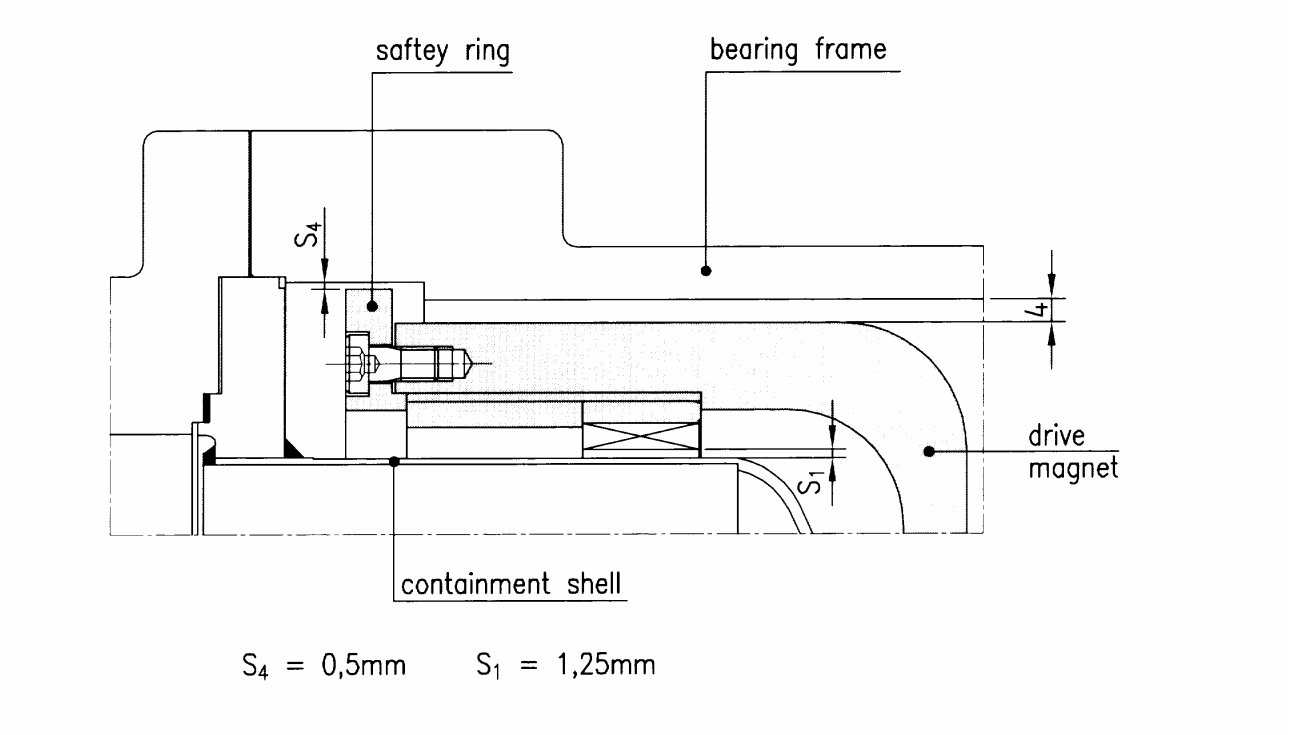

Figure 29: Saftey problem of seal-less driven impeller pumps

Electromagnetic pumps (EMPs)

EMPs use Lorentz-forces to move the liquid in the flow channel. Therefore, the liquid has to be electrically conductive. One can divide EMP in conduction and induction pumps. Conduction pumps conduct an electric current from the tube walls through liquids. Furthermore, they provide also a magnet which yields to a magnetic field in the liquid. Induction pumps do not have devices to send an electric current directly through the liquid. They impose the electric current inside the liquid through the magnetic field they build in the liquid.

Conduction pumps are simple to build but have a poor efficiency [Barker]. Two induction EMPs are investigated: permanent magnet pump (PMP) and an annular linear pump.

Permanent magnet pump (PMP) [Bucenieks a]

The so called permanent magnet pumps (PMP) are a more recent development. In former days, the permanent magnets were not very strong, the efficiency of this kind of pump was not exceptionally high, because of the resulting slip between magnets and the pumped liquid. As magnets have become stronger, permanent magnet pumps can compete with the classical induction pumps. The magnets are rotated by a usual electromotor. The IPUL institute at Riga has built very innovative PMPs with several advantages. IPUL builds two types of PMPs:

- Cylindrical type
- Disk type

These differ in the arrangement. Both channels have a rectangular cross section. In a PMP, the channel is bended around the magnets, that lie (with a very small gap) on top of the (radial) inner surface of this channel. The disk type channel is a U-shape and the magnets are placed on the top of the channel. Figure 30 and 31 compare both pump designs.

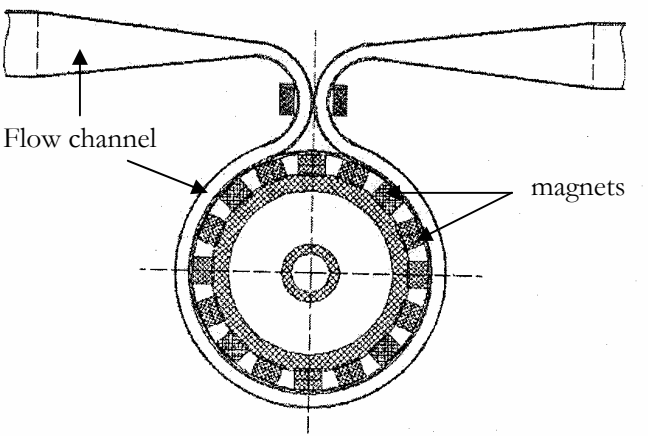

Figure 30: Cut through a cylindrical PMP

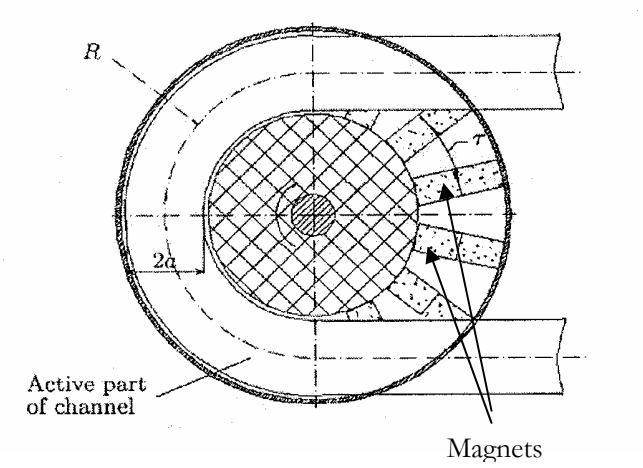

Figure 31: Cut through a disc type PMP

Cylindrical PMPs can withstand higher pressure than disc type pumps because of the geometry of those flow channel (compare the flat channel of disc type with the tube shape of cylindrical PMP). Unfortunately, the high pressure inside the loop causes thick flow channel walls inside the PMPs, calculations with Ansys will show that. Thicker walls lower the efficiency of the pump, the following equation for the maximal (head) pressure P_{max} developed by the pump illustrates this. P_{max} is a quadratic function of the magnetic field B. Coefficient σ denotes the electrical conductivity of the liquid metal, w_B the average magnetic field velocity, s the slip, l_{ch} the length of the active channel part and k transversal end effects.

$$P_{\max} = 0.5 \cdot \sigma \cdot w_B \cdot B^2 \cdot s \cdot l_{ch} \cdot k \quad (8)$$

Dimensioning for the flow channel was done in reference to the proposed cylindrical pump for ESS and in cooperation with IPUL. The mercury velocity inside the pump was set at 1.5m/s, wall material is 316L stainless steel and the height of the channel is 20mm. Eurisol flow rate is 180 kg/s, at a working temperature of 60°C. Consequently, the demanded flow cross section A is $8.9*10^{-3}$ m² and the width of the channel, $2a$, has to be 445mm.

$$A = \frac{\dot{m}}{\rho w} = \frac{180}{13482 * 1.5} = 8.9 \cdot 10^{-3} m^2$$

$$2a = \frac{A}{b} = \frac{8.9 \cdot 10^{-3} m^2}{20 \cdot 10^{-3} m} = 445 mm$$

The similar conditions have, as a consequence, a similar channel width as in ESS. The channel is also subdivided by columns into three parts to achieve higher stiffness of the channel. Normally, the wall thickness is about 2-3mm. To estimate the deformation and stress, calculations in ANSYS (for one part of the channel) were carried out with a wall thickness of 5mm. The calculations show that even for 5mm wall thickness, the applied pressure is too high and, therefore, a PMP could not be used (details see below).

The length of one of the three parts of the flow channel is about 160mm. The deformation at the middle of the cross section is over 4 mm, which is much too high. Such a deformation would oblige a higher gap between magnets and wall, or to form the magnets according to the assumed deformation. In addition, there are too high stresses (about 800MPa) in the middle of the channel (stresses in the edges could be reduced by fillets). Design stress for 316L at 60°C is 115MPa.

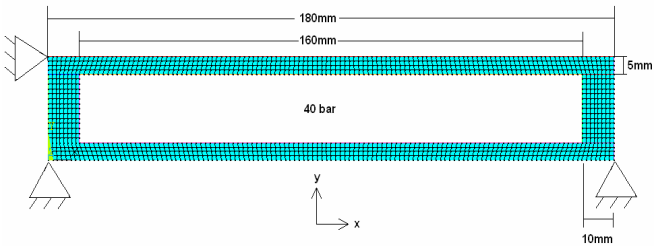

Figure 32: Model

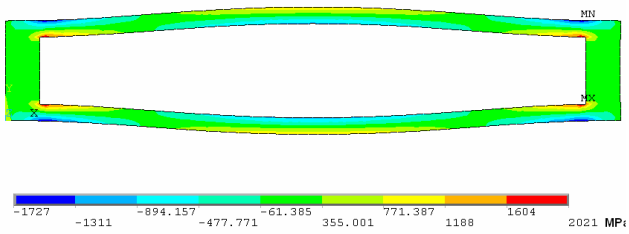

Figure 33: Stress in x-direction

Annular linear induction pump [Barker]

Annular linear induction pumps differ from flat linear induction pumps only in the shape (as the name already impies). Figure 34 shows a cross section of a flat one on the right hand side, and a cross section of a annular on the left.

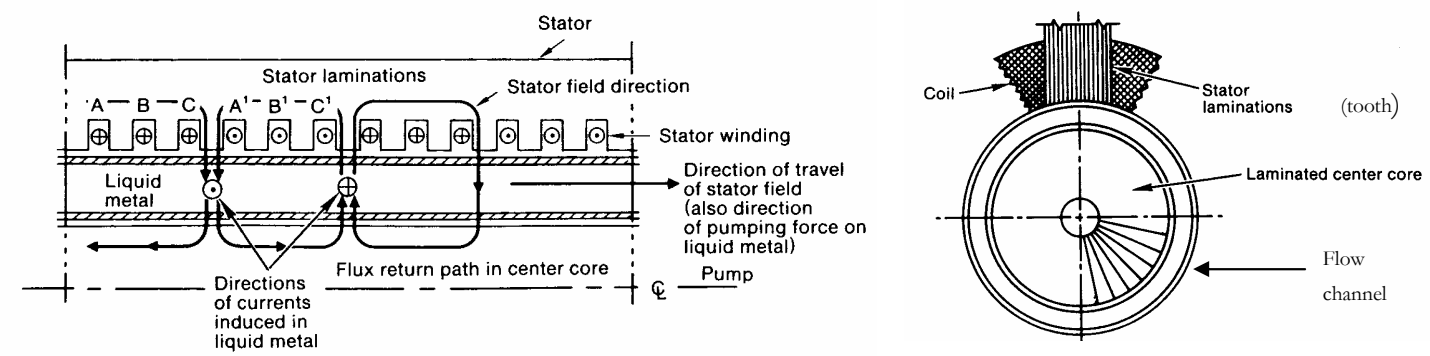

Figure 34: Sketch of an flat EMP (left) and an annular EMP (rigth)

Annular pumps can withstand higher pressure than flat ones, due to their shape. In cooperation with IPUL a lay-out of an EMP for the loop was carried out. As flow velocity inside the pump 1.5m/s and a pump channel heigth of 14mm were chosen. Accordingly, the pump channel has an inner diameter of 399mm and an outer diameter of 413mm. Stresses inside the tube walls (2mm) were studied with ANSYS on two designs. The first one is conventional (EMP1), the second one has additional ribs (EMP2).

The conventional lay out (normal tube) imposes high precision during fabrication because the teeth have also the task of supporting the tube wall. ANSYS calculation (with an axial symmetric model) was done with the following assumptions: no gap between teeth and wall, and infinite stiffness of the teeth. Absence of a gap could be achieved by tight fit and a very high stiffness through additional metal rings around the teeth. The length of the tube (2mm thick) between two teeth is maximal 15mm. Results are shown in the following two figures.

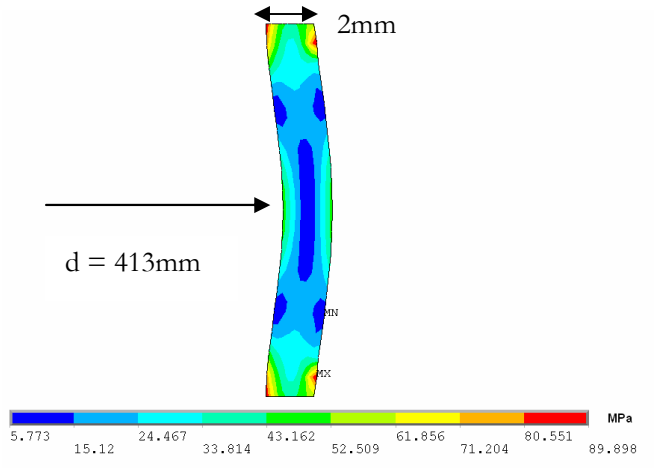

Figure 35:Von mises stress (EMP1)

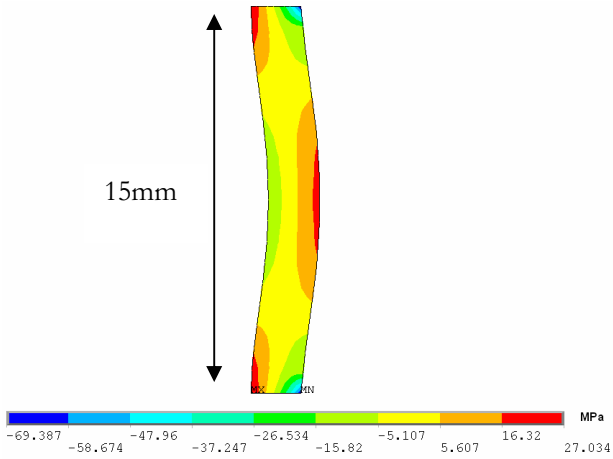

Figure 36: Z-Stress (EMP1)

IPUL carried out calculations for this type. Some important parameters of the pump calculated are listed in table 10 Finally, this lay out uses smaller tubes than the first set and, therefore, higher velocity of 2.6 m/s is also the result.

Provided pressure	5.2 bar	Number of slots	32
Internal pressure drop	0.58 bar	Length of slot	14 mm
Pressure head	4.62 bar	Total length of pump	1.5 m
		Length of core	1.0 m
Current in coils (two parallel connected)	2 * 50A (at 50Hz)	Magnetic field	0.15 T
Electric power	163 kW	Provided flow rate	180 kg/s
Active power	102 kW	Inner and outer tube of flow channel	85mm x 1.5mm 117mm x 2.0mm
Efficiency (of active power)	6 %	Velocity in flow channel	2.6 m/s

Table 10: Parameters of EMP draft (IPUL)

Active power includes thermal losses and the acceleration of mercury. Accordingly, an efficiency of 6% for active power results in thermal losses of maximal 100 kW inside the mercury. Electric power includes also power for the magnetic field. To reach the desired pressure head of 8 bar, two cores of this type can be connected in a series. Total length of this pump is 2.5m, total pressure head 9.2 bar, and the heat transferred to the mercury is maximal 200 kW. Weight of the channel is 10kg, the weight of mercury 140kg. Total pump weight of 350kg is estimated.

In the end, a new shape of the outer flow channel tube shall be mentioned (same tube diameter). This shape has ribs on the surface and can withstand the pressure of 40 bars on its own. In particular, the teeth do not need to support the wall, and less precision during production and assembling is required. On the other hand, problems with the coil assembly can occur. Figure 37 shows the result for a tube with ribs of 4mm in length and 40mm in height. For every slot remains 11mm length (15mm for EMP1). Table 11 sums up the result for different heights of the ribs (all 4mm in length).

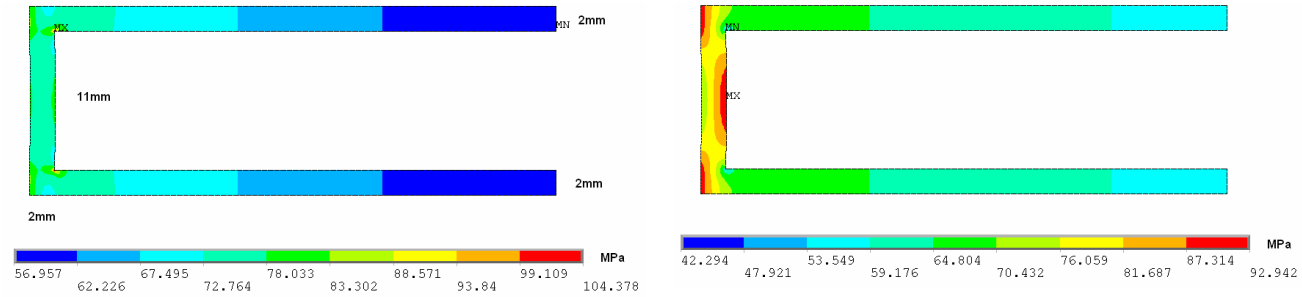

Figure 37: EMP2 (left: von Mises stress, right Z-sttress)

Max. Stress / Length rips	15mm	20mm	40mm
Von Mises [MPa]	171.5	127.2	104.4
Z [MPa]	194.1	139.3	92.9

Table 11: Stresses of EMP draft 2, depending on ribs

3.2 Heat exchanger

The heat exchanger has to be capable of removing 3.0 MW of heat. The deposited heat in the target is about 2.5MW, the transferred heat inside the pump is maximal 200 kW, and the decay heat can be neglected. The mercury is cooled down from 180°C to 60°C, cooling water is heated from 30°C to 50°C, water flow rate is 24kg/s. A shell & tube heat exchanger was chosen. Before dimensioning the heat exchanger, some general ideas about heat transfer are given.

Theory

There are three kinds of heat exchange. First, there is conduction, which is an energy transfer in a material from a high temperature region to a low temperature region. Secondly, there is convection, which is the transport of potential energy; for example heat, through currents within a fluid. Thirdly, there is radiation heat transfer, which can transfer energy also through a vacuum [Holman, chapter 1]. Therefore, only the first two kinds of exchange are of interest for this heat exchanger.

Conduction is usually described in a linear fashion with the conduction coefficient, respectively convection with the convection coefficient, with the following two formulas,

$$\dot{Q} = -kA\frac{\partial T}{\partial x} \quad (9)$$

$$\dot{Q} = hA(T_w - T_\infty) \quad (10)$$

where A is the surface area of the conduction process or the convection process, T_w is the temperature on the limiting wall and T_∞ the temperature of the fluid outside the convection area.

Values for the conduction coefficient can be found through experiments and can easily be looked up in books. The convection value depends strongly on the situation. There is a standard approach for calculating the coefficient h in tubes with the so called Nusselt number, Nu . The convection coefficient, h, of the fluid within the tube is determined by formula 11, with the convection coefficient, k, of the fluid and the inner diameter d_i of the tube. There exist different formulas for the Nusselt number, depending on the Prandtl number Pr and Reynolds number Re of the fluid. The most popular formula for common fluids is (12), where n is 0.3 for heating and 0.4 for cooling. [Holman, p.286]. Nusselt number for liquid metal, especially mercury, can be determined according to empirical formula 13 [Kirillov, p.2]. Pe (equal Re·Pr) is called Peclet number. Both formulas were used for dimensioning of the heat exchanger.

$$h = Nu\frac{k}{d_i} \quad (11)$$

$$Nu = 0.023\,\mathrm{Re}^{0.8}\,\mathrm{Pr}^{n} \quad (12)$$

$$Nu = 4.3 + 0.025Pe^{0.8} \quad (13)$$

If the fluid does not flow in a tube, but in a more complex device (as the water does in the heat exchanger shell), one can calculate an equivalent hydraulic diameter, d_h, according to formula 14, with the flow surface A and the wetted perimeter U.

$$d_h = \frac{4 \cdot A}{U} \quad (14)$$

To get the estimation of the surface area, or the transferred heat, respectively, one can use the equation with the so called overall heat transfer coefficient, U, and the log mean temperature difference, ΔT_{lm}, which are calculated as shown. R_f is the fouling resistance (dirt and scale accumulated on the walls during operation), Th_t is the thickness of the tube and k_t the conductivity of the tube walls. The inversion of h and the factor Th/k is also called resistance. The higher the resistance is, the lower the heat flow.

$$\dot{Q} = UA\Delta T_{lm} \quad (15)$$

$$\frac{1}{U} = \frac{1}{h_{hg}} + R_{f,hg} + \frac{Th_t}{k_t} + R_{f,water} + \frac{1}{h_{water}} \quad (16)$$

$$\Delta T_{lm} = \frac{\left(T_{hg,out} - T_{water,in}\right) - \left(T_{hg,in} - T_{water,out}\right)}{\ln\left(\frac{T_{hg,out} - T_{water,in}}{T_{hg,in} - T_{water,out}}\right)} \quad (17)$$

If the outer and inner surface of the exchange area differ, i.e. the thickness of the wall is not neglected in a geometrical way, one has to define a reference area. The choice of the reference heat exchange area A is arbitrary (e.g. inner tube area, outer tube area, mean value). Typically, the outer area is used and one has to calculate $1/U$ as described in (18). Subscript i means the inner, subscript o the outer tube whereas w means the wall and A_{lm} the logarithmic mean value of the heat exchange surface [Goedecke, p.284]. In further discussions the heat exchange area is meant to be the total outer surface of the tubes.

$$\frac{1}{U} = \frac{A/A_i}{h_i} + R_{f,i} + \frac{A/A_{lm}}{(k/Th)_w} + R_{f,o} + \frac{A/A_o}{h_o} \quad (18) \quad with$$

$$A = A_o \quad and \quad A_{lm} = \frac{A - A_i}{\log(\frac{A}{A_i})} \quad \Rightarrow$$

$$A/A_i = d_{t,o}/d_{t,i}$$

$$A/A_{lm} = \frac{d_{t,a} \cdot \log(\frac{d_{t,a}}{d_{t,i}})}{2 \cdot Th_t}$$

As the parameters, especially the Prandtl number, depend highly on the temperature, this is just a rough estimation and after the lay out, one has to confirm the functionality of the chosen heat exchanger. In general,

one does this with an iterative method. The chosen iterative method is described in [Kuppan, p.208ff] and was implemented in matlab (name).

After the initialization (with an assumed heat exchanger efficiency and the calculated outlet temperatures), one calculates the mean temperatures of the fluids. Then one can determine the temperature depending values (the Prandtl number, conductivity and specific heat) and calculate with this data the number of transfer units (*NTU*), which is defined as follows:

$$NTU = \frac{UA}{C_{\min}} \quad (19)$$

$$C = \dot{m} \cdot c_p \quad (20)$$

whereby *C* is the so called heat capacity rate. $C_{\min}$ denotes the minimal heat capacity rate, which is in this case the heat capacity rate of mercury. The flow with the smaller heat capacity rate is also called "weak" stream. [Kuppan, p. 30]. With the heat capacity ratio C^* between $C_{\max}$ and $C_{\min}$, one can calculate the efficiency of a counterflow heat exchanger according to [Wong, p. 160f]

$$\varepsilon = \varepsilon(NTU, C^*, \textit{flowtype}) = \frac{B - e^{-NTU}}{B - C^* e^{-NTU}} \quad (21) \qquad \textit{with}$$

$$C^* = \frac{C_{\max}}{C_{\min}}$$

$$B = e^{-(NTU)\cdot C^*}$$

With the efficiency one can calculate the new inlet and outlet temperatures.

$$t_{h,out} = t_{h,in} - \varepsilon \frac{C_{\min}}{C_h} \cdot (t_{h,in} - t_{c,in}) \quad (22a)$$

$$t_{c,out} = t_{c,in} + \varepsilon \frac{C_{\min}}{C_c} \cdot (t_{h,in} - t_{c,in}) \quad (22b)$$

This method uses in each step the log mean temperature in order to specify the thermophysical properties of the two liquids and reaches so a higher precision. Therefore, there were calculated functions for the needed properties of water in a range between 20°C and 80°C and for mercury between 20°C and 200°C. This was done in a very simple fashion with a matlab linear interpolation.

For a single pass counterflow heat exchanger, an effectiveness of 80%-85% is standard. Because the heat exchanger lay out does not uses fins for improvement of heat transfer, the factors η_f and η_o which describe this phenomena are in that case just 1 (for details see 7.4).

Dimensioning

A shell & tube heat exchanger was chosen for the Eurisol loop. It provides good pressure stability and a simple design. The main issue is to prevent leaks, otherwise, the cooling water could be highly contaminated. The best safety against leakage is a double walled tube. That means that two tubes have with an interspatial gas between them, under higher pressure than the two fluids. If there is a leak, this pressure drives the gas outside, the decrease of the gas pressure can be measured and the loop will be stopped. The gap has to be very small for good heat conduction. To ensure an easy production of the double walled tubes, a single pass heat exchanger was chosen with counterflow. In addition, this design has the highest heat exchange efficiency. The Oak Ridge heat exchanger study was chosen for a first reference. As the material for the two (inner) tubes stainless steel 316L was chosen. To take the gap between the two tubes into account the conductivity of stainless steel was decreased about 10% to 15W/mK (17 W/mK at 125°C), the tube wall thickness is 2.49mm. According to [ESS, p.4-57], very small gaps can be neglected. Also, the fouling resistance on the water side as well as on the mercury side, is assumed as in the Oak Ridge report ($8.8 \cdot 10^{-5}$ mK/W each side) [OakRidge_b].

Water velocity (shell side)	0.12 m/s
Hg velocity (tube side)	0.57 m/s
Double-wall tubes	
Outer	15.9 mm outer diameter * 1.24 mm wall
Inner	12.7 mm outer diameter * 0.89 mm wall
Effective Length	2.74
Number	330
Thickness of 2 walls and gap	2.49 mm
Gap between tubes	0.36 mm
Fouling resistance	$8.85 \cdot 10^{-5}$ mK/W

Table 12: Parameters of Oak Ridge heat exchanger

The main dimensioning parameter for heat exchangers is the surface area, on which the heat flux occurs. Estimation of the area with a one tube model yields to 60-120m², depending on the parameters of the fluids. Three lay outs were studied with the implemented matlab code ("HeatExchanger.m").

	# tubes	Tube dia. [mm]	Shell dia. [mm]	Effective length [m]	A [m²]	Velocity Hg [m/s]	Velocity Water [m/s]
Lay Out (1)	330	15.9	1000 (D_h 146.7)	6.0	98.9	0.5439	0.0992
Lay Out (2)	660	15.9	2000 (D_h 306.8)	3.0	98.9	0.2720	0.0237
Lay out (3)	660	15.9	1038.3 (D_h 79.0)	3.0	98.9	0.2720	0.0992

Table 13: Main parameters of compared heat exchangers

The result for lay out 1 is Q = 2.74 MW at an efficiency of 0.688 with a mercury outlet temperature of 61.3 °C and a water outlet temperature of 47.6 °C. This type heat exchanger would satisfy the conditions, but is too long.

The result for layout 2 is Q = 1.22 MW at an efficiency of 0.307 with a mercury outlet temperature of 110.2°C and a water outlet temperature of 32.2 °C. Heat transfer is too low due to too less convection on the water side.

The result for layout 3 is Q = 2.87 MW at an efficiency with a mercury outlet temperature of 57.4°C and a water outlet temperature of 48.9°C.

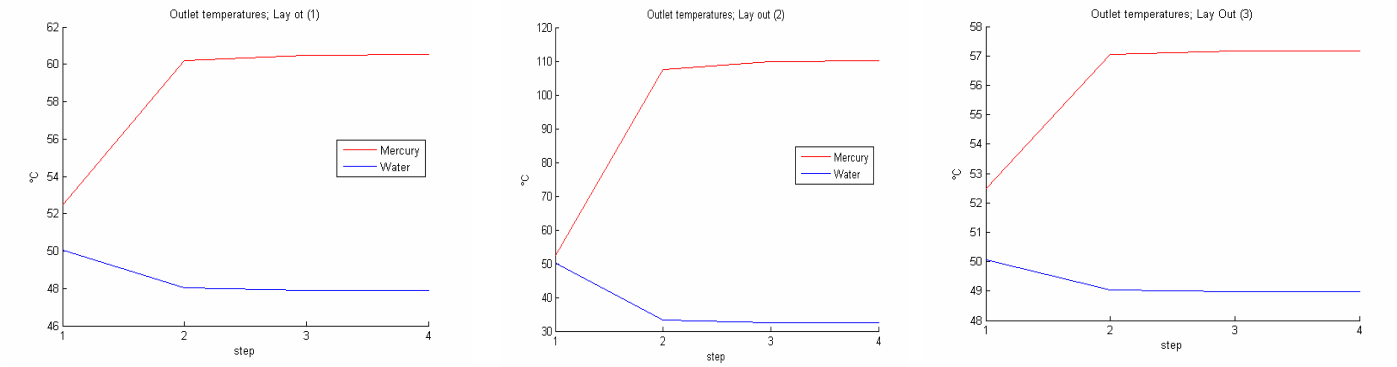

Figure 38: Outlet temperatures (lay-out 1, 2 and 3)

Table 14 shows the resistances of the three lay outs. The main contribution to the total resistance is on the water side.

R [m°C/W]	Tube side	Water side	Total fouling	Wall
Lay out (1)	$2.43*10^{-5}$	$2.2*10^{-3}$	$1.76*10^{-4}$	$1.67*10^{-4}$
Lay out (2)	$3.94*10^{-5}$	$7.9*10^{-3}$	$1.76*10^{-4}$	$1.67*10^{-4}$
Lay out (3)	$4.26*10^{-5}$	$1.8*10^{-3}$	$1.76*10^{-4}$	$1.67*10^{-4}$

Table 14: Resistance of the lay-outs

Formula (12) inserted in (11) describes the convection of water, which should be increased. Therefore, a smaller equivalent hydraulic diameter and a higher velocity are desired.

$$h = (0.023 \cdot \left(\frac{wD_h}{\gamma} \right)^{0.8} + \mathrm{Pr}^{0.4}) \cdot \frac{k}{D_h} \quad (23)$$

So, lay out (3) has the best convection of water, and also the best cooling results for mercury. Lay out (2), with the highest hydraulic diameter and the lowest velocity of water, is the worst heat exchanger. Of course, there are limitations for decreasing the hydraulic diameter as well as for increasing the velocity. The tubes may not be too close together and the water needs some time to heat up.

The next step is to optimize the exchanger in respect to its size as well as its pressure drop and should be carried out by a specialist. Of course, the pressure drop depends on the construction and so the calculated pressure drop (see 2.7) is just an estimation. Often, it can be decreased by baffles and smooth devices. Weight of this heat exchanger is 4.3t (2.5t of mercury and 1.8t of steel).

Outlook

[Kuppan] suggests on page 273 a determination of the tube bundle size and tube length. There is recommended a ratio between tube length and the square tube bundle diameter of 8 for first lay outs. This would lead to a bundle diameter d_{tb} of 375 mm for 3 meter tube length and 750 mm bundle diameter D_{tb} for 6 meter tube length. Following formula defines the distance between the inner tubes L_{tp} (tube pitch) where θ_{tp} describes the angle between the tubes (see appendix).

$$N_t = \frac{0.78 \cdot d_{tb}^2}{C_1 \cdot L_{tp}^2} \qquad C_1 = 0.86 \quad for \quad \theta_{tp} = 30$$

$$C_1 = 1 \quad for \quad \theta_{tp} = 45^o \; and \; 90^o$$

There should be a assumed distance of 10mm between the outer tubes of the bundle and the inner diameter of the shell. In the case of a rectangular pattern the tube pitch length L_{tp} for the 3 lay outs are shown in table 3.

	Lay out (1)	Lay out (2)	Lay out (3)
L_{tp} [mm]	47.64	68.07	35.01

Table 15: Tube pitches of lay outs

A tube bundle diameter of 375 mm for 660 tubes would lead to a tube pitch of 13.60 mm which is less than the diameter of the tubes. As that kind of heat exchanger is too compact the ratio of 8 can not be applied. The result for the 6 meter heat exchanger and 330 tubes is a tube pitch of 37.44 mm.

3.3 Expansion tank and gas separator

This device is placed on the highest part of the loop. It provides space for the thermal expansion of mercury. It has to be clarified if this device also has to separate gas out of the mercury. Two lay outs will be shown. The first one will mainly serve as an expansion tank, but also has some separating capability (draft 1). The second one is a standard approach for separating gas, and will also provide space for thermal expansion (draft 2).

Both types will have a mercury surface covered with gas (Argon is suggested). A maximal cover gas pressure, which does not exceed, in addition with the maximal static pressure of mercury and pressure head of the pump, the lay out pressure of 40 bar, has to be defined.

The possible detection of 1l mercury leakage is examined for both drafts.

Specification

Mercury is filled into the loop at room temperature (20°C). The mean temperature of the loop during operation is assumed to be 100°C. Heating 20t of mercury from 20°C to 100°C yields 21.4 litres of thermal expansion. The lay-out space of the expansion tank is 25litres. The separator should be able to remove 8 norm-litres of gas per month.

The tank should include mercury leakage detection capabilities. The leakage of mercury results in a lower level inside the tank. This could be measured with the static pressure difference of mercury between two points (of different height). The second possibility is measuring the cover gas pressure, which will decrease, due to the increasing cover gas volume.

Draft 1

Draft 1 aims to minimize the cover gas volume. Accordingly, the gas supply tank can be smaller. In addition, the leakage of mercury inside the tank can be discovered easier. The cover gas surface is 15cm x 15cm. The cover gas volume is about 3 litres (13cm in height).

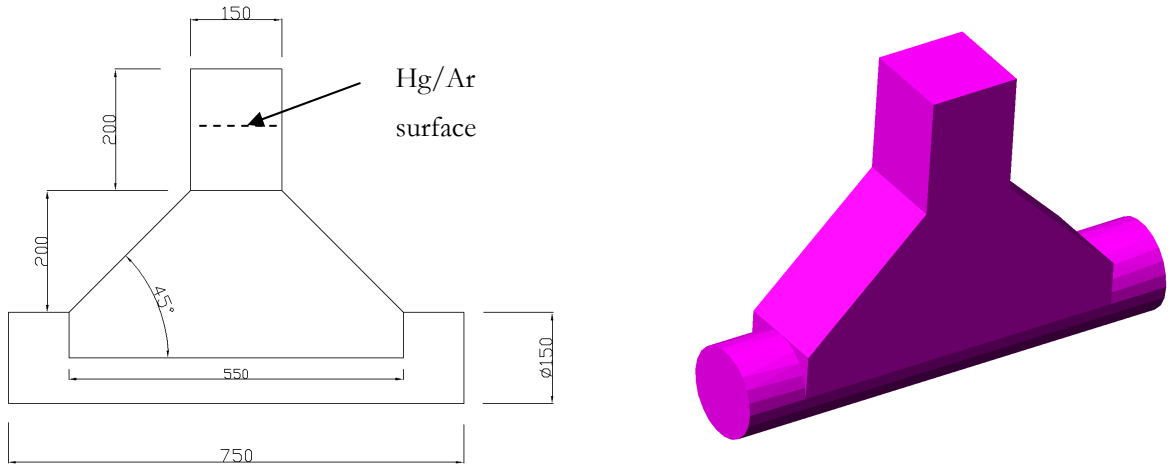

Figure 39: Draft 2 of expansion tank/gas separator

The resulting cover gas pressure is shown in table 16 (all given values in bar), for 1l of leaked mercury. Argon and Helium are examined. The van-der-Waals equation was used, and the implemented matlab code ("dPExpansionTank.m") is attached on the CD.

Initial pressure	1	5	10	20
Argon	0.75	3.75	7.51	15.0
Helium	0.75	3.75	7.48	14.9

Table 16: Cover gas pressure in draft 1 after 1l mercury leakage, depending on initial pressure (all values in bar)

Leakage of 1 litre mercury causes a 4.4cm decrease of the level. This results in a decrease of the static pressure inside the mercury of only 0.058bar.

Draft 2

The draft for the separator can be found in [Bucenieks_b, p.21f]. Within the gas separator, a stream velocity of roughly 0.1 m/s is desired, therefore, the inner diameter of the separator is 474mm. The total length of the separator is estimated at 1m, the sketch is shown in figure 40. Separating cover gas surface is estimated to be 60cm x 10cm. With a height of 10cm, the cover gas volume is 6litres; cover gas pressure after 1l mercury leakage is given in table 17.

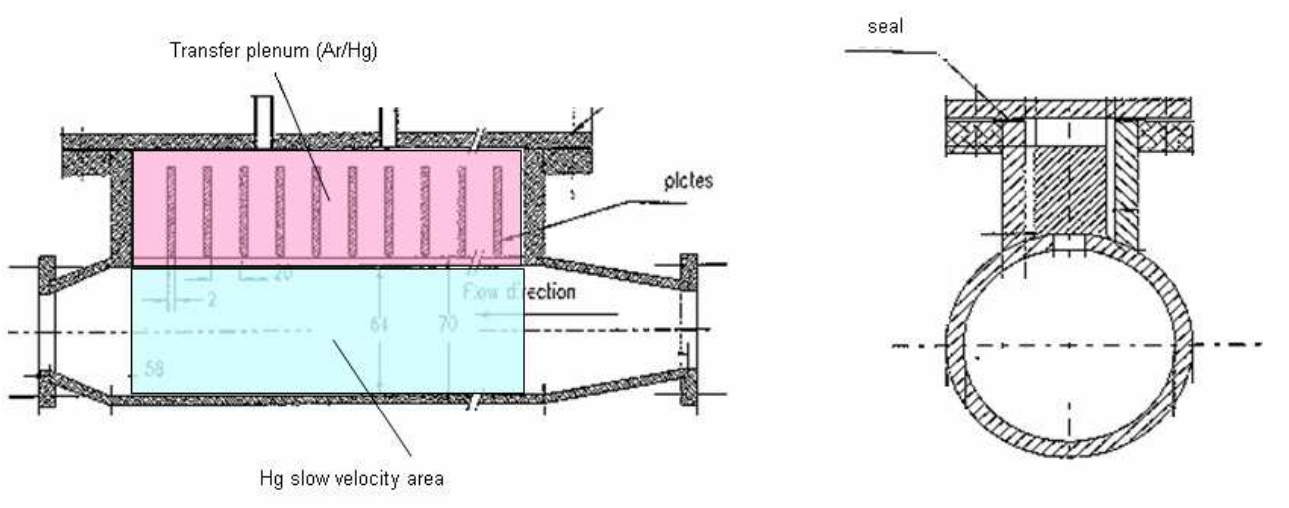

Figure 40: Draft 2 of expansion tank/gas separator

Initial pressure	1	5	10	20
Argon	0.86	4.29	8.58	17.2
Helium	0.86	4.28	8.56	17.1

Table 17: Cover gas pressure in draft 2 after 1l mercury leakage, depending on initial pressure (all values in bar)

The leakage would result in a 1.6cm decrease of the mercury level, which is equivalent to 0.022bar in static pressure.

Results

The static pressure difference is not suitable for leakage detection. The behaviour of Argon does not differ much from Helium, as the pressure (and temperature) are not very high. Pressure drops of both drafts are big enough to identify a mercury leakage of 1l. The weight of draft 1 is not considered (only few mercury inside), draft 2 weights about 2.1t (2t of mercury, 100kg steel).

Gas could also separate in the drain tank, after the mercury has been drained. The final decision, which kind of expansion tank is to be installed, should take this into consideration as well.

3.4 Drain Tank

Dimensioning

The task of the drain tank is to store the mercury if maintenance work on the loop or an emergency shut down are necessary. The drain tank was layed out for 20t of mercury (equals to 1.5m³). During an emergency shut down, there is no time to reduce the cover gas pressure before opening the draining valves, and therefore, the drain tank has the same lay out pressure level as the loop (40 bar). The drain tank should be installed on an inline.

The high pressure invokes a large thickness of the walls; hence, a round shape for the tank should be preferred. The middle part of the suggested drain tank consists of a 1.10m long tube with an outer diameter of 1067mm. The end caps are half spheres, accordingly, the total length of the tank is about 2.20m. Plates with fillets, used as end caps, would require too thick walls.

The required tube thickness s is calculated with formula). C_1 describes the fabrication tolerance, c_2 the corrosion and abrasion, σ_{zul} the highest stress allowed (115MPa for 100°C) and the factor υ_N describes the connections (high quality weldings factor 1). With a tolerance of 3mm and 1mm of corrosion, the wall has to be at least 8.56mm thick.

$$s = s_v + c_1 + c_2 \quad (24)$$

$$s_v = \frac{d_a \cdot p}{(2\sigma_{zul} - p) \cdot \upsilon_N + 2p} \quad (25)$$

The thickness of the flat plates as end caps are calculated according to formula 26; *C* denotes a constant (0.3 in this case), *r* the fillet radius. A fillet radius of 200mm would result to a thickness, s_v, of 48.5mm, a radius of 400mm result to 37.4mm. Formula 27 describes the required wall thickness for an end sphere, with its radius *r*. With a tolerance of 2mm and 1mm of corrosion, the wall has to be at least 12.28mm thick. Next norm wall thickness according to DIN V EN V 10 220 (2), (see appendix) is 13.1mm.

$$s_v = C(d_i - r) \cdot \sqrt{\frac{p}{\sigma_{zul}}} \quad (26)$$

$$s_v = \frac{p \cdot r}{2 \cdot \sigma_{zul}} \quad (27)$$

Decay heat removal

The decay heat of mercury (see 2.3) has to be removed. Therefore, the drain tank is embedded in a water basin. The water could be cooled by natural convection (additional water buffer) or by a provided water flow. Natural convection does not depend on an additional pump or the main water cooling circuit. This is an advantage during an emergency. The drawback of this system is the further storage tank (water buffer). In the loop lay-outs, a water buffer (length 2.50m, height 1.3m, width 0.75m; 2.4m³) was included. The natural convection was simulated with a matlab code "NaturalConvection.m". It simulates the natural convection due to density

differences and the resulting forces. Temperature in the mercury, as well as in the water buffer and the water surrounding the drain tank in a smaller tank, is homogenous. The result for an assumed friction coefficient of 0.05 and a water mass of 500kg in the small tank is shown in the left chart of figure 41. The right chart shows the water flow rate. As simulation does not consider the heat conduction process inside mercury, the temperature of mercury in the middle of drain tank is higher than calculated. Still, this kind of heat removal should work, as the heat conduction in metals is good.

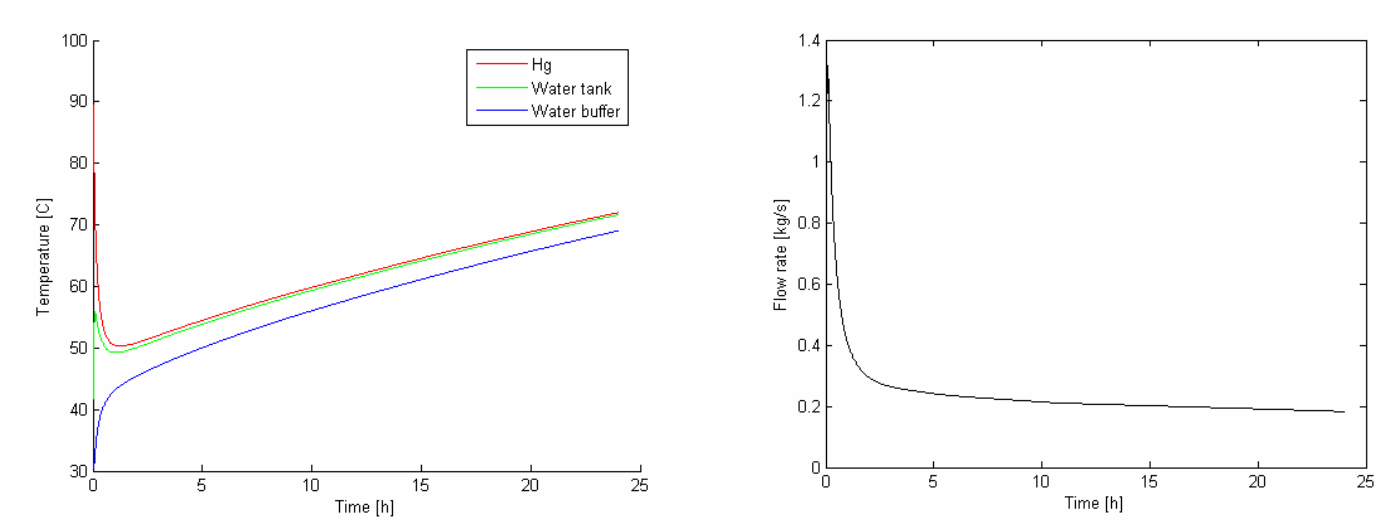

Figure 41: Natural convecion for drain tank cooling

The cooling water flow could also be provided by a pump and the water buffer could be saved.

4 Measurement devices

The main challenge for measurement devices and valves in the loop is radiation (mainly gamma ray from the tubes and neutrons from the target). Electrical devices should not be used. It will probably not be possible to reach the estimated life-time of 20 years with the devices described in chapter 4. Therefore, a redundant lay out is important, but, still some of them have to be replaced. Easy replacement has to be ensured as well.

4.1 Temperature

A very important issue while running the loop is to measure the temperature at certain points. In particular, the knowledge of the temperature at the exit of the target is of high interest. This temperature is an important shut down criteria, as boiling mercury within the target would damage the target and, therefore, result in a leak.

There are two types of temperature measurement. One includes contact with the medium in order to measure and the other is without contact. Measurement devices without contact often use pyrometers for determining the heat radiation of the medium. In this way, one can also get an image of the temperature allocation on the plates or in space.
Measurement devices with contact to the medium can be distinguished by the mode of operation. There are three types which use:

- mechanical properties (thermal elongation coefficient)
- phase properties
- electrical properties

for assessing the temperature of the medium. Classical thermometers are mechanical. The most famous is the mercury thermometer. More modern thermometers are the bimetallic ones, which use two metals with different thermal expansion coefficients. They are normally shaped as a helix or a screw. An example for a thermometer using the phase properties is the so called "Seger cone". The cone, made of a material with a well known melting point, is installed on a surface. If the surface reaches the melting point, the cone will start melting and consequently it will topple down. These cones are used for testing the refractability of materials.
The electrical thermometers are divided in three subcategories:

- electrical resistance thermometers
- semiconductor sensors
- thermocouples.

Electrical resistance thermometers use the effect that hot metals have a higher electrical resistance than cold metals. Also, the electrical conductivity of semiconductors depends highly on the temperature [Strohrmann].

To measure the temperature in the loop, thermocouples were chosen. They have proven to be very reliable. Electrical resistance thermometers and semiconductor sensors are more precise, but have several disadvantages. The main disadvantage is that the connection cables to these devices are, in general, normal cables, isolated with synthetic material; these are damaged by irradiation. Furthermore, 4 conductors are necessary to eliminate the influence of errors based on cable length. This, and a very unusual isolation, would result to a very high price. In addition, these devises are surrounded by a rigid metal protection body and therefore not flexible.

Thermocouples are divided in different type classes, which depend on the materials of conductors. These determine the working temperature range. The delivery program of Thermocoax is stated below [Thermocoax].

Type	Temperature range	Material
K	-200°C … + 1000°C	Chromel® (+) / Alumel® (-)
J	-40°C … + 750°C	Iron (+) / Constantan® (-)
N	-40°C … + 1300°C	Nicrosil® (+) / Nisil® (-)
E	-200°C … + 900°C	Chromel® (+) / Constantan® (-)
T	-200°C … + 350°C	Copper (+) / Constantan® (-)

Table 18: Thermocouples of Thermocoax

There are three types of tips, as illustrated in figure 42; grounded and, especially, exposed tips have a very fast response to temperature change. As this feature is not important within the loop, an ungrounded tip is preferred. First, it provides better mechanical and radiation protection. Secondly, the operational reliability of thermocouples with this tip can be easily checked. As the insulation is also high at the tip, one can check mechanical damage of the insulation by measuring the electrical resistance. If the resistance is remarkably lowered, it means that there is mechanical damage of the insulation, and that the thermocouple should be replaced. This check is not possible with the two other tip styles.

Figure 42: Thermocouples tip styles [http://www.omega.com/prodinfo/thermocouplesensor.html]

Thermocouples type K with a diameter of 1.5mm, with an ungrounded tip and Ac as mantel material were selected. Connection with the hot cell can be done with norm clips, which do not necessarily have to be made of the same material as the thermocouples.

4.2 Pressure

In the hot cell, pressure measurement is challenging, as electric devices should not be used inside the cell. However, there are four possible applications for pressure measurement. The first two mentioned points are direct pressure measurements, the last two points involve relative pressure measurement.

- Pressure of cover gas
- Mercury pressure near or inside target (could indicate begin of boiling of mercury)
- Mercury pressure difference inside a Venturi flow meter
- Mercury static pressure difference inside expansion tank (indicating level)

It is necessary to know the cover gas pressure, as this pressure prevents mercury inside the target from cavitation. Furthermore, this pressure can indicate mercury leakage, as shown in 3.3.

All pressure measurements should be realized with so called „transducers". They transduce the pressure from the mercury via a membrane through a small channel filled with fluid. In this way, electronic equipment inside the hot cell can be avoided. Membranes are made of metal. There are special transducing oils which are stated to be "irradiation resistible" (e.g. "Spezialöl N" from the company Bachofen). However, one has to verify the dose rate implied on the oil. Especially measurement near the target could yield to early damage of the oil. The production of gases in the oil during irradiation changes its compressibility, leading to mistakes in the measurement, which are difficult to correct.

4.3 Level meter

A mercury level meter is placed in the expansion tank. It is absolutely necessary during the filling of the loop for indicating when the mercury has reached the correct level. During the process, the level meter must be capable of warning of too high or too low mercury levels, because this would damage the loop.
Common level meters use several heater/thermocouple bundles. The heater heats the thermocouple to a certain temperature. The power required for this in the cover gas, is different from heating a bundle in mercury (due to different convection and conduction). So, each bundle registers if it is surrounded by the cover gas or by mercury. With several of these bundles, one can get a discrete image of the level. It is suggested to use 5 levels. The level indicates: "too low", "low", "nominal", "high" or "too high". The first and the last level bundles have to be layed out redundantly.

More sophisticated level meters could indicate unusual level due to

- mercury leackage
- uncommon beam

- vibrations.

The most important of these points is mercury leakage. Unfortunately, irradiation radically reduces the possible devices (e.g. no laser level meters). The only reliable possibility is a continuous level meter, could measure the static pressure difference inside mercury by transducers. The static pressure difference of mercury per centimetre is 0.0132bar.

4.4 Flow meter

Flow meters could be installed for measuring the flow rate of mercury. Possible applications are.

- Independent check, if the pump is working correctly (before starting the beam)
- Data for checking temperature measurements (flow rate, proton power and temperature are known)
- Independent indicating of pump failure (decrease of flow) during operation.

The pump can additionally provide a self-check. The last point implies a short reaction time of the flow meter. In addition, the flow will have some small fluctuations.

Possible flow meters are:

- Venturi tube
- Electromagnetic flow meter
- Ultra sound flow meter

A Venturi tube was dimensioned according to EN ISO 5167-1 and this yielded to a length between 1.0m-1.6m. Venturi flow meters are reliable (if the pressure measurement works), but require sealing. EM flow meters as well as flow meters using ultra sound do not have this disadvantage. Furthermore, they are smaller. Ultra sound flow meters are precise, but up till now, no radiation resistible one exists. It is suggested to use an EM flow meter in the loop, but it has to be located at least half a meter away from the EMP; otherwise, the EM-field of the pump would influence the flow measurement.

4.5 Mercury concentration in the air

Measurement of the mercury concentration in the hot cell air has to be provided. The concentration in the air could range between 0 and 30 mg/m^3. Depending on their location and precision, they could be used as leakage detectors.

5 Design of the loop

Within this chapter, the dimensioning of the tubes and the flanges is carried out. Furthermore, compensation of thermal expansion is discussed as well as possible valves.

5.1 Dimensioning of the tubes

This section deals with dimensioning the thickness of the tubes, bends and T-connectors (tees) for PN 40. To get an inner diameter of at least 150mm for the tubes, an outer diameter of 168.3 mm was selected, referring to DIN V EN V 10 220 (2) (see appendix). The material of the tubes is stainless steel 316L. The design stress for 316L is 108 MPa (200 °C). The total weight of 15m tubes is 4.1t (3.6t of mercury, 0.5t of steel).
Within the steel, higher stresses than 108 MPa should not occur; which means that the deformation is elastic. Therefore, the influence of cycles (beam shut downs) can be neglected. According to [RRC-MR, p.31], the influence of operating hours is neglectable for temperatures under 425°C.

Tube

The required tube thickness, s, is calculated with formula 24 (compare chapter drain tank). C_1 describes the fabrication tolerance, c_2 the corrosion and abrasion, respectively.

$$s = s_v + c_1 + c_2$$

$$s_v = \frac{d_a \cdot p}{(2\sigma_{zul} - p) \cdot \upsilon_N + 2p} = 2.89mm$$

A feasible value for c_1 is 1.0mm, c_2 was assumed to be maximal 3.0 mm. The minimal thickness, s, is 6.89mm and the next higher norm is 7.39mm. Accordingly, the inner tube diameter is 153.52mm.

Elbow

The inner and outer tube thickness of the elbows was calculated in relation to AD 2000 (B1 Anlage1). The radius of the elbows is 230mm, the inner diameter d_i 153.52 mm. With the same c1 and c2, this leads to an inner wall thickness, s_i, of 7.66 mm and an outer wall thickness s_o of 6.52 mm.

$$s_{v,i} = s_v \cdot B_i$$

$$s_{v,o} = s_v \cdot B_o$$

$$B_i = \frac{r}{s_v} - \frac{d_i}{2s_v} - \sqrt{\left(\frac{r}{s_v} - \frac{d_i}{2s_v}\right)^2 - 2 \cdot \frac{r}{s_v} + \frac{d_i}{2s_v}}$$

$$B_o = \sqrt{\left(\frac{r}{s_v} + \frac{d_i}{2s_v}\right)^2 + 2 \cdot \frac{r}{s_v} + \frac{d_i}{2s_v}} - \frac{d_i}{2s_v} - \frac{r}{s_v}$$

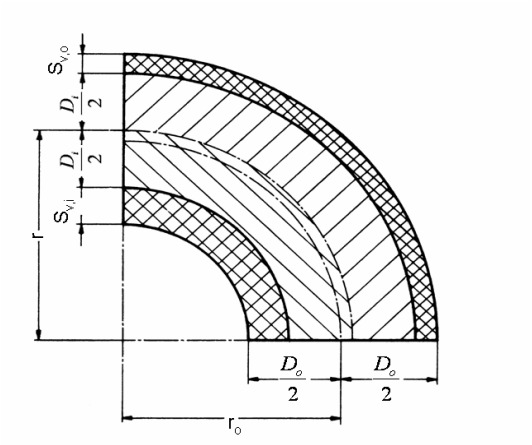

Figure 43: Elbow

Tee

The tees used for draining should have the same diameter as the tubes of the loop. In this way, a rapid draining is ensured in an emergency. With the given values ($s_{v,0}$ = $s_{v,1}$ = 7.39mm; d_i = 152mm), the results are (subscript 0 denotes the main tube, subscript 2 denotes the branch tube):

a0 = 21.0mm, *a1* = 26.3mm and $s_{vt,0}$ = $s_{vt,1}$ = 11.37mm. The parameter *a* is the required length of the fortification.

$$s_{vt,0} = \frac{s_{v,0}}{v_A}$$

$$s_{vt,1} = \frac{s_{v,1}}{v_A}$$

$$a_0 = \sqrt{(d_{i,0} + s_{v,0}) \cdot s_{v,0}}$$

$$a_1 = 1.25 \cdot \sqrt{(d_{i,1} + s_{v,1}) \cdot s_{v,1}}$$

$$v_A = \frac{a_0 + a_1 \cdot \frac{s_{v,1}}{s_{v,0}} + s_{v,1}}{a_0 + s_{v,1} + \frac{d_{i,1}}{2} + \frac{d_{i,1}}{d_{i,0}} \cdot (a_1 + s_{v,0})}$$

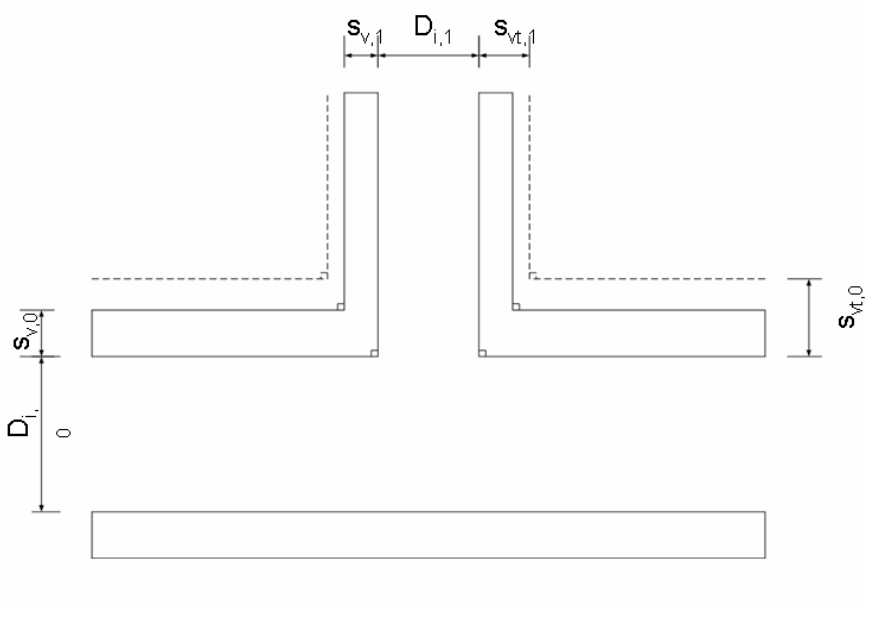

Figure 44: Tee

5.2 Flange

DIN 2635 serves as a draft for the flange design at a pressure of 40 bar (for PN25 DIN2634, for PN16 DIN 2633) [Flansche, p.170ff]. DIN 2635 can be looked up in the appendix, DIN 2634 and 2633 can be found on the CD.

Thermal stress can be higher in the flanges, due to their more complex shape (compared to a normal tube). Thermal gradients exist during

- nominal operation
- starting up of the beam
- beam failure (cold slag).

During nominal operation, the temperature gradient is very small (the surrounding air has a poor convection capability). When the beam starts, the mercury could be heated from room temperature to 180°C. As it takes several seconds to reach the full power of the beam, this case is neglected. The failure of the beam is very prompt and a slug of cold mercury (60°C) follows the hot mercury (180°C).
This case was studied first as a static problem (60°C on the mercury side and 180°C on the air side). Because very high stresses were calculated (up to 300MPa in the middle of the flange on the mercury side), transient simulations were carried out. The calculated maximal stresses are still in the same range. Figure 45 illustrates the static simulation, figure 46 the transient one (10 seconds after begin of the cold slag).

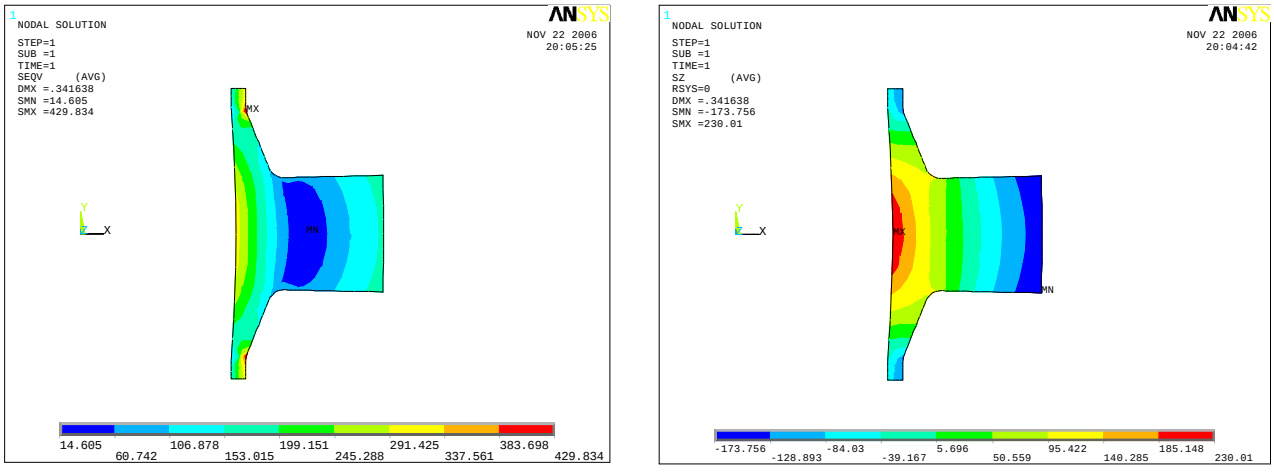

Figure 45: Flange, static case (left: von der Mises stress, right: z-stress; in MPa)

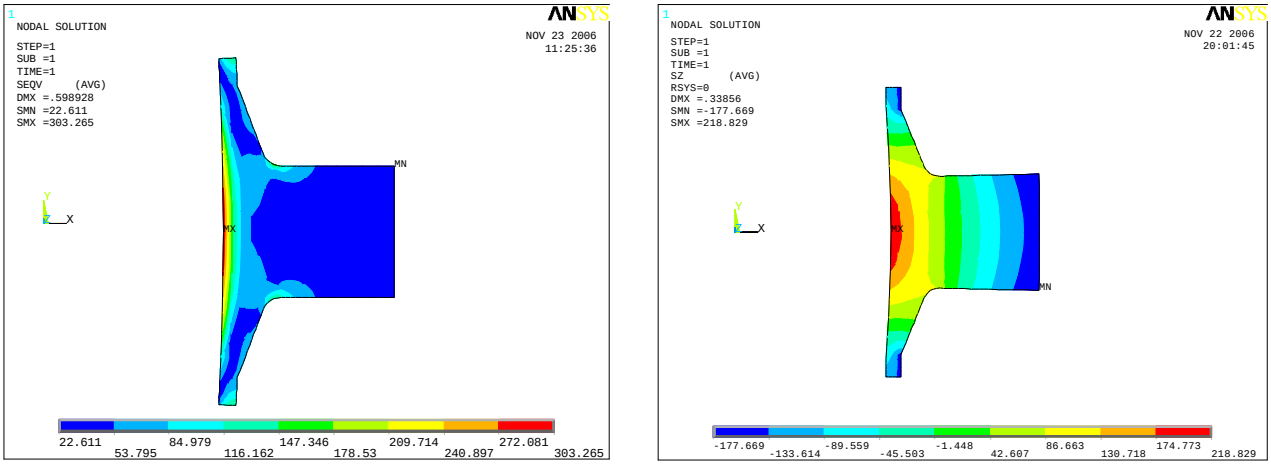

Figure 46: Flange, transient case (left: von der Mises stress, rigth: z-stress; in MPa)

5.3 Compensation of thermal expansion

The tube between the target and the heat exchanger gets heated, and, therefore is a point of special investigations. Thermal expansion could be compensated by bellows. Unfortunately, their usage includes the danger of leakage. A safer way of compensating the expansion is a special tube arrangement. U-shaped tube structures are very common for this purpose. Due to lay-out reasons, an S-shaped arrangement is preferred in this case.

The tube will be assembled at room temperature and get heated to the nominal temperature of 180°C. With a safety a margin, a temperature difference of 200°C was taken for the thermal expansion calculations in ANSYS ("S_compensator.lgw"). Linear heat expansion coefficients of 316L steel at 20°C, 100°C and 200°C were used for interpolation. Figure 47 shows a typical result, all calculated data is given in 7.6.

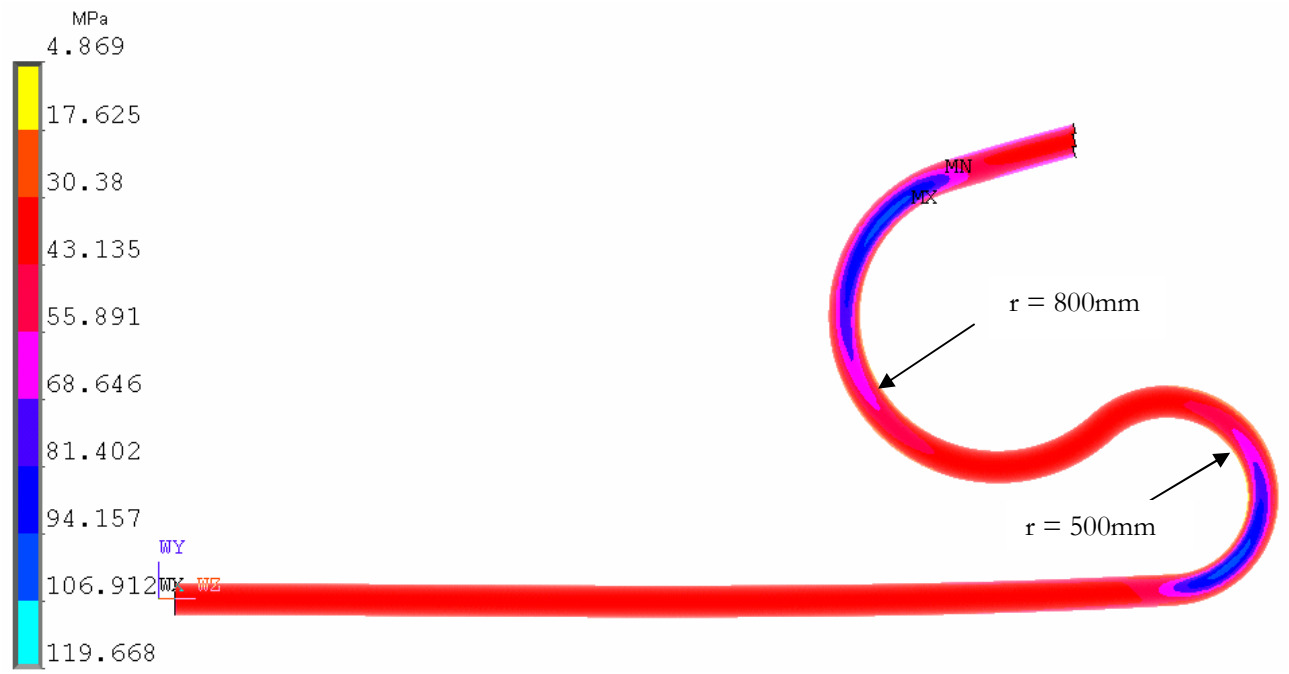

Figure 47: Von Mises stress for tubes (S-arrangent)

5.4 Valves

There are three types of valves directly linked with the loop, all of them should be opened and closed from the control room:

- draining valves
- gas valves (expansion tank and drain tank)
- release valves (in the local highest points of the loop to release gas pockets)
- safety valve (rupture disc in drain tank)

The rupture disk should be made of metal and fail at norm pressure in order to release the over pressure and, in the worst case, also some mercury into the emergency tank. One of the biggest he challenges are the draining valves. The company Phoenix has got some experience with mercury valves. Drawing of a mercury valve and a photo is attached on the CD and can be used as draft.

5.5 Design

Two loop designs were done with IDEAS. The files are saved on the CD "names". Both lay out loops consist of

- heat exchanger (3 meter long, 1.0 meter in diameter)

- pump (2.50 meter long, 1.0 meter in diameter)
- gas separator draft 2 (1.0 meter long, diameter 50cm)
- drain tank (not visible; length 2.20m, diameter 1.0m) in surrounding water tank (length 2.65m, diameter 1.30m)
- water buffer (length 2.50m, height 1.3m, width 0.75m)
- shielding I (4.0 meter thick, 3 meter in width)
- space for shielding II
- redundant valves for draining at the lowest point(s) in the loop

The first draft is optimized for operation. A second draft was sketched out, because draft 1 was too big.

Draft 1

Draft 1 includes S-arrangement of the tubes for thermal expansion compensation. In addition, one flow meter (1 meter Venturi tube) is placed after the heat exchanger and a second one (1.6 meter) is placed after the gas separator. There is only one lowest point and the slope is 8%, the total height is 6.50m, the length 6m and the width (as by draft 2) 3m (dimensions except shielding I).

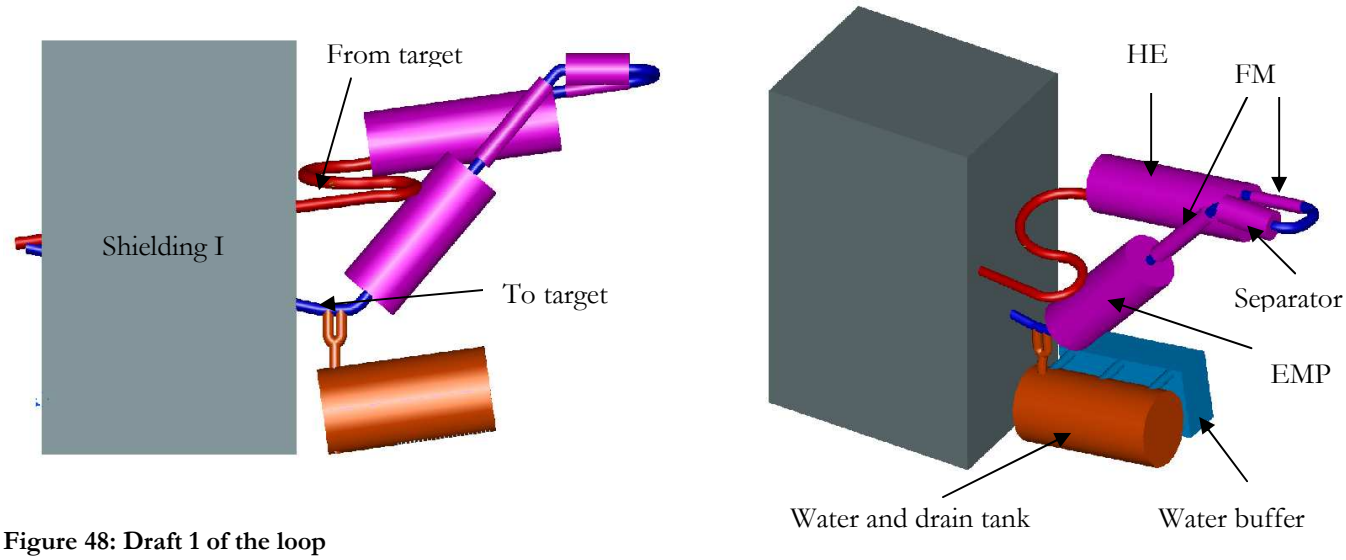

Figure 48: Draft 1 of the loop

Draft 2

To reduce the height, only one electromagnetic flow meter (length 20cm) is installed. Bellows are mounted before and after the drain tubes. The slope within the loop is 2%, the total height is 4.50m, the length 4.50m and the width (as by draft 1) 3m (dimensions except shielding I).

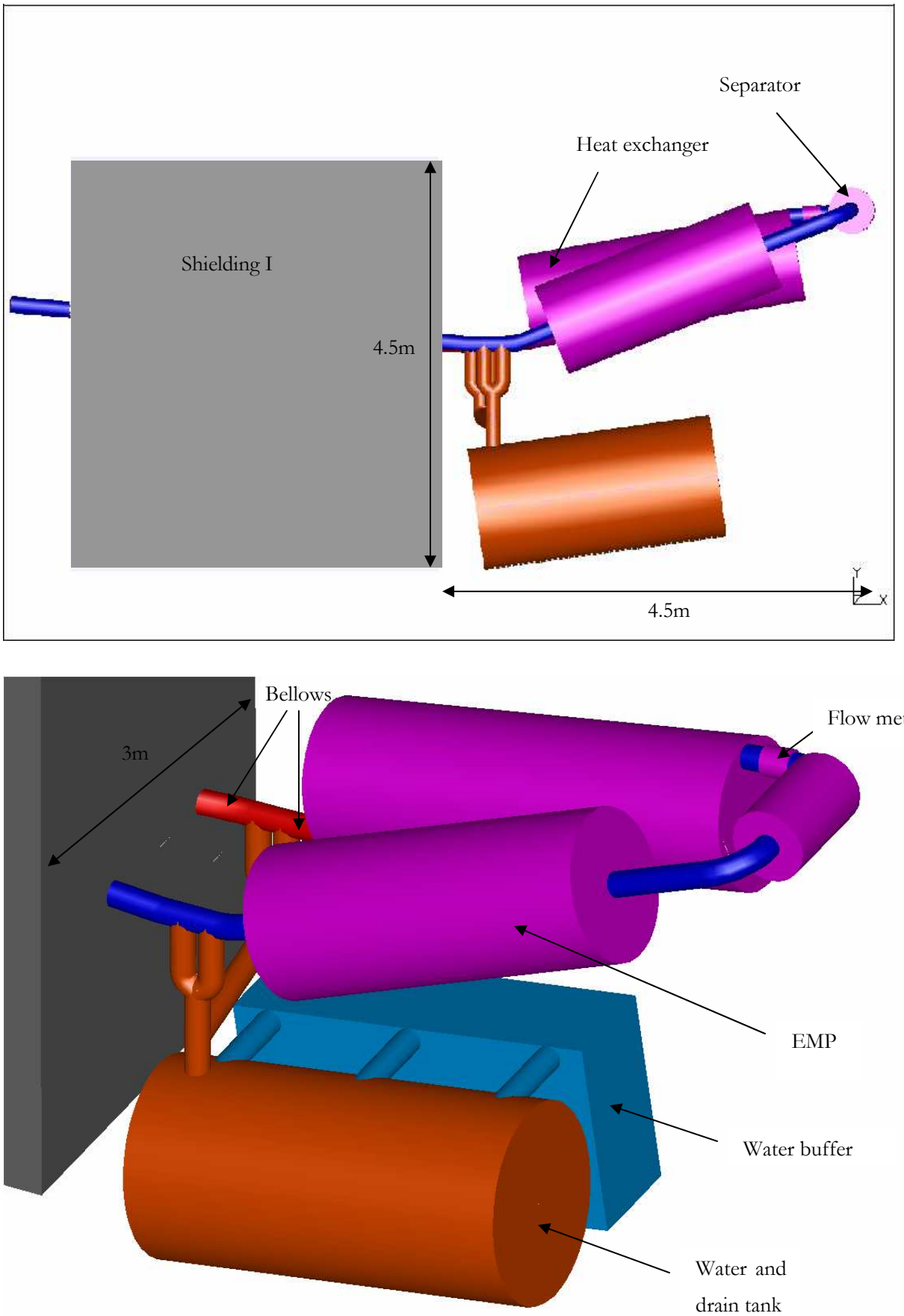

Figure 49: Draft 2 of loop

5.6 Operation of the loop

Several situations shall be discussed in the following. It has to be ensured that there is only the chosen cover gas inside the expansion tank and no air. The oxygen in the air would cause corrosion (see 2.2).

5.6.1 Installation of loop

After the loop has been installed air should be sucked out and the loop should be rinsed by Argon. After that, a pump device has to safely transfer the mercury inside the drain tank. It is suggested that this fill-in tube is used as transfer a tube for an emergency expansion tank. The hole should be closed by a safety valve which crumbles at the lay-out pressure of 40bar.

5.6.2 Filling of loop

Pressurized gas (Argon is suggested) will drive the mercury from the drain tank into the tubes of the loop. The gas pressure has to exceed the maximal static pressure of the mercury. This means an Argon pressure of 6.0 bar (height of loop 4.50m, mercury density 13500kg/m^3). When the level meter in the expansion tank shows the correct level, the further pressurizing of Argon is stopped by closing the Argon valves. Then, the mercury valves are closed. For pressurizing the drain tank (1.5m^3) with 6.0bar at norm temperature, 14.8kg (8900 norm-litres) of Argon is necessary (calculated with van-der –Waals equation). Within the target, due to its design, there will probably be a local highest point, and, hence also a gas pocket, and, thus, there should be also a release valve.

5.6.3 Normal operation

Before launching the proton beam, the pump has to deliver the nominal flow rate of 180kg/s. This can be checked via flow meter and verified by the pump itself (e.g. power consumption). Afterwards, the cooling water pump has to be started, providing the nominal flow rate of 24kg/s and then beam can be launched.

5.6.4 Draining of loop

Before starting of draining, the beam has to be shut down, as well as the pump. Electromagnetic pumps without fluid are not damaged immediately, but, as the heat is not removed by the mercury, it is preferable to shut down the pump before draining. After opening the valves, the mercury flows into the drain tank by the force of gravity.

5.6.5 Emergency shut down

There are four criteria for shut down. All of them could cause an increase of pressure and, therefore, damaging the loop. Accordingly, each criteria cause an emergency shut down.

- Target influx temperature too high (heat exchanger defect)
- Loss of flow, heat can not be removed properly (pump defect)
- Leakage of mercury, resulting in loss of flow and, furthermore, contaminating the hot cell (tube defect)
- Leakage of cover gas, resulting in danger of cavitation in target (expansion tank or valve defect)

Moreover, it has to be ensured that the proton beam does not exceed the nominal power of 4MW. The power of the beam line after the accelerator is higher (four additional targets with each 100kW) and distraction of the beam could be possible.

In case of an emergency, first proton beam has to be stopped, then the drain valves must be opened and then the loop pump must be stopped. If there is not water buffer for drain tank cooling, the cooling water flow has to be provided. Finally, the pump for the heat exchanger cooling water can be stopped.

5.7 Weight

Table 19 lists the components and their weight. The total weight is 240t.

	Steel/concrete [t]	Mercury [t]	Total [t]
Tubes (15m)	0.5	3.6	
Heat exchanger	1.8	2.5	
Gas separator	0.1	2.0	
Pump	0.01	0.14	
Shielding I	215	0	
Shielding II	14	0	
Sum	231.41	8.24	239.65

Table 19: Weight of loop (in tons)

6 Conclusion and future work

Two designs for the mercury loop were described. The dimensions of first draft are too big, therefore, a second draft was carried out. The length of the second loop is about 4.50m, height 4.50m and width 3m. The dimensions could be reduced by optimizing the main components, in particular the heat exchanger. Total weight of the loop is 240t (shielding I weights 215t). In order to reduce the weight that has to be transported by the trolley, shielding I should be optimized. A constructional solution should be found, where only the necessary part of shielding I has to be moved, the part which enclosures the mercury tubes.

Furthermore, the design of the target has a large influence on the loop lay out. Future work is listed below in order of importance:

- Final decision of beam parameters
- Final design of target
- Radiation problems (design of shieldings, investigation of irradiated tube surface, filter)
- Design of heat exchanger and pump
- Defining of the isotopes which should be separated
- Testing of the filtering methods and mounting in the loop design
- Constructional design of loop

Further future work will be designing the heat exchanger, detailed planning of the pump and if necessary, testing the separator or the whole loop. A decision has to be made whether or not separation of the gas is important. A final decision has to be made on the instrumentation and valves. Construction drawings must be issued and a cost analysis carried out.

7 Appendix

7.1 Material data

Material data according to [CRC,][Landolt] and [Wong].

Mercury

T [C]	ϱ [kg/m3]	Cp [J/kgC]	γ[m2/s]	k [W/mK]	Pr []
0	13628.22	140.3	1.24*10^-7	8.20	2.88*10^-6
20	13579.04	139.4	1.14	8.69	2.49
50	13505.84	138.6	1.04	9.40	2.07
100	13384.58	137.3	9.28*10^-8	10.51	1.62
150	13264.28	136.5	8.53	11.49	1.34
200	13144.94	135.9	8.02	12.34	1.16
250	13024.60	135.7	7.65	13.07	1.03

Table 20: Mercury data

Boiling temperature:

	Torr			Atm				
P	100	400	760	2	5	10	20	40
T [C]	260	330	365.9	398	465	517	581	657

Table 21: Boiling temperatures of mercury:

Vapour pressure:

D. Dampfdruck des Quecksilbers.

1. Dampfdruck des Quecksilbers in Torr zwischen —40 und +358 °C[1]).

Zehner \ Einer	ϑ in °C +0	+2	+4	+6	+8	
— 40	0,1793	0,2354	0,3066	0,4005	0,5195	× 10^{-5} Torr
— 30	0,6696	0,8559	1,090	1,383	1,747	
— 20	2,200	2,771	3,479	4,379	5,425	
— 10	0,6734	0,8343	1,032	1,279	1,553	× 10^{-4} Torr
0	1,898	2,314	2,811	3,407	4,130	
+ 10	0,4971	0,5980	0,7193	0,8658	1,024	× 10^{-3} Torr
+ 20	1,220	1,448	1,713	2,023	2,385	
+ 30	2,801	3,289	3,852	4,503	5,257	
+ 40	0,6118	0,7109	0,8240	0,9532	1,101	× 10^{-2} Torr
+ 50	1,272	1,464	1,679	1,930	2,210	
+ 60	2,526	2,883	3,285	3,738	4,243	
+ 70	4,823	5,463	6,177	6,979	7,869	
+ 80	0,8865	0,9975	1,120	1,2575	1,408	× 10^{-1} Torr
+ 90	1,576	1,761	1,965	2,190	2,439	
+100	2,713	3,014	3,343	3,706	4,009	
+110	4,535	5,010	5,527	6,095	6,722	
+120	0,7383	0,8113	0,8908	0,9772	1,094	Torr
+130	1,173	1,283	1,400	1,530	1,672	
+140	1,821	1,983	2,158	2,346	2,549	
+150	2,768	3,001	3,252	3,522	3,812	
+160	4,126	4,458	4,813	5,194	5,599	
+170	6,034	6,494	6,990	7,521	8,063	
+180	8,678	9,311	9,988	10,706	11,47	
+190	12,28	13,13	14,04	15,01	16,03	
+200	17,12	18,26	19,47	20,75	22,10	
+210	23,52	25,03	26,65	28,27	30,06	
+220	31,92	33,87	35,93	38,09	40,36	
+230	42,75	45,25	47,90	50,64	53,54	
+240	56,57	59,79	63,12	66,60	70,28	
+250	74,12	78,13	82,30	86,68	91,26	
+260	95,98	100,97	106,15	111,6	117,2	
+270	123,14	129,3	135,6	142,3	149,4	
+280	156,55	164,1	171,9	180,1	188,5	
+290	197,31	206,4	215,9	225,8	236,0	
+300	246,55	257,5	268,9	280,7	293,0	
+310	305,63	318,7	332,4	346,6	361,1	
+320	376,2	391,7	407,9	424,4	441,7	
+330	459,5	477,9	496,7	515,2	536,5	
+340	557,6	579,0	601,2	624,2	647,6	
+350	672,3	697,4	723,1	749,7	777,0	

2. Dampfdruck des Quecksilbers in atm zwischen +350 und 675 °C[1]).

Zehner \ Einer	ϑ in °C +0	+5	+10	+15	+20	+25
+350	0,8847	0,9690	1,060	1,157	1,259	1,375
380	1,497	1,623	1,762	1,909	2,064	2,230
410	2,408	2,597	2,799	3,014	3,248	3,480
440	3,733	4,000	4,281	4,577	4,889	5,219
470	5,567	5,929	6,310	6,713	7,132	7,568
500	8,035	8,517	9,016	9,550	10,08	1,065
530	11,27	11,89	12,51	13,22	13,92	14,65
560	15,41	16,20	17,01	17,86	18,79	19,65
590	20,60	21,57	22,58	23,63	24,72	25,83
620	26,97	28,16	29,38	30,65	31,96	33,30
650	34,68	36,10	37,57	39,08	40,63	42,21

[1]) Die Berechnung erfolgte unter Verwendung der in den Tabellen A, B und C angegebenen Konstanten.

Grau / Schäfer

Table 22: Vapour pressure of mercury

Water:

T [C]	ϱ [kg/m3]	Cp [J/kgC]	γ[m2/s]	k [W/mK]	Pr []
20	1000.52	4182	10.01*10^-6	0.597	7.02
40	994.59	4178	6.58	0.628	4.34
60	985.46	4184	4.78	0.651	3.02
80	974.08	4196	3.64	0.668	2.22

Table 23: Water data

Steel 316L

Young's modulus

T [C]	20	100	150	200	250
E [GPa]	192	186	182	178	174

Table 24: Young's modulus of 316L stainless steel (interpolation allowed)

Linear thermal expansion coefficient

T [C]	20	50	100	150	200	250
α [10^{-6}/K]	15.2	15.7	16.5	17.2	17.8	18.4

Table 25: Linear thermal expansion coefficient (316L)

Poission coefficient

T [C]	20	100	200
V []	0.291	0.298	0.307

Table 26: Poisson coefficient (316L)

Thermal conductivity

T	21	38	66	93	121	149	177	204
Λ [W/mK]	13.3	13.7	14.2	14.5	15.1	15.6	15.9	16.4

Table 27: Thermal conductivity (316L)

Density and specific heat

T	20	93	204
ϱ [kg/m3]	7958	7925	7883
Cp [J/kgC]	452	486	528

Table 28: Density and specific heat (316L)

7.2 Irradiation data

Long term decay heat (drain tank) after 200 days built up (source data from "LongDecay. Multiplied by target volume)

Time [days]	0	0.5	1	2	5	10	24	48	72
Power [kW]	14.7	8.9	7.7	6.6	5.3	4.3	3.2	2.6	2.2

Table 29: Decay heat (after 200d build up)

Short term gamma distribution/photon release rate (part of "ShortDecay.dec")

Elow MeV	Ehigh MeV	Time Unit=Sec Initial	1.50E+01	6.00E+01
0.000-	0.020	5.59E+09	5.58E+09	5.55E+09
0.020-	0.035	5.30E+10	5.29E+10	5.27E+10
0.035-	0.050	2.11E+10	2.11E+10	2.10E+10
0.050-	0.075	1.16E+11	1.16E+11	1.15E+11
0.075-	0.125	5.78E+11	5.75E+11	5.70E+11
0.125-	0.175	4.12E+11	4.02E+11	3.93E+11
0.175-	0.250	5.62E+11	5.60E+11	5.55E+11
0.250-	0.400	2.04E+12	2.02E+12	2.01E+12
0.400-	0.900	5.53E+12	5.38E+12	5.11E+12
0.900-	1.350	6.96E+11	6.89E+11	6.82E+11
1.350-	1.800	3.09E+11	3.06E+11	3.02E+11
1.800-	2.200	1.56E+11	1.55E+11	1.53E+11
2.200-	2.600	7.33E+10	7.25E+10	7.19E+10
2.600-	3.000	3.24E+10	3.23E+10	3.21E+10
3.000-	3.500	1.45E+10	1.44E+10	1.42E+10
3.500-	4.000	4.31E+08	4.03E+08	3.69E+08
4.000-	4.500	1.28E+08	1.08E+08	8.23E+07
4.500-	5.000	1.85E+07	1.43E+07	1.11E+07
5.000-	6.000	1.28E+08	2.19E+07	1.31E+07
6.000-	7.000	8.26E+07	2.11E+07	1.14E+06
7.000-	8.000	7.17E+06	2.04E+06	9.37E+04
8.000-	9.000	4.50E+04	6.45E+02	1.90E-03
9.000-	10.000	4.50E+04	6.45E+02	1.90E-03
OTotal Flux		1.06E+13	1.04E+13	1.01E+13
OEnergy Flux MeV/Sec		5.69E+12	5.58E+12	5.41E+12
ODose (Sv/h @ 1m)		7.58E-01	7.44E-01	7.21E-01

Table 30: Gamma spectrum (short term)

Long term gamma distribution/ photon release rate (part of "LongDecay.dec")

Elow MeV	Ehigh MeV	Time Unit=Hrs Initial	5.00E-01	1.00E+00	2.00E+00	5.00E+00	1.00E+01	2.40E+01	4.80E+01	7.20E+01
0.000-	0.020	4.82E+09	4.55E+09	4.53E+09	4.49E+09	4.36E+09	4.13E+09	3.65E+09	3.14E+09	2.82E+09
0.020-	0.035	5.05E+10	3.96E+10	3.09E+10	2.02E+10	1.02E+10	5.29E+09	2.00E+09	1.25E+09	1.00E+09
0.035-	0.050	1.51E+10	1.27E+10	1.16E+10	1.05E+10	9.26E+09	8.22E+09	6.50E+09	5.13E+09	4.54E+09
0.050-	0.075	1.05E+11	1.01E+11	9.80E+10	9.36E+10	8.39E+10	7.22E+10	5.12E+10	3.25E+10	2.33E+10
0.075-	0.125	5.37E+11	4.44E+11	4.08E+11	3.69E+11	3.09E+11	2.62E+11	1.99E+11	1.40E+11	1.05E+11
0.125-	0.175	3.87E+11	2.94E+11	2.64E+11	2.40E+11	2.09E+11	1.79E+11	1.38E+11	1.05E+11	8.68E+10
0.175-	0.250	5.39E+11	4.10E+11	3.66E+11	3.22E+11	2.59E+11	2.12E+11	1.54E+11	1.10E+11	8.99E+10
0.250-	0.400	1.70E+12	1.49E+12	1.38E+12	1.24E+12	1.01E+12	7.93E+11	5.25E+11	3.87E+11	3.33E+11
0.400-	0.900	5.42E+12	3.03E+12	2.53E+12	2.07E+12	1.52E+12	1.12E+12	7.03E+11	4.69E+11	3.66E+11
0.900-	1.350	6.85E+11	5.46E+11	4.79E+11	4.13E+11	3.28E+11	2.56E+11	1.57E+11	9.01E+10	6.00E+10
1.350-	1.800	3.05E+11	2.56E+11	2.31E+11	2.03E+11	1.63E+11	1.24E+11	7.13E+10	4.45E+10	3.49E+10
1.800-	2.200	1.48E+11	1.30E+11	1.20E+11	1.10E+11	9.68E+10	8.67E+10	7.19E+10	5.96E+10	5.22E+10
2.200-	2.600	6.95E+10	5.99E+10	5.30E+10	4.44E+10	3.75E+10	3.55E+10	3.29E+10	3.03E+10	2.82E+10
2.600-	3.000	3.23E+10	2.60E+10	2.04E+10	1.34E+10	8.27E+09	6.76E+09	4.55E+09	2.89E+09	2.01E+09
3.000-	3.500	1.45E+10	7.86E+09	4.65E+09	2.38E+09	1.18E+09	1.08E+09	9.65E+08	7.42E+08	5.46E+08
3.500-	4.000	4.31E+08	1.44E+08	6.55E+07	1.88E+07	5.56E+06	4.06E+06	2.09E+06	7.53E+05	2.84E+05
4.000-	4.500	1.28E+08	6.04E+06	4.70E+06	3.52E+06	2.29E+06	1.38E+06	4.33E+05	7.29E+04	1.26E+04
4.500-	5.000	1.85E+07	1.81E+06	1.24E+06	8.99E+05	6.06E+05	3.64E+05	1.17E+05	2.01E+04	3.48E+03
5.000-	6.000	1.28E+08	3.27E+03	2.01E+00	5.06E-05	1.26E-17	0.00E+00	0.00E+00	0.00E+00	0.00E+00
6.000-	7.000	8.26E+07	2.25E-04	3.30E-14	0.00E+00	0.00E+00	0.00E+00	0.00E+00	0.00E+00	0.00E+00
7.000-	8.000	7.17E+06	0.00E+00	0.00E+00	0.00E+00	0.00E+00	0.00E+00	0.00E+00	0.00E+00	0.00E+00
8.000-	9.000	4.50E+04	0.00E+00	0.00E+00	0.00E+00	0.00E+00	0.00E+00	0.00E+00	0.00E+00	0.00E+00
9.000-	10.000	4.50E+04	0.00E+00	0.00E+00	0.00E+00	0.00E+00	0.00E+00	0.00E+00	0.00E+00	0.00E+00
OTotal Flux		1.00E+13	6.85E+12	6.00E+12	5.15E+12	4.04E+12	3.17E+12	2.12E+12	1.48E+12	1.19E+12
OEnergy Flux MeV/Sec		5.46E+12	3.78E+12	3.29E+12	2.80E+12	2.19E+12	1.72E+12	1.14E+12	7.99E+11	6.45E+11
ODose (Sv/h @ 1m)		7.28E-01	5.01E-01	4.37E-01	3.71E-01	2.90E-01	2.27E-01	1.50E-01	1.04E-01	8.39E-02
OSurf.-Dose (Sv/h)		6.67E+05	4.74E+05	4.13E+05	3.51E+05	2.76E+05	2.18E+05	1.47E+05	1.03E+05	8.35E+04

Table 31: Gamma spectrum (long term)

7.3 Tube dimension norm

Tabelle 2.3 Rohre zur allgemeinen Verwendung, Maße und längenbezogene Masse, Gruppe 1 nach DIN V EN V 10 220 (2)

Außendurchmesser mm Reihe 1	2	3	Wanddicke, mm 0,5	0,6	0,8	1	1,2	1,4	1,6	1,8	2	2,3	2,6	2,9	3,2	3,6	4	4,5	5	5,4*	5,6	6,3
			längenbezogene Masse, kg/m																			
10,2			0,120	0,142	0,185	0,227	0,266	0,304	0,339	0,373	0,404	0,448	0,487									
	12		0,142	0,169	0,221	0,271	0,320	0,366	0,410	0,453	0,493	0,550	0,603	0,651	0,694							
	12,7		0,150	0,179	0,235	0,289	0,340	0,390	0,438	0,484	0,528	0,590	0,648	0,701	0,750							
13,5			0,160	0,191	0,251	0,308	0,364	0,418	0,470	0,519	0,567	0,635	0,699	0,758	0,813	0,879						
		14	0,166	0,198	0,260	0,321	0,379	0,435	0,489	0,542	0,592	0,664	0,731	0,794	0,852	0,923						
	16		0,191	0,228	0,300	0,370	0,438	0,504	0,568	0,630	0,691	0,777	0,859	0,937	1,01	1,10	1,18					
17,2			0,206	0,246	0,324	0,400	0,474	0,546	0,616	0,684	0,750	0,845	0,936	1,02	1,10	1,21	1,3	1,41				
		18	0,216	0,257	0,339	0,419	0,497	0,573	0,647	0,719	0,789	0,891	0,987	1,08	1,17	1,28	1,38	1,50				
	19		0,228	0,272	0,359	0,444	0,527	0,608	0,687	0,764	0,838	0,947	1,05	1,15	1,25	1,37	1,48	1,61	1,73			
	20		0,240	0,287	0,379	0,469	0,556	0,642	0,726	0,808	0,888	1,00	1,12	1,22	1,33	1,46	1,58	1,72	1,85			
21,3			0,256	0,306	0,404	0,501	0,595	0,687	0,777	0,866	0,952	1,08	1,20	1,32	1,43	1,57	1,71	1,86	2,01	2,12		
		22	0,265	0,317	0,418	0,518	0,616	0,711	0,805	0,897	0,986	1,12	1,24	1,37	1,48	1,63	1,78	1,94	2,10	2,21		
	25		0,302	0,361	0,477	0,592	0,704	0,815	0,923	1,03	1,13	1,29	1,44	1,58	1,72	1,90	2,07	2,28	2,47	2,61	2,68	2,91
		25,4	0,307	0,367	0,485	0,602	0,716	0,829	0,939	1,05	1,15	1,31	1,46	1,61	1,75	1,94	2,11	2,32	2,52	2,66	2,73	2,97
26,9			0,326	0,389	0,515	0,639	0,761	0,890	0,998	1,11	1,23	1,40	1,56	1,72	1,87	2,07	2,26	2,49	2,70	2,86	2,94	3,20
		30	0,364	0,435	0,576	0,715	0,852	0,987	1,12	1,25	1,38	1,57	1,76	1,94	2,11	2,14	2,56	2,83	3,08	3,28	3,37	3,68
	31,8		0,386	0,462	0,612	0,760	0,906	1,05	1,19	1,33	1,47	1,67	1,87	2,07	2,26	2,50	2,74	3,03	3,30	3,52	3,62	3,96
	32		0,388	0,465	0,616	0,765	0,911	1,06	120	1,34	1,48	1,68	1,89	2,08	2,27	2,52	2,76	3,05	3,33	3,54	3,65	3,99
33,7			0,409	0,490	0,649	0,806	0,962	1,12	1,27	1,42	1,56	1,78	1,99	2,20	2,41	2,67	2,93	3,24	3,54	3,77	3,88	4,26
		35	0,425	0,509	0,675	0,838	1,00	1,16	1,32	1,47	1,63	1,85	2,08	2,30	2,51	2,79	3,06	3,38	3,70	3,94	4,06	4,46
	38		0,462	0,553	0,734	0,912	1,09	1,26	1,44	1,61	1,78	2,02	2,27	2,51	2,75	3,05	3,35	3,72	4,07	4,34	4,47	4,93
	40		0,487	0,583	0,773	0,962	1,15	1,33	1,52	1,70	1,87	2,14	2,40	2,65	2,90	3,23	3,55	3,94	4,32	4,61	4,75	5,24
42,4			0,517	0,619	0,821	1,02	1,22	1,42	1,61	1,80	1,99	2,27	2,55	2,82	3,09	3,44	3,79	4,21	4,61	4,93	5,08	5,61
		44,5	0,543	0,650	0,862	1,07	1,28	1,49	1,69	1,90	2,10	2,39	2,69	2,98	3,26	3,63	4,00	4,44	4,87	5,21	5,37	5,94
48,3				0,706	0,937	1,17	1,39	1,62	1,84	2,06	2,28	2,61	2,93	3,25	3,56	3,97	4,37	4,86	5,34	5,71	5,90	6,53
	51			0,746	0,990	1,23	1,47	1,71	1,95	2,18	2,42	2,76	3,10	3,44	3,77	4,21	4,64	5,16	5,67	6,07	6,27	6,94
		54		0,790	1,05	1,31	1,56	1,82	2,07	2,32	2,56	2,93	3,30	3,65	4,01	4,47	4,93	5,49	6,04	6,47	6,68	7,41
	57			0,835	1,11	1,38	1,65	1,92	2,19	2,45	2,71	3,10	3,49	3,87	4,25	4,74	5,23	5,83	6,41	6,87	7,10	7,88
60,3				0,883	1,17	1,46	1,75	2,03	2,32	2,60	2,88	3,29	3,70	4,11	4,51	5,03	5,55	6,19	6,82	7,31	7,55	8,19
	63,5			0,931	1,24	1,54	1,84	2,14	2,44	2,74	3,03	3,47	3,90	4,33	4,76	5,32	5,87	6,55	7,21	7,74	8,00	8,89
	70				1,37	1,70	2,04	2,37	2,70	3,03	3,35	3,84	4,32	4,80	5,27	5,90	6,51	7,27	8,01	8,60	8,89	9,90
		73			1,42	1,78	2,12	2,47	2,82	3,16	3,50	4,01	4,51	5,01	5,51	6,16	6,81	7,60	8,38	9,00	9,31	10,4
76,1					1,49	1,85	2,22	2,58	2,94	3,30	3,65	4,19	4,71	5,24	5,75	6,44	7,11	7,95	8,77	9,42	9,74	10,8
		82,5			1,61	2,01	2,41	2,80	3,19	3,58	3,97	4,55	5,12	5,69	6,26	7,00	7,74	8,66	9,56	10,3	10,6	11,8
88,9					1,74	2,17	2,60	3,02	3,44	3,87	4,29	4,91	5,53	6,15	6,76	7,57	8,38	9,37	10,3	11,1	11,5	12,8
	101,6						2,97	3,46	3,95	4,43	4,91	5,63	6,35	7,06	7,77	8,70	9,63	10,8	11,9	12,8	13,3	14,8
		108					3,16	3,68	4,20	4,71	5,23	6,00	6,76	7,52	8,27	9,27	10,3	11,5	12,7	13,7	14,1	15,8
114,3							3,35	3,90	4,45	4,99	5,54	6,35	7,18	7,97	8,77	9,83	10,9	12,2	13,5	14,5	15,0	16,8
	127								4,95	5,56	6,17	7,07	7,98	8,88	9,77	11,0	12,1	13,6	15,0	16,2	16,8	18,8
	133								5,18	5,82	6,46	7,41	8,36	9,30	10,2	11,5	12,7	14,3	15,8	17,0	17,6	19,7
139,7									5,45	6,12	6,79	7,79	8,79	9,78	10,8	12,1	13,4	15,0	16,6	17,9	18,5	20,7
		141,3							5,51	6,19	6,87	7,88	8,89	9,90	10,9	12,2	13,5	15,2	16,8	18,1	18,7	21,0
		152,4							5,95	6,69	7,42	8,51	9,61	10,7	11,8	13,2	14,6	16,4	18,2	19,6	20,3	22,7
		159							6,21	6,98	7,74	8,89	10,0	11,2	12,3	13,8	15,3	17,1	19,0	20,5	21,2	23,7
168,3									6,58	7,39	8,20	9,42	10,6	11,8	13,0	14,6	16,2	18,2	20,1	21,7	22,5	25,2
		177,8								7,81	8,67	9,95	11,2	12,5	13,8	15,5	17,1	19,2	21,3	23,0	23,8	26,6
		193,7								8,52	9,46	10,9	12,3	13,6	15,0	16,9	18,7	21,9	23,3	25,1	26,0	29,1
219,1										9,65	10,7	12,3	13,9	15,5	17,0	19,1	21,2	23,8	26,4	28,5	29,5	33,1
		244,5									12,0	13,7	15,5	17,3	19,0	21,4	23,7	26,6	29,5	31,8	33,0	37,0
273											13,4	15,4	17,3	19,3	21,3	23,9	26,5	29,8	33,0	35,6	36,9	41,4
323,9													20,6	23,0	25,3	28,4	31,6	36,4	39,3	42,4	44,0	49,3
355,6													22,6	25,2	27,8	31,3	34,7	39,0	43,2	46,6	48,3	54,3
406,4													25,9	28,9	31,8	35,8	39,7	44,6	49,5	53,4	55,4	62,2
457															36,8	40,3	44,7	50,2	56,7	60,1	62,3	70,0
508															39,8	44,8	49,7	55,9	62,0	66,9	69,4	77,9
		559													43,9	49,3	54,7	61,5	68,3	73,7	76,4	85,9
610															47,9	53,8	59,8	67,2	74,6	80,5	83,5	93,8
		660															64,7	72,7	80,8	87,2	90,4	102
711																	69,7	78,4	87,1	94,0	97,4	109
	762																74,8	84,1	93,3	101	104	117
813																	79,8	89,7	99,6	108	112	125
		864															84,8	95,4	106	114	119	133
914																	89,8	101	112	121	125	141
1016																	99,8	112	125	135	140	157
1067																			131	141	147	165
1118																			137	148	154	173
	1168																		143	155	161	180
1219																			150	162	168	188
	1321																				182	204
1422																					196	220
	1524																					236
1626																						252
	1727																					
1829																						
	1930																					
2032																						
	2134																					
2235																						
	2337																					
	2438																					
2540																						

* Wanddicke 5,4 mm gibt es bei nahtlosen und geschweißten Rohren nicht.

Lieferbereich der geschweißten Stahlrohre nach DIN EN 10217-2

Lieferbereich der nahtlosen Stahlrohre nach DIN EN 10216-2

Table 32: Excerpt of DIN V EN V 10 220 (2)

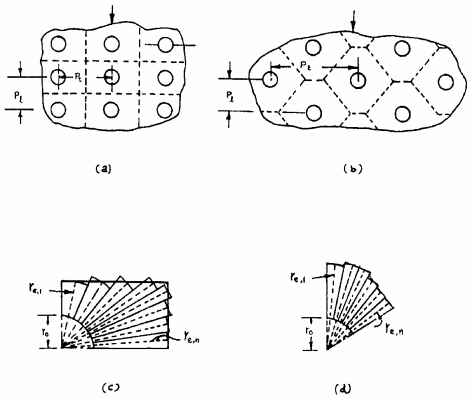

Figure 37 Fin sectors to determine fin efficiency of continuous finned tube heat exchanger.

1. Surface geometrical properties. These include

   A_o, minimum free flow area
   A, heat-transfer surface area (total of primary surface area, A_p, and secondary surface area, A_f)
   L, flow length
   D_h, hydraulic diameter
   β, heat-transfer surface area density
   σ, ratio of minimum free flow area to frontal area
   l_f, fin length
   t_f, fin thickness

   Also included are specialized dimensions used for heat-transfer and pressure-drop correlations.
2. Fluid physical properties. Determine the thermophysical properties at bulk mean temperature for each fluid, namely, hot and cold fluids. The properties needed for the rating problem are μ, c_p, k, and Pr. Since the outlet temperatures are not known for the rating problem, they are guessed initially. Unless it is known from the past experience, assume an exchanger effectiveness as 60–75% for most single-pass crossflow exchangers, and 80–85% for single-pass counterflow and two-pass cross-counterflow exchangers. For the assumed effectiveness, calculate the fluid outlet temperatures by

$$t_{h,o} = t_{h,i} - \varepsilon \frac{C_{min}}{C_h}(t_{h,i} - t_{c,i}) \tag{110}$$

$$t_{c,o} = t_{c,i} + \varepsilon \frac{C_{min}}{C_c}(t_{h,i} - t_{c,i}) \tag{111}$$

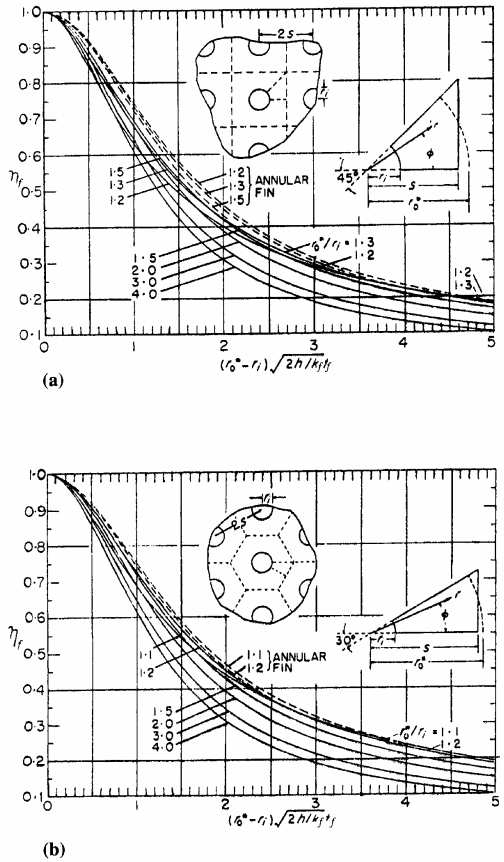

Figure 36 Fin efficiency for a continuous finned tube heat exchanger. (a) Square fin; (b) hexagonal fin.

Hence, the solution procedure is outlined using the ε-NTU method. The rating procedure given here is as in Refs. 24 and 63.

7.1 Rating of Single-Pass Counterflow and Crossflow Exchangers

The basic steps of the rating problem are shown in Fig. 38 and involve the determination of the following parameters.

Initially, assume $C_c/C_h \approx M_c/M_h$ for a gas-to-gas exchangers, or $C_c/C_h = (Mc_p)_c/(Mc_p)_h$ for a gas-to-liquid exchanger with approximate values of $c_p s$. For exchangers with $C^* \geq 0.5$ (usually gas-to-gas exchangers), the bulk mean temperature on each side will be the arithmetic mean of the inlet and outlet temperatures on each side. For exchangers with $C^* < 0.5$ (usually gas-to-liquid exchangers), the bulk mean temperature is calculated as given in Table 2.

Once the bulk mean temperatures are obtained on each side, obtain the fluid properties from thermophysical property tables or from standard thermal engineering books.

3. Reynolds numbers. Calculate the Reynolds number and/or any other pertinent dimensionless groups needed to determine j or Nu and f of heat-transfer surfaces on each side of the exchanger.
4. Compute j or Nu and f factors.
5. Correct Nu (or j) and f for variable fluid property effects in the second and subsequent iterations.
6. From Nu or j, determine heat-transfer coefficient for both the fluid streams.

$$h = \frac{\mathrm{Nu}k}{D_h} \tag{112a}$$

or

$$h = jG\, C_p Pr^{-2/3} \tag{112b}$$

7. Determine the fin efficiency η_f and the overall surface efficiency η_o given by

$$\eta_f = \frac{\tanh ml}{ml} \tag{113}$$

$$\eta_o = 1 - \frac{A_f}{A}(1 - \eta_f) \tag{114}$$

8. Overall conductance. Calculate the wall thermal resistance, R_w. Knowing the fouling resistances $R_{f,h}$ and $R_{f,c}$ on the hot and cold fluid sides, respectively, calculate the overall thermal conductance UA from

$$\frac{1}{\mathrm{UA}} = \frac{1}{(\eta_o hA)_h} + \frac{R_{f,h}}{(\eta_o A)_h} + R_w + \frac{1}{(\eta_o hA)_c} + \frac{R_{f,c}}{(\eta_o A)_c} \tag{115a}$$

$$= R_h + R_1 + R_w + R_2 + R_c \tag{115b}$$

Table 2 Approximate Bulk Mean Temperature on the Hot and Cold Side of a Two-Fluid Heat Exchanger for $c^* < 0.5$ [24,63]

C_{max} = hot fluid C_{min} = cold fluid	C_{max} = cold fluid C_{min} = hot fluid
$t_{h,m} = \frac{t_{h,i} + t_{h,o}}{2}$	$t_{c,m} = \frac{t_{c,i} + t_{c,o}}{2}$
$t_{c,m} = t_{h,m} - \Delta t_{lm}$	$t_{h,m} = t_{c,m} + \Delta t_{lm}$
$\Delta t_{lm} = \frac{(t_{h,m} - t_{c,i}) - (t_{h,m} - t_{c,o})}{\ln\left(\frac{t_{h,m} - t_{c,i}}{t_{h,m} - t_{c,o}}\right)}$	$\Delta t_{lm} = \frac{(t_{h,i} - t_{c,m}) - (t_{h,o} - t_{c,m})}{\ln\left(\frac{t_{h,i} - t_{c,m}}{t_{h,o} - t_{c,m}}\right)}$

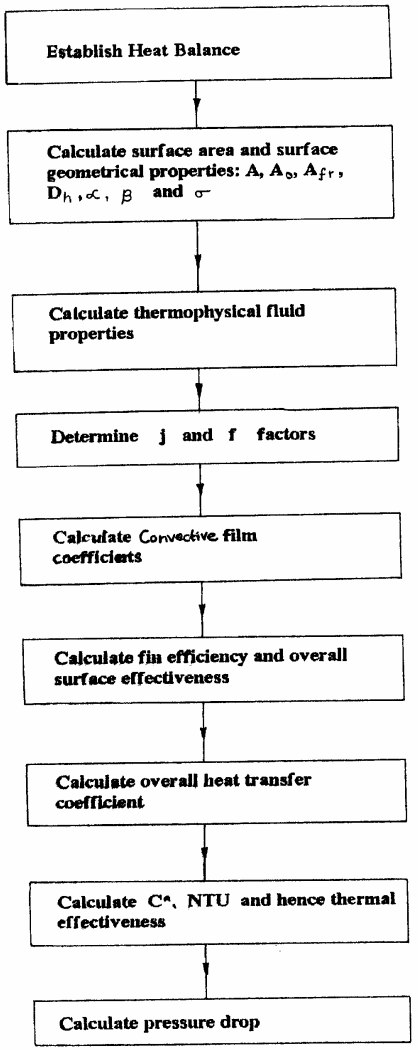

Figure 38 Rating of a compact heat exchanger.

9. Calculate NTU, C^*, and exchanger effectiveness, ε. If the thermal effectiveness is above 80%, correct for wall longitudinal conduction effect.
10. Compute the outlet temperature from Eqs. 110 and 111. If these outlet temperatures differs significantly from those assumed in step 2, use these outlet temperatures in step 2 and continue iterating steps 2–9 until the assumed and computed outlet temperatures converge within the desired degree of accuracy. For a gas-to-gas exchanger probably one or two iterations will be sufficient.
11. Compute the heat duty from

$$q = \varepsilon C_{\min}(t_{h,i} - t_{c,i}) \tag{116}$$

12. Calculate the core pressure drip. The friction factor f on each side is corrected for the variable fluid properties as discussed in Chapter 3. The wall temperature T_w is computed from

$$T_{w,h} = t_{m,h} - q(R_h + R_1) \tag{117}$$

$$T_{w,c} = t_{m,c} + q(R_c + R_2) \tag{118}$$

7.2 Shah's Method for Rating of Multipass Counterflow and Crossflow Heat Exchangers

The rating procedure for multipass crossflow exchangers with fluids mixed between passes is described by Shah [63]. The solution procedure for rating problem for the two-pass crossflow exchangers with flows unmixed in the passes but mixed between passes is also very similar to the sizing of single-pass crossflow. Only some of the calculations on the two pass side need to be modified, and only those points are summarized here.

1. In order to compute fluid bulk mean temperature and thermophysical properties of fluids, first guess the overall thermal effectiveness, ε_N. Assume it to be 80–85% unless it is known from the past experience. .Assume that the NTU per pass is same. The individual pass effectiveness ε_p is related to overall effectiveness ε_N for the case of fluids mixed between passes. Compute approximate values of C_c and C_h since we don't know yet the accurate values of the specific heats.
2. Determine the intermediate and outlet temperature by solving the following individual pass effectiveness and overall effectiveness equations:

$$\varepsilon_{p1} = \frac{C_c(t_{c,o} - t_{c,int})}{C_{\min}(t_{h,i} - t_{c,int})} \tag{120}$$

$$\varepsilon_{p2} = \frac{C_c(t_{c,int} - t_{c,i})}{C_{\min}(t_{h,int} - t_{c,i})} \tag{121}$$

$$\varepsilon = \frac{C_c(t_{c,o} - t_{c,i})}{C_{\min}(t_{h,i} - t_{c,i})} \tag{122}$$

In the foregoing three equations there are three unknowns: $t_{c,o}$, $t_{c,int}$, and $t_{h,int}$. Hence, they can be evaluated exactly and then from the overall energy balance $t_{h,o}$ is calculated.

$$C_c(t_{c,o} - t_{c,i}) = C_h(t_{h,i} - t_{h,o}) \tag{123}$$

Since we know all terminal temperatures for each pass, we can determine the bulk mean temperature for each fluid in each pass and subsequently the fluid properties separately for each pass.

DK 621.643.412.6 März 1975

Vorschweißflansche

Nenndruck 40

DIN 2635

Welding neck flanges, nominal pressure 40
Brides à souder à collerette; pression nominale 40

Maße in mm

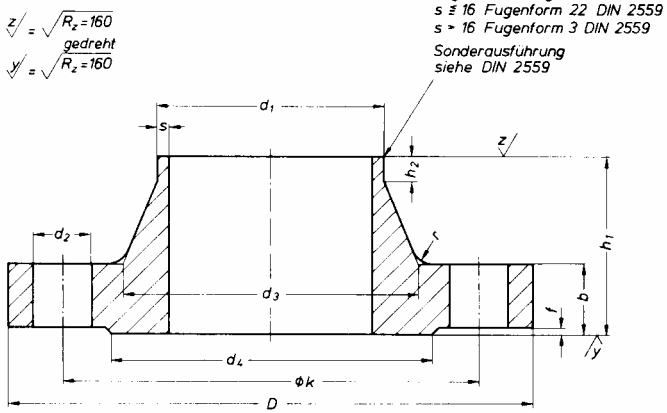

Bezeichnung eines Vorschweißflansches mit Dichtleiste Form C von Nennweite 400 für Rohr-Außendurchmesser d_1 = 406,4 mm aus C 22:

Flansch C 400 x 406,4 DIN 2635 – C 22

Fachnormenausschuß Rohre, Rohrverbindungen und Rohrleitungen (FR) im Deutschen Normenausschuß (DNA)

Rohr-Anschlußmaße Nennweite	d_1 Reihe 1	d_1 Reihe 2	Flansch D	b	k	h_1	Ansatz d_3	s	r	h_2 ≈	Dichtleiste d_4	f	Schrauben Anzahl	Gewinde	d_2	Gewicht eines Flansches (7,85 kg/dm³) kg ≈
10	–	14	90	16	60	35	25	1,8	4	6	40	2	4	M 12	14	0,661
	17,2	–					28									
15	–	20	95	16	65	38	30	2	4	6	45	2	4	M 12	14	0,746
	21,3	–					32									
20	–	25	105	18	75	40	38	2,3	4	6	58	2	4	M 12	14	1,06
	26,9	–					40									
25	–	30	115	18	85	40	42	2,6	4	6	68	2	4	M 12	14	1,29
	33,7	–					46									
32	–	38	140	18	100	42	52	2,6	6	6	78	2	4	M 16	18	1,88
	42,4	–					56									
40	–	44,5	150	18	110	45	60	2,6	6	7	88	3	4	M 16	18	2,33
	48,3	–					64									
50	–	57	165	20	125	48	72	2,9	6	8	102	3	4	M 16	18	2,82
	60,3	–					75									
65	76,1	–	185	22	145	52	90	2,9	6	10	122	3	8	M 16	18	3,74
80	88,9	–	200	24	160	58	105	3,2	8	12	138	3	8	M 16	18	4,75
100	–	108	235	24	190	65	128	3,6	8	12	162	3	8	M 20	22	6,52
	114,3	–					134									
125	–	133	270	26	220	68	155	4	8	12	188	3	8	M 24	26	9,07
	139,7	–					162									
150	–	159	300	28	250	75	182	4,5	10	12	218	3	8	M 24	26	11,8
	168,3	–					192									
(175)	193,7	–	350	32	295	82	218	5,6	10	15	260	3	12	M 27	30	18,2
200	219,1	–	375	34	320	88	244	6,3	10	16	285	3	12	M 27	30	21,5
250	–	267	450	38	385	105	298	7,1	12	18	345	3	12	M 30	33	34,9
	273	–					306									
300	323,9	–	515	42	450	115	362	8	12	18	410	4	16	M 30	33	49,7
350	355,6	–	580	46	510	125	408	8,8	12	20	465	4	16	M 33	36	68,1
	–	368														
400	406,4	–	660	50	585	135	462	11	12	20	535	4	16	M 36	39	96,5
	–	419														
500	508	–	755	52	670	140	562	14,2	12	20	615	4	20	M 39	42	117

Eingeklammerte Nennweite möglichst vermeiden.
Rohr-Anschlußmaße der Reihe 1 sind international, die der Reihe 2 werden in Deutschland noch angewendet.

Werkstoff: C 22 nach DIN 17 200

Flansche aus C 22, die den hier festgelegten Maßen entsprechen, können bis zu Temperaturen von 120 °C für Betriebsdrücke in Höhe des Nenndruckes verwendet werden. Bei höheren Temperaturen als 120 °C bis 300 °C ist der Abfall der Streckgrenze zu berücksichtigen.

Andere Werkstoffe nach Vereinbarung.

Herstellverfahren, Lieferzustand und Kennzeichnung: nach DIN 2519

Dichtungsarten:

Regelausführung mit Dichtleiste Form C nach DIN 2526.

Weitere mögliche Dichtungsarten siehe DIN 2526

Hinweise auf weitere Normen

Flansche; Allgemeine Angaben, Übersicht siehe DIN 2500
Stahlflansche; Technische Lieferbedingungen siehe DIN 2519
Stahlrohre siehe DIN 2448 und DIN 2458

7.6 Study of tube S-arrangement

R1	R2	Alpha1	Alpha2	L2	dL (L1)	Van Mises Stress
600	600	214.5	200	10	3300 (4500)	123.6
600	600	234.5	220	10	4200 (5300)	142.4
600	600	224.5	210	10	4200 (5300)	138.2
600	600	214.5	200	10	4200 (5300)	133.3
600	600	204.5	190	10	4200 (5300)	136.1
600	600	195.5	180	10	4200 (5300)	138.0
600	600	214.5	200	100	4200 (5300)	136.8
600	700	214.5	200	10	4200 (5300)	122.7
700	600	214.5	200	10	4200 (5300)	123.8
550	750	214.5	200	10	4200 (5300)	121.7
650	650	214.5	200	10	4200 (5300)	123.8
500	800	214.5	200	10	4200 (5300)	119.7

Table 33: Study of tube S-arrangement

7.7 Implemented matlab code

NaturalConvicion.m

```
function DrainTankSim( tges, flag )
%
% tges [std]
% flag ['uncooled', 'cooled']

% Geometry
Lpipes = 1+ 1 +1; % [m]
Dpipes = 0.1;       % [m]
H      = 1.3;       % [m]
thWall = 0.013;     % Thickness of wall [m]
Atank  = 2.2*pi;      % Surface of Me tank Steel [m2]


% Masses [kg]
mMe    = 20000;
mW1    = 500;
mW2    = 2400;

% Starting temperatures
TMe    = 100;
TW1    = 30;
TW2    = TW1;

% Heating
% see loc_decayheat

% Material properties
k     = 14;              % Conductivity tank Steel [W/mK]
cpMe  = 136.5;
cpW   = 4178;

% Constants
g      = 9.81;
lambda = 0.05;
dt     = 10;  % [sec] % 1   -> each step 1 sec
                      % 60  -> each step 1 min
                      % 120 -> each step 2 min


Apipe = 1/4 * pi * Dpipes^2;
psi   = (lambda * Lpipes / Dpipes); % + 4 Bends;
dm    = 0;
n     = (tges * 3600)/dt;
EtotZu= 0;
for i = 1 : 1: n

    % Natuerliche Konvektion (Wasser im Tank - Wasser ausserhalb)
    rhoW1    = loc_density( TW1(i) );
    rhoW2    = loc_density( TW2(i) );
    rhoDif   = rhoW2 - rhoW1;
    wW      =  ( 2* ( rhoDif * g * H / ( rhoW2 * psi ) ) );

    dm(i+1)  = rhoW2 * Apipe * wW * dt;   % [kg]
        % Mischungstemperatur der 2 Wasser
    TW1(i+1) = ( (mW1-dm(i+1))/mW1* TW1(i) ) + ( dm(i+1)/mW1 * TW2(i) );
    switch flag
```

```
        case 'cooled'
            TW2(i+1) = TW2(i);
        case 'uncooled'
            TW2(i+1) = ( ( dm(i+1)/mW2)* TW1(i) ) + ( (mW2-dm(i+1))/mW2 *TW2(i)
);
        otherwise
            disp('flag unknown!');
    end

    % Energiebilanz in Me
    Qab      = k * Atank * ( TMe(i) - TW1(i)) / thWall;
    Qzu      = loc_decayrate( (i-1)*dt );
    QMe      = Qzu - Qab;
    TMe(i+1) = (QMe / (mMe * cpMe) * dt) + TMe(i);
    EtotZu   = (Qzu * dt) + EtotZu;

    % Waermezufuhr nach Wasser in (von Me)
    TW1(i+1) = ( Qab / (mW1 *cpW) * dt) + TW1(i+1);

end

disp('disposed energy');
EtotZu
hold on
tAxes = [1:length(TMe)] ./ (3600/dt);
plot(tAxes, TMe, '-r');
plot(tAxes, TW1, '-g');
plot(tAxes, TW2, '-b');
figure
plot(tAxes, dm/dt, '-k');

disp('TW1 , TW2 and TMe');
TW1(end)
TW2(end)
TMe(end)

return

function Q = loc_decayrate( t )

    T = [0, 0.5, 1, 2, 5, 10, 24, 48, 72]; % h
    T = T.*3600; % s
    Q = [14.7, 8.9, 7.7, 6.6, 5.3, 4.3, 3.2, 2.6, 2.2]; % [kW]
    Q = Q*1000; % [W]
    S = 1;

    Q = interp1( T, S*Q, t );

return

function rho = loc_density( T )

    p = [-0.00340625,-0.101624999999994,1003.9624999999999;];
    rho = polyval( p, T );

return
```

```
function data = HeatExchanger( Ds, Dt, L, Nt, Wth, kt, Rf , eff, m1, m2, T1in,
T2in)
%
% HeatExchanger( Ds, Dt, L, Nt, Wth, kt, Rf , eff, m1, m2, T1in, T2in)
% calculates transfered heat and outlet temperatures of s&t HE
% (counterflow, one pass) using mercury (hot medium) and water (cold medium)
%   Ds   : Inner diameter of shell     [mm]
%   Dt   : Outer diameter of tubes     [mm]
%   L    : Length of tubes             [m]
%   Nt   : Number of tubes             []
%   Wth  : Wall thickness of tube      [mm]
%   kt   : Conductivity of tube        [W/mK]
%   Rf   : Total resistance of fouling [m2°C/W]
%   eff  : Initial effectiveness of HE []
%   m1   : Mass flow hot fluid         [kg/s]
%   m2   : Mass flow cold fluid        [kg/s]
%   T1in : Temperature hot fluid in    [°C]
%   T2out: Temperature cold fluid in   [°C]
%
% source: Karrasik, p.30, p.177, p.209ff
% 2006, Andreas Vetter, PSI -- last change: -

    rho1   = 13384; % (at 100°C)
    rho2   = 994;   % (at 40°C)
    lambda = 0.03;
    Dd     = 0.15;  % Delivery tube diameter [m]

    Ds  = Ds * 0.001;  % [m]
    Dt  = Dt * 0.001;  % [m]
    Wth = Wth * 0.001; % [m]
    Dti = Dt - (2*Wth);% [m]
    At  = 1/4 * Dt^2 * pi;              % section area of 1 tube
    Ati = 1/4 * Dti^2 * pi;             % inner section area of 1 tube
    A0  = (1/4 * Ds^2 * pi) - (Nt * At); % free flow section area (shell side)
    A   = Nt * Dt * pi * L              % Total heat Exchange area (outer
tubes)
    Dh  = 4*A0 / ( Ds*pi + Nt*Dt*pi ) ;  % Hydraulic diameter

    A_Ai  = Dt / (Dt - 2*Wth);
    A_Alm = Dt * log(A_Ai) / (2*Wth);
    Rw    = Wth/kt;

    w1 = m1/(rho1 * Nt*Ati)
    w2 = m2/(rho2 *  A0   )

    % Initialising
    C1  = loc_C( T1in, m1, 'Mercury');;
    C2  = loc_C( T2in, m2, 'Water');
    if (C1 < C2)
        Cmin = C1;
        Cmax = C2;
        flag = 1;
    else
        Cmin = C2;
        Cmax = C1;
        flag = 2;
    end
    if ((Cmin/Cmax) >= 0.5)
        flag = 3;
    end
```

```
T1out = T1in - ( eff * Cmin /C1* (T1in-T2in));
T2out = T2in + ( eff * Cmin /C2* (T1in-T2in));

data = [T1out; T2out; eff];
Zaehler = 1;
stop = 0;
while (~stop)
    Zaehler = Zaehler + 1;

    [T1m T2m] = loc_Temp( T1in, T1out, T2in, T2out , flag);
    C1 = loc_C( T1m, m1, 'Mercury');
    C2 = loc_C( T2m, m2, 'Water');
    if (C1 < C2)
        Cmin = C1;
        Cmax = C2;
        flag = 1;
    else
        Cmin = C2;
        Cmax = C1;
        flag = 2;
    end
    if ((Cmin/Cmax) >= 0.5)
        flag = 3;
    end
    Cs = Cmin/Cmax;
    if (Cmin > Cmax)
        disp('Warning: Cmin > Cmax!)');
    end

    % Tube Side
    Pr1 = fun_Prandtl(T1m, 'Mercury')
    Re1 = loc_ReynoldsNumber( w1, Dt, T1m, 'Mercury')
    Nu1 = 5 + 0.025*( Re1*Pr1 )^0.8
    k1  = fun_conductivity( T1m, 'Mercury');
    h1  = Nu1 * k1/ Dt;

    % Shell Side
    Pr2 = fun_Prandtl(T2m, 'Water');
    Re2 = loc_ReynoldsNumber( w2, Dh, T2m, 'Water');
    Nu2 = 0.023 * Re2^0.8 * Pr2^0.4
    k2  = fun_conductivity( T2m, 'Water');
    h2  = Nu2 * k2/ Dh;

    R1 = 1/h1;
    R2 = 1/h2;
    U  =  1 /( (A_Ai*R1) + (A_Alm*Rw) + Rf + R2 );

    % Step 9
    Cs = Cmin/Cmax;    % C*
    NTU = U*A/Cmin;
    eff = loc_Effectiveness(NTU, Cs);
        % Longitudinal correction NYI
    if (eff > 0.85)
       eff = 0.85 ;
       disp('longitudinal correction not implemented!');
    end
    % Step 10
    T1out = T1in - ( eff * Cmin /C1* (T1in-T2in) );
    T2out = T2in + ( eff * Cmin /C2* (T1in-T2in) );


    if (Zaehler > 8)
```

```
            stop = 1;
        end
        data(:,end+1) = [T1out; T2out; eff];
    end


    % OUTPUT
    hold on
    i=[1:Zaehler];
    plot( i, data(1,:), '-r' );
    plot( i, data(2,:), '-'  );
    xlabel('step');
    ylabel('°C');

    Q  = eff * Cmin * (T1in - T2in)
    Q1 = m1 * fun_HeatCapacity( ((T1in+T1out)/2), 'Mercury' ) * (T1in - T1out)
    Q2 = m2 * fun_HeatCapacity( ((T2in+T2out)/2), 'Water' ) * (T2out - T2in)

    R1 = R1;
    R2 = R2;
    Rw = Rw;
    Cs = Cs;

    dP = loc_PressureDrop( Dd, Ati*Nt, lambda*L/Dti , w1 , rho1 );

return

function eff = loc_Effectiveness(NTU, R)
% source: Wong, p.160f
% R here heat capacity ratio C*

    B = exp(-NTU*R);

    eff = (B - exp(-NTU)) / ( B - R*exp(-NTU) );

return

function C = loc_C( T, m, medium);

    cp = fun_HeatCapacity( T, medium );
    C  = m * cp;

return

function Re = loc_ReynoldsNumber( w, D, T, medium )

    Re = w * D / fun_kinViscosity(T, medium) ;

return

function [T1m, T2m] =loc_Temp( T1in, T1out, T2in, T2out, flag)
% for Cmax = cold fluid, Cmin = hot fluid, C<0.5
% see Karrasik p.211

    switch (flag)
        case 1
            T2m  = (T2in + T2out) /2;  % mean temperature cold fluid
            dTa  = T1in  - T2m;
            dTb  = T1out - T2m;
            LMTD = ( dTa - dTb ) / ( log( dTa /dTb ) );
            T1m  = T2m + LMTD;

        case 2
```

```
            T1m  = (T1in + T1out)/2;
            dTa  = T1m - T2in;
            dTb  = T1m - T2out;
            LMTD = ( dTa - dTb ) / ( log( dTa / dTb) );
            T2m  = T1m - LMTD;

        case 3 % (C* >= 0.5)
            T1m = (T1in + T1out) /2;
            T2m = (T2in + T2out) /2;

        otherwise
            disp('Error, flag nicht bekannt');
    end
return

function dP = loc_PressureDrop( Dd, At, sigT, w, rho )
% Dd  : (inner) Delivery tube diameter [m]
% At  : Total inner section surface of tubes [m2]
% sigT: Sigma of tube (=lambda*L/Dt)
% w   : velocity in tubes [m/s]
% rho : density [kg/m^3]

    Ad    = 1/4 * pi * Dd^2;                                    % surface area of
delivery tube
    dPin  = (1 - Ad/At)^2 * rho * w^2 /2 * 10^-5             ; % influx
    dPt   = sigT * rho * w^2 / 2  * 10^-5                    ; % tube flow
    dPout = 0.5* ((1 - Ad/At)^(3/4)) * rho * w^2 /2  * 10^-5 ; % outflux
    dP    = dPin + dPt + dPout

    Ps = (dPt/dP)
return
```

dPExpansionTank.m

```
function dP = dP_ExpansionTank( Vn, Tn, Pn , Medium, dV)
%
% dP = dP_ExpansionTank( Vn, Tn, Pn , Medium, dV)
% Calculates decrease of pressure, due to loss of mercury (dV)
%   Vn       : Nominal volume cover gas [liter]
%   Tn       : Nominal temperature cover gas [K]
%   Pn       : Nominal pressure cover gas [atm]
%   Medium   : Cover gas ['Ar', 'He']
%   dV       : Delta Volume [liter]
%
% 2006, Andreas Vetter, PSI -- last change: -
% source: Handbook of chemistry and physics (69th edition) p.D-188

R = 0.08206;  % [litres*atm/mole/K]

switch Medium
    case 'Ar'
        a = 1.345;   % [liters^2*atm/mole^2]
        b = 0.03219; % [liters/mole]

    case 'He'
        a = 0.03412;
        b = 0.02370;

    otherwise
        disp('Medium unknown');
        return
end

AA = - a*b;
BB =   a*Vn;
CC = -(Pn*b*Vn^2 + R*Tn*Vn^2);
DD =   Pn*Vn^3;

nn = roots([AA BB CC DD]); % [mole]

c = 0;
for i=1:3
    if (isreal(nn(i)))
        c = c+1;
        n = nn(i);
    end
end

if (c>1)
    disp('More than 1 real solution');
    nn
    pause
end

V = Vn + dV;
P = (n*R*Tn/ (V-n*b) ) - a * (n/V)^2
```

7.8 References

Barker	Barker R.S., Tessier M.J., "Handbook of Electromagnetic Pump Technology", Elsevier Science Publishing Inc, New York 1987
Bucenieks_a	Bucenieks I.E., "High pressure and high flowrate induction pumps with permanent magnets", Magnetohydrodynamics Vol. 39 (2003), No. 4, pp. 411-417
Bucenieks_b	"Layout, Design and Operation of an InGsSn-Eutectic Liquid Metal Loop", IPUL report, 1998
CRC	"CRC Handbook of Chemistry and Physics", B&T, New York 1989
ESS	Volume III Update Report, Chapter 4, Target Systems
Eurisol_a	Eurisol Report (December 2003), Internet "Eurisol.org"
Eurisol_b	"Report of the Target and Ion Source Task Group, Appendix C", December 2003, Internet "Eurisol.org"
Flansch	„Flansche und Wekstoffe, Normen und Tabellen", 3.Auflage, Beuth Verlag, Berlin 1995
Goedecke	Goedecke R., "Fluidverfahrenstechnik", Wiley-VCH, New York, 2006
Hinterberger	Hinterberger F., "Physik der Teilchenbeschleuniger und Ionenoptik", Springer, Berlin 1997
Holman	Holman J.P.: "Heat Transfer", 8th Edition, McGraw-Hill, New York 1997
Idelchik	Idelchik I.E.: "Handbook of Hydraulic Resistance", 3rd Edition, Begell House, New York 1996
Karassik	Karrasik I.J., Messina J.P., Cooper P., Heald C.C.: "Pump Handbook", 3rd Edition, McGraw-Hill, New York 2001
Kirillov	Kirillov P.L., "Liquid Metalls", Atomizdat, Moscow 1967
Kuppan	Kuppan T.: "Heat Exchanger Handbool", 1st edition, Dekker, New York 2000
Landolt	Landolt H., Börnstein R., Schäfer K., Borchers H., Bartels J., "Zahlenwerte und Funktionen aus Physik, Chemie, Astronomie, Geophysik und Technik", Teil 2, 6. Auflage, Springer, Berlin 1960
Merck	Sicherheitsdatenblatt (Quecksilber reinst), Firma Merck, 2004

OakRidge_a	Internal report, see attached CD (folder "OakRidgeHeatExchanger")
OakRidge_b	Pawel S.J., Taleyarkhan R.P., Felde D.K., Manneschmidt E.T., "Influence of mercury velocity on compatibility with type 316L/316LN stainless stell in a flow loop", Journal of Nuclear Materials, Vol. 318, 2003, p. 313-324
RCC-MR	RCC-MR Code, Ensemble de caractèristiques 3S, Edition Mai 1993
Schommer	Schommer H., "Sealless magnetic driven centrifugal and side channel pumps", Faragallah, Sulzbach 2004
Strohrmann	Strohrmann G., "Messtechnik im Chemiebetrieb", 10.Auflage, Oldenbourg Industrieverlag, Oldenburg 2004
Thermocoax	Thermocoax®, "Einsatzfertige Mantelthermoelemente", Product Catalogue, 2006
Wagner	Wagner W.: "Strömung und Druckverlust", 5.Auflage, Vogel Verlag, Wuerzburg 2001
Wille	Wille K., "The Physics of Particle Accelerators", Oxford University Press, Oxford 2000
Wong	Wong H.Y.: "Handbook of Essential Formulae and Data on Heat Transfer for Engineers", 1st edition, Longman, London 1977
Zalvutinov	"A study on martensitic and austenitic steels after exposure in mercury at 573K up to 5000h", Zalavutidinov R.Kh., Dai Y., Gorodetsky A.E, Bauer G.S., Alimov V.Kh., Zakharov A.P., Journal of Nuclear Materials 296 (2001), p. 219-224, see attached CD

7.9 Eidesstattliche Erklärung

Die selbständige und eigenhändige Anfertigung versichere ich an Eides statt.

Datum Unterschrift